NASA TECHNICAL NOTE

NASA TN D-7916

2.4/4

NASA TN D-7916 c.1

LOAN COPY: RETU
AFWL TECHNICAL L
KIRTLAND AFB, N

TECH LIBRARY KAFB, NM
0136613

INDUCED PRESSURE DISTRIBUTION OF A JET IN A CROSSFLOW

Richard L. Fearn and Robert P. Weston

Langley Research Center
Hampton, Va. 23665

NATIONAL AERONAUTICS AND SPACE ADMINISTRATION • WASHINGTON, D. C. • JULY 1975

TECH LIBRARY KAFB, NM
0133613

1. Report No.	2. Government Accession No.	3. Recipient's Catalog No.
NASA TN D-7916		

4. Title and Subtitle	5. Report Date
INDUCED PRESSURE DISTRIBUTION OF A JET IN A CROSSFLOW	July 1975
	6. Performing Organization Code
7. Author(s)	8. Performing Organization Report No.
Richard L. Fearn and Robert P. Weston	L-9894
	10. Work Unit No.
9. Performing Organization Name and Address	505-10-31-02
NASA Langley Research Center Hampton, Va. 23665	11. Contract or Grant No.
	13. Type of Report and Period Covered
12. Sponsoring Agency Name and Address	Technical Note
National Aeronautics and Space Administration Washington, D.C. 20546	14. Sponsoring Agency Code

15. Supplementary Notes

Richard L. Fearn is Assistant Professor of Engineering, University of Florida, Gainesville, Florida.

16. Abstract

An experimental investigation of the turbulent flow of a subsonic round jet exhausting perpendicularly from a flat plate into a subsonic crosswind of the same temperature has been conducted in the Langley V/STOL tunnel. The large test section of this tunnel made it possible to use a jet with the relatively large diameter of 10.16 cm (4.00 in.). Pressures were measured on the flat plate at over 400 locations to provide a detailed description of the static pressure distribution. Results are presented in tabular and graphical forms for jet to crossflow velocity ratios ranging from 2 to 10, and comparisons are made with results of other experiments. The results indicate that the dominant flow parameter affecting the pressure distributions is the ratio of jet to crossflow velocities. The distribution of turbulence on the plate also appears to be a function of velocity ratio.

17. Key Words (Suggested by Author(s))	18. Distribution Statement
Jet plume Subsonic crossflow Pressure distribution Jet in a crossflow	Unclassified – Unlimited New Subject Category 34

19. Security Classif. (of this report)	20. Security Classif. (of this page)	21. No. of Pages	22. Price*
Unclassified	Unclassified	105	$5.25

*For sale by the National Technical Information Service, Springfield, Virginia 22151

INDUCED PRESSURE DISTRIBUTION OF A JET IN A CROSSFLOW

Richard L. Fearn* and Robert P. Weston
Langley Research Center

SUMMARY

An experimental investigation of the turbulent flow of a subsonic round jet exhausting perpendicularly from a flat plate into a subsonic crosswind of the same temperature has been conducted in the Langley V/STOL tunnel. The large test section of this tunnel made it possible to use a jet with the relatively large diameter of 10.16 cm (4.00 in.). Pressures were measured on the flat plate at over 400 locations to provide a detailed description of the static pressure distribution. Results are presented in tabular and graphical forms for jet to crossflow velocity ratios ranging from 2 to 10, and comparisons are made with results of other experiments. The results indicate that the dominant flow parameter affecting the pressure distributions is the ratio of jet to crossflow velocities. The distribution of turbulence on the plate also appears to be a function of velocity ratio.

INTRODUCTION

In the transition between hover and wingborne flight, a significant part of the lift of a VTOL aircraft is furnished by direct engine thrust. This injection of a high velocity jet of air at almost right angles to the crossflow caused by the aircraft's forward motion produces a complicated flow field which affects the aerodynamic characteristics of the aircraft. Several wind-tunnel tests have been conducted to measure these jet-induced effects on the pressure loading and aerodynamic coefficients for specific aircraft configurations (refs. 1 to 9).

In an attempt to describe in general the essential features of this complicated flow field, many investigators have concentrated on a simplified version of the situation and studied the turbulent flow of a subsonic round jet exhausting perpendicularly through a large flat plate into a subsonic crossflow. Such a study has application to areas other than V/STOL aerodynamics such as the process of cooling combustion gases in gas-turbine combustors or the discharge of an effluent into a waterway. For several decades experiments have been conducted on certain aspects of this jet in a crossflow problem, namely

*Assistant Professor of Engineering, University of Florida, Gainesville, Florida.

the path of the jets (refs. 10 to 16) and the pressure distribution on the flat plate (refs. 15 and 17 to 23). However, the pair of contrarotating vortices, which constitutes one of the dominant features of the velocity field, has only recently received detailed attention (refs. 15, 16, 24, and 25). Due to limitations in wind-tunnel size, most previous experiments have been restricted to jets with rather small diameters of 0.6 to 2.5 cm (0.25 to 1.0 in.) to avoid wind-tunnel wall effects. An extensive bibliography for work done prior to 1969 is given by R. J. Margason in reference 26.

An experimental investigation of the pressure and velocity fields associated with a jet in a crossflow for flows of the same temperature was conducted in the Langley V/STOL tunnel whose large test section made it feasible to use a jet with the relatively large diameter of 10.16 cm (4.0 in.). The investigation included measurements of the pressure distribution on the flat plate and the velocity field in the jet and resulted in a quantitative description of the pair of contrarotating vortices associated with the jet (ref. 25). The measured pressure distributions on the flat plate are presented in this report in tabular and graphical form for jet to crossflow velocity ratios ranging from 2 to 10.

A comparison of the results of the present experiment with those of a similar experiment conducted at the Office National d' Études et de Recherches Aérospatiales (ONERA) (refs. 21 and 22) is given also. This comparison is significant because the ONERA experiment is the only other one to date which utilized a jet of comparable size and is included herein because the results have heretofore received only limited distribution. Comparison is also made with the results of experiments using smaller jets (refs. 15, 17, 18, 20, and 23).

SYMBOLS

Values are given both in SI Units and U.S. Customary Units. The measurements and calculations were made in U.S. Customary Units.

A area of jet orifice, m^2 (ft^2)

A_j jet exit area corrected for nozzle boundary-layer thickness, m^2 (ft^2)

C_p pressure coefficient, $\frac{p - p_\infty}{q_\infty}$

$\overline{C}_p$ time average of C_p at a point

C_p' fluctuations of C_p about its time-average value, $\overline{C}_p$

D jet diameter, cm (in.)

H	height of plate above tunnel floor in jet diameters
M	Mach number
$\dot{m}$	mass flow rate in jet nozzle, kg/sec (slugs/sec)
N_{Re}	Reynolds number based on jet diameter and crossflow velocity
n	integer
p	static pressure, N/m^2 (lb/ft^2)
p_t	total pressure in jet plenum, N/m^2 (lb/ft^2)
q	dynamic pressure, N/m^2 (lb/ft^2)
R	effective velocity ratio defined by equation (1)
$\bar{R}$	gas constant, m-N/kg-K (ft-lb/slug-^oR)
r	radial distance from origin of X,Y coordinate system, cm (in.)
T	temperature, K (^oR)
U	velocity, m/sec (ft/sec)
X,Y	coordinate system in plane of flat plate (see fig. 1(b))
γ	ratio of specific heat at constant pressure to specific heat at constant volume for a gas
θ	angle measured from negative X-axis, degrees (see fig. 1)
ν	kinematic viscosity, m^2/sec (ft^2/sec)
ρ	mass density, kg/m^3 ($slugs/ft^3$)
σ	standard deviation of fluctuations in C_p

Subscripts:

j	denotes static property of jet fluid at nozzle-exit plane
t	denotes stagnation property of fluid in jet plenum
∞	denotes static property of crossflow fluid

APPARATUS

This experiment was conducted in the Langley V/STOL wind tunnel which is a closed return atmospheric tunnel with a test section 4.42 by 6.63 m (14.50 by 21.75 ft). Test-section airspeeds for this investigation ranged from 23 to 66 m/sec (75 to 215 ft/sec), or free-stream Mach numbers of 0.07 to 0.19. Jet Mach numbers ranged from 0.09 to 0.95.

The flat plate was originally constructed from a 1.22-m or 12D by 2.44-m or 24D (4.0- by 8.0-ft) sheet of 1.91-cm (0.75-in.) plywood with an overlay of 1.59-mm-thick (0.0625-in.) formica on the upper surface. A hole for the nozzle was centered midway between the long sides of the plate and 6D aft of its leading edge. The plate was mounted 3D above the wind-tunnel floor to remove the plate from the tunnel boundary layer, which was about 1.5D thick. In addition, boundary-layer suction could be applied to the tunnel floor upstream of the plate to reduce the tunnel-boundary-layer thickness.

Four hundred and fifty-nine static pressure orifices were placed on the original flat plate at selected intersections of ray and circles centered at the jet orifice as indicated in figure 1(a). Each static pressure port was made of 1.02-mm (0.040-in.) inside diameter stainless-steel thin-wall tubing mounted flush with the upper surface of the flat plate and protruding several centimeters through the lower surface. Sheet metal fairing was used on the underside of the plate to protect the static pressure leads and to streamline the nozzle-plenum assembly.

The majority of the data presented in this report was taken using a 24D by 27D plate resulting from front and side extensions to the original plate (fig. 1(b)) and with the plate mounted 4.5D above the wind-tunnel floor. For both sizes of the flat plate, the leading edge was rounded with a radius of about 1.02 cm (0.40 in.) and a transition strip was placed 3.8 cm (1.5 in.) aft of the leading edge.

The jet of air was formed by using a plenum chamber and a 20:1 convergent nozzle (ref. 27) designed to provide a flat velocity profile at the 10.16-cm-diameter (4.00-in.) nozzle exit. In order to measure the static pressure in the jet as close to the plane of the plate as possible, a small ring (0.125D) was installed at the jet orifice with four static pressure ports spaced equally around the inside surface of this jet exit ring 0.635 cm

(0.25 in.) from the exit plane. When the plate was mounted 4.5D above the tunnel floor, a constant diameter cylindrical extension was used to extend from the convergent nozzle to the jet exit ring. Figure 2 is a sketch of the nozzle-plenum assembly with the extension in place, and figure 3 is a photograph of the plate and jet orifice in the wind tunnel. Supply air for the jet was heated so that the temperature at the jet orifice would be approximately the same as that of the crossflow. A Venturi flowmeter in the air supply line was used to measure the mass flow rate of the jet.

All pressures were measured with pressure transducers which were calibrated with water or mercury manometers. The leads from the static pressure ports on the flat plate and from the boundary-layer mouse, which was used to measure the boundary layer on the flat plate, were connected by plastic tubing to 11 pressure scanning devices mounted on the underside of the plate. Each device consisted of a single pressure transducer which could be connected sequentially to each of 48 pressure tubes. The output of each pressure transducer was fed into a r.c. low pass filter to attenuate fluctuations in the transducer output signal. One second after each static pressure port was connected to the pressure transducer, the signal from the filter was sampled and recorded on magnetic tape.

TEST PROCEDURES AND CONDITIONS

Jet-Nozzle Characteristics

Prior to the wind-tunnel test, the jet-nozzle characteristics were investigated with no crossflow. A total pressure probe and a static pressure probe were used for surveys in the nozzle-exit plane and in several parallel planes up to 20D from the exit plane. These pressures were measured with water and with mercury manometers. The turbulent boundary-layer displacement thickness of the jet at the nozzle-exit plane (without extensions) was determined to be $(2.8 \pm 0.5) \times 10^{-3}$ D. Outside of the nozzle boundary layer the exit-plane velocity profile was flat to within 0.5 percent of the velocity measured at the center of the jet. The jet core extended almost 6D from the exit plane. The jet fluid at the exit had low turbulence, but once outside the jet core, fluid mixing created large turbulence in the jet.

Test Conditions

The investigation of the pressure distribution on the flat plate was conducted during three separate wind-tunnel tests. In the first test, the original flat plate (12D by 24D) was mounted 3D above the tunnel floor. Results of this experiment caused doubts about the accuracy of the measured pressures near the leading and side edges of the plate. It was decided to repeat the test to study the effect on the pressure distribution of changing various test conditions. The diagnostic phase of the second test included the test conditions shown in table 1.

TABLE 1.- TEST CONDITIONS

H	Extensions to flat plate	Boundary-layer suction on wind-tunnel floor
3.0	None	On
3.0	None	Off
3.0	Leading edge	On
3.0	Leading edge	Off
4.5	Leading edge and side	On
4.5	Leading edge and side	Off

The remainder of the second test was made with the plate 4.5D above the floor, all extensions in place, and with no boundary-layer suction on the wind-tunnel floor. The pressure distribution was measured for a range of effective jet to crossflow velocity ratios, holding the jet Mach number constant. This was repeated for jet Mach numbers of 0.50, 0.75, and 0.93. Data for comparison with ONERA (ref. 21) were taken by matching wind-tunnel and jet Mach numbers as well as the effective velocity ratios. For comparison with the results of other experiments (refs. 15, 17, 18, and 23), only the effective velocity ratios were matched.

During a third wind-tunnel test, the pressure at selected ports was measured as a function of time for effective velocity ratios of 4 and 8 in an attempt to understand the nature of scatter in the data of the previous tests for certain locations on the plate. This was accomplished by sampling the output of the transducer connected to a given static pressure port for an interval of 10 seconds at a sampling rate of 31 times per second. The data were taken both with and without the low pass filters in the circuit. In this test, the plate was mounted 3D above the tunnel floor and consisted of the original plate with the leading-edge extension only. This configuration was used since the results of the diagnostic tests showed the leading-edge extension to be the only significant change in the conditions.

Effective Velocity Ratio

The properties of a jet in a crossflow depend primarily on the ratio of the momentum flux across the jet orifice to the momentum flux of the crossflow over an equal area. It is useful to define an effective velocity ratio as the square root of this ratio of momentum fluxes

$$R = \left(\frac{\int_A \rho_j U_j^2 \, dA}{\rho_\infty U_\infty^2 A} \right)^{1/2} \tag{1}$$

The reciprocal of equation (1) is used by some investigators and it is usually referred to by the same name.

If the jet and crossflow fluids are the same and obey the ideal gas equation of state, and if the speed U_j is constant across the jet orifice, then the effective velocity ratio may be written: $R = \frac{M_j}{M_\infty}\left(\frac{p_j}{p_\infty}\right)^{1/2}$. In the experiment, this equation could be used in four ways to calculate the effective velocity ratio. The first involves measurements of the mass flow rate of the jet, the total temperature and total pressure of the jet, and the area of the jet orifice. Using the nozzle boundary-layer displacement thickness measured with no crossflow to give an estimate of the jet exit area A_j, the jet Mach number can be calculated, assuming isentropic flow, from $M_j\left(1 + 0.2M_j^2\right)^{-3} = \frac{\dot{m}}{p_t A_j}\left(\frac{\overline{R}T_t}{\gamma}\right)^{1/2}$. With M_j known, the jet-exit-plane pressure can be calculated from $p_j = p_t\left(1 + 0.2M_j^2\right)^{-3.5}$. A second way of using the equation for the effective velocity ratio makes use of the average pressure measured by the jet exit ring to give the static pressure at the jet exit plane. Isentropic expansion to this average pressure gives the jet Mach number from the relation $M_j = \left\{5\left[\left(\frac{p_t}{p_j}\right)^{2/7} - 1\right]\right\}^{1/2}$. In reality, the pressures at the four jet-exit-ring ports differed greatly and it is questionable whether their average pressure actually represents the jet pressure at the exit.

If the jet static pressure at the exit plane is assumed equal to the crossflow static pressure, the equation for the effective velocity ratio simplifies to a ratio of the jet to crossflow Mach numbers. Additionally, if the jet and crossflow temperatures are equal, this becomes the actual velocity ratio, $R = \frac{U_j}{U_\infty}$. For use in the equation $R = \frac{M_j}{M_\infty}$, the jet Mach number can be calculated by two methods: using (1) the mass flow rate of the jet or (2) the jet total pressure. The isentropic relations for these are

$$M_j(\dot{m}) = \frac{\dot{m}}{p_\infty A_j}\left(\frac{\overline{R}T_j}{\gamma}\right)^{1/2}$$

or

$$M_j(p_t) = \left\{5\left[\left(\frac{p_t}{p_\infty}\right)^{2/7} - 1\right]\right\}^{1/2}$$

Differences in jet Mach number of up to 0.08 and in R of up to 14 percent are obtained between calculations using expansion to average jet-exit-ring pressure and expansion to crossflow static pressure. For presentation of results in this report the calculations are based on expansion to crossflow static pressure because of uncertainties in the

jet exit pressures due to difficulties in their measurement. In addition, calculating R from expansion to crossflow static pressure provides consistent comparison with data from the other investigators who calculate their velocity ratios in a similar way.

Flat-Plate Boundary Layer

The boundary layer on the flat plate was measured at several locations along the upstream ray from the jet for each test condition (see table 1). It was found that changing the test conditions had little effect on the behavior of the boundary layer on the plate. There was a separation bubble at the rounded leading edge of the plate and reattachment of the flow as a thickened turbulent boundary layer. Whether the jet was on or off did not significantly affect the measured boundary-layer velocity profiles. The estimated displacement thickness of the boundary layer at the location of the jet was 0.07D, based on boundary-layer measurements upstream of the jet.

PRESENTATION OF RESULTS

The pressure distribution on the flat plate is presented in terms of a pressure coefficient $C_p = \frac{p - p_\infty}{q_\infty}$, where p is the measured static pressure at a specific location on the plate. Except when otherwise noted, p is the difference between the pressure measured at the test condition $\left(R = \frac{M_j}{M_\infty}\right)$ and the pressure measured with the jet off $\left(M_j = 0\right)$, and with the tunnel Mach number unchanged.

The results of the wind-tunnel investigation of the pressure distribution of the flat plate are presented as follows:

	Figure	Table
Values of C_p for a range of R	4 to 11	
Time variation for C_p at selected locations for R = 4.1 and R = 8 . .	12 to 16	2
Uncertainty bands for contour plots	17	
Effect of changing jet Mach number holding R constant	18	
Comparison with the results of other experiments	19 to 23	3

RESULTS AND DISCUSSION

Pressure Distribution on the Flat Plate

Detailed descriptions of the measured pressure distribution on the flat plate are presented in figures 4 to 11 for effective velocity ratios of 2.2, 2.8, 3.9, 5.1, 6.1, 7.0, 8.0, and 10.0, respectively. Each figure presents the pressure distribution for one effective velocity ratio in four different formats. Numerical values of C_p are presented in tabular form in part (a). The pressure distribution as a function of radial distance from the jet for each ray of pressure ports is shown in part (b), and in part (c) it is shown as a

function of angular position for selected circles of pressure ports close to the jet orifice. Part (d) shows contours of constant pressure coefficient. These C_p contour plots are useful as a convenient means for qualitative comparisons with the results of other test conditions or with the results of other experiments. Construction of the contour plots involved smoothing the data from the ray and circle plots.

From these figures some observations can be made about the effect on the flat-plate pressure distribution of changing the effective velocity ratio:

1. For all velocity ratios there is a positive pressure region upstream of the jet, but in general, the maximum pressure attained and the extent of this region decrease with increasing velocity ratio. This is probably due to the increased entrainment of crossflow fluid as the relative jet velocity increases.

2. The ray plots indicate a large radial component of the pressure gradient in the region close to and to the side of the jet. Recent analysis indicates that these gradients may be induced by the location of the counter-rotating vortices in the vicinity of the jet.

3. From the circle plots, it is seen that the angular position of the minimum pressure point moves upstream from about 110° for $R = 2.2$ to about 75° for $R = 10$. The value of the minimum pressure coefficient measured on the inner circle of ports is also a function of velocity ratio and appears to reach its lowest value of about -4.7 at the velocity ratio of 6.1. As a comparison, for potential flow over a circular cylinder the minimum pressure coefficient occurs at 90° and has a value of -1.5.

4. In the wake region along the 180° ray, the radial component of the pressure gradient is less than it is in the region to the side of the jet. The minimum pressure coefficient attained on this ray is about -2 for velocity ratios of 2 to 5. For velocity ratios above 5 the minimum value of C_p on this ray gradually becomes less negative with increasing velocity ratio, indicating a more rapid pressure recovery in the wake region for the larger velocity ratios. This is consistent with the physical observation that at the lower velocity ratios the deflected jet plume is closer to the flat plate, introducing a wake effect. At higher velocity ratios, the plume will be higher and the wake effect therefore less apparent.

5. An interesting behavior of the pressure distribution along the rays from 160° to 180° is noted for $R \geq 4$. There appears to be a small region close to and in the wake of the jet where a flat spot (very small radial component of the pressure gradient) or, perhaps even a hook, in the ray plot occurs. This behavior, however, is masked by the relatively large scatter of the data in the wake region.

6. An anomaly in the pressure distribution in the wake occurs for a velocity ratio of 3.9. The minimum pressures along the 170° and 180° rays, for example, are lower than the corresponding pressures for all other velocity ratios. The implication of this behavior is that there is a slower pressure recovery in the wake region for a velocity ratio of 4 than for the other velocity ratios.

7. For circles of pressure ports near the jet orifice, the value of C_p at a given angular position in the left half-plane ($-\theta$) is consistently more negative than the value for the symmetry point in the right half-plane ($+\theta$). This is due to misalinement between the nozzle and flat plate. The nozzle was displaced 0.02D in the negative Y-direction with respect to the point of intersection of the rays of pressure ports.

Most of the effects described above are also evident in the C_p contour plots. For example, the slow pressure recovery in the wake region is described by contours that extend far downstream before intersecting the X-axis, whereas a more rapid pressure recovery is described by these same contours intersecting the X-axis much closer to the jet. It is also noted that the lobe of each contour appears to be swept back more for lower velocity ratios. Thus, the direction of maximum influence of the pressure field is a function of the velocity ratio.

The pressures at selected locations on the flat plate were also measured as a function of time for effective velocity ratios of 4.1 and 8. This was accomplished by sampling the output of the pressure transducer connected to a given port for approximately 10 seconds at a sampling rate of 31 times per second. These measurements were taken with the output of the pressure transducer filtered by a low pass filter and, also, unfiltered. For the latter case, the amplitude of pressure fluctuations with a frequency above about 15 cps should have been attenuated in the tubing connecting the static pressure port on the flat plate to the transducers. For the results of both cases, it is convenient to write the pressure coefficient at a given time as the sum of an average value over the time interval, of measurement and a fluctuation about this average value; $C_p = \overline{C}_p + C'_p$ where $\overline{C}_p = \frac{1}{n} \sum_{i=1}^{n} C_{p_i}$, and where n is the total number of times the pressure C_{p_i} at the port was measured. For this phase of the experiment, the jet-off pressures were not adequately measured so the values of p are not corrected for the jet-off condition but are instead referenced to free-stream pressure. The standard deviation of the fluctuations of the pressure coefficient about its mean value is also calculated:

$$\sigma = \left[\frac{1}{n} \sum_{i=1}^{n} \left(C'_{p_i} \right)^2 \right]$$

Results of these calculations are presented in table 2 and in figures 12 to 15. Figure 12 shows the time variation of the pressure coefficient for selected pressure ports for an effective velocity ratio of 4.1 and for the output of the pressure transducer filtered.

TABLE 2.- PRESSURE-COEFFICIENT STANDARD DEVIATIONS

r/D	Pressure-coefficient standard deviations at θ of –										
	60^o	75^o	90^o	105^o	120^o	135^o	150^o	160^o	170^o	180^o	-170^o
R = 4.1; M_j = 0.48; pressure-transducer output filtered											
0.58	0.07	0.09	0.12	0.21	0.22	0.12	0.16	0.16	0.12	0.11	
.66		.07	.10	.17	.18	.12	.14	.14	.11	.09	0.12
.70		.05	.09	.14	.13	.09	.11	.11	.08	.07	.11
.80		.05	.06	.09	.09	.09	.11	.11	.09		.09
1.20		.02	.03	.05	.06	.06	.08	.09	.09		.12
2.50		.01	.01	.01	.02	.03	.03	.05	.07	.06	.06
3.75		.00	.01	.01	.01	.02	.02	.03	.06	.09	.06
R = 4.1; M_j = 0.48; pressure-transducer output unfiltered											
0.58	0.45	0.72	1.31	2.53	2.35	1.75	1.95	1.35	0.85	0.70	
.66		.60	1.12	1.96	2.02	1.54	1.57	1.25	.75	.59	0.78
.70		.58	1.04	1.72	1.94	1.54	1.60	1.26	.86	.73	.93
.80		.44	.82	1.33	1.70	1.40	1.29	1.17	.78		.81
1.20		.20	.37	.51	.73	.74	.71	.82	.70		
2.50		.04	.06	.07	.12	.19	.22	.34	.46		.49
3.75		.02	.03	.03	.04	.07	.10	.16	.30	.46	.43
R = 8.0; M_j = 0.93; pressure-transducer output filtered											
0.62	0.13	0.18	0.26	0.33	0.24	0.20	0.16	0.12	0.09	0.09	
.66		.12	.19	.25	.18	.15	.14	.10	.08	.07	0.09
.70		.11	.17	.22	.16	.14	.12	.09	.07	.07	.09
.80		.10	.15	.18	.15	.13	.12	.09	.07	.06	.08
1.00		.06	.08	.09	.09	.06	.07	.05	.04	.04	.05
2.00		.01	.02	.02	.02	.03	.04	.04	.03		
2.50		.01	.01	.01	.01	.01	.01	.02	.02	.03	
5.00		.01	.01	.01	.01	.01	.01	.01	.02	.02	
R = 8.0; M_j = 0.93; pressure-transducer output unfiltered											
1.00		0.53	0.74	0.92	0.65	0.55	0.59	0.48	0.36	0.25	0.24
2.00		.24	.33	.40	.40	.37	.53	.41	.27	.25	.31
3.50		.07	.13	.10	.14	.15	.20	.21	.22	.44	.46
5.00		.03	.08	.05	.07	.10	.12	.14	.14		.14

Results are shown for circles of pressure ports close to the jet orifice and for pressure ports on rays of 105° and 170°. For the circles of ports close to the jet the maximum standard deviations occur at an angular location of 105°, which coincides with the location of the point of minimum pressure (see fig. 6(c)). However, the standard deviation of the fluctuations decreases more rapidly with the distance along the 105° ray than along the 170° ray. Thus, for values of r/D greater than about 1, the maximum fluctuations occur in the wake region.

Results for the same test conditions, but with the low pass filters removed from the circuit, are shown in figure 13. The standard deviations of the fluctuations in the measured pressure are an order of magnitude greater, and higher frequencies are recorded, but the qualitative observations made for figure 12 are applicable. Results for $R = 8$ are shown in figures 14 and 15. It appears that the fluctuations in C_p for $R = 8$ are greater than those for $R = 4$ in the region 60° to 105° but are less than those for $R = 4$ in the wake region. These differences indicate that the distribution of turbulence on the plate is a function of effective velocity ratio.

The response of the pressure transducers connected to the static pressure ports on the jet exit ring indicate that the flow in the jet near the orifice had a relatively low level of turbulence as was expected. The fluctuations in the pressures measured on the jet exit ring were about three orders of magnitude smaller than those in the pressures measured on the plate near the orifice.

Although it was not the intent of this experiment to study the turbulent fluctuations of the pressure distributions on the flat plate, some feeling for the extent of the high turbulence region around the jet and a rough estimate of the turbulent intensities can be obtained from the values of σ listed in table 2. Contours of constant σ are plotted in figure 16 for velocity ratios of 4.1 and 8.0. Note that near the jet orifice, the shapes of these contours are similar to the shapes of the respective pressure contours. Since each data point for figures 4 to 11 represents a single random sample of the pressure-transducer output, the distribution of σ on the flat plate when the low pass filters are in the circuit is a measure of the distribution of uncertainty in the pressure coefficient. The large values of σ near the jet and in the wake help explain the scatter in the data for these regions.

While the C_p contour plots are the most convenient means of comparing one measured pressure distribution with another, care must be taken to recognize the effect of a given uncertainty in C_p on the location of each contour. If, for a given position on the flat plate, the pressure coefficient has an uncertainty of $\pm\Delta C_p$, then there is a corresponding uncertainty $\pm\Delta s$ in the location of the contour passing through that point. This uncertainty is given by $\Delta s = \Delta C_p / |\text{grad } C_p|$. Calculation of the uncertainty band width ($2\,\Delta s$) for a contour thus requires a knowledge of the gradient of the pressure distribution at that point. From values of σ in table 2 and the measured pressure distribution for $R = 3.9$

from figure 6 the shaded uncertainty bands shown in figure 17(a) have been constructed. Note that the uncertainty bands become larger as the absolute magnitude of the pressure coefficient decreases; this is because the pressure gradient is decreasing with distance from the jet more rapidly than σ. Since no measurements of the pressure fluctuations were made for $\theta < 75^{\circ}$ no estimate of the uncertainty bands from fluctuations in C_p could be made in this region.

Another source of positional uncertainty in the C_p contours would be inherent errors in the pressure transducers themselves. Although this type of error would be difficult to estimate accurately, a realistic value would be 0.5 percent of full-scale deflection. Such an error would result in the uncertainty bands shown in figure 17(b) for the same test conditions as those shown in figure 17(a). For this case of a constant uncertainty ΔC_p, the bandwidth at any location of the contour is determined solely by the magnitude of the gradient of C_p at that location. The extreme width of the uncertainty bands for the contours -0.1, 0.0, and +0.1 except in the region near the jet indicates that using these contours to compare two separately determined pressure distributions could be misleading.

The C_p contours shown in figure 17 represent three different determinations of the pressure distribution at the same jet and free-stream Mach numbers for the last three test conditions listed in table 1. The differences appear not to be significant. Although not shown here, the differences in the pressure distributions for the first three conditions of table 1 indicated that the leading-edge extension was needed. It appears that the leading edge needs to be 8D to 10D upstream of the jet exit to obtain stable boundary-layer conditions in the region of interest. Therefore, all the data presented in this report was taken with the leading-edge extension added to the flat plate. The effects on the pressure distribution of changing the jet Mach number while holding the effective velocity ratio constant are shown in figure 18 for effective velocity ratios of 4, 5, 6, 7, 8, and 10. Using figure 17 as a guide for the uncertainties in contour locations, it is concluded that within the 0.45 to 0.95 range of jet Mach number studied this effect is small compared to the effect of changing the effective velocity ratio except in the wake of the jet. Note that the anomaly of relatively slow pressure recovery in the wake for $R = 4.0$ and $M_j = 0.75$ is supported by the results for $R = 4.0$ and $M_j = 0.44$.

Comparisons With the Results of Other Experiments

Comparisons of the results of the present experiment with those of several other experiments are provided in this section. These comparisons are made with C_p contour plots in figures 19 to 23. Table 3 provides a summary of the test conditions for each experiment.

TABLE 3.- TEST CONDITIONS FOR VARIOUS EXPERIMENTS

Experiment	Jet diameter		Test-section size	Flat-plate dimensions	Tunnel speed		N_{Re} $(U_\infty D/\nu_\infty)$
	cm	in.			m/sec	ft/sec	
Soullier (ref. 21)	12.0	4.7	43D × 63D	21D × 21D	30 to 90	98.4 to 295	(24 to 72) × 10^4
Present study	10.2	4.0	44D × 65D	24D × 27D	23 to 62	75.5 to 203.4	(16 to 42) × 10^4
Mosher (ref. 28)	5.1	2.0	54D (circular)	24D × 33D	15	49	5.1 × 10^4
Vogler (ref. 17)	2.5	.98	84D × 144D	24D × 40D	93	305	15 × 10^4
Bradbury (ref. 18)	2.5	.98	102D × 138D	72D × 84D	18	59	3.0 × 10^4
Thompson (ref. 15)	2.5	.98	48D × 60D	Tunnel floor*	12	39	2.0 × 10^4
Ousterhout (ref. 23)	1.0	.39	75D × 107D	69D × 96D	28	91.9	1.8 × 10^4

*Applied wind-tunnel boundary-layer suction.

The experiment chosen for the most extensive comparison was conducted by A. Soullier (ref. 21) at ONERA. As seen from table 3, the test conditions for this experiment are quite similar to those of the present study. Both effective velocity ratio and free-stream Mach number were matched for each comparison. Figure 19 presents the results. Although some of the low magnitude C_p contours (±0.1 and ±0.2) are as much as 1D apart, from the foregoing discussion it is believed that this behavior is not significant. Agreement between the contours for the larger values of C_p is fairly good, but sometimes there are significant though not drastic differences, for example, the differences shown in figure 19(a) for $C_p = -1.0$.

Figures 20 to 23 compare the results of the present study with those of the other experiments listed in table 3. For these comparisons effective velocity ratios were matched, but crossflow velocities were not matched. Agreement among the contour plots of Mosher (fig. 20), Thompson (fig. 21), Bradbury and Wood (fig. 21), Vogler (fig. 22), and the present study is fairly good, but for some contours there are discrepancies which would seem to exceed the experimental errors. For example, for $R = 4$ the contour indicates a more rapid pressure recovery in the wake for the results of Thompson and of Bradbury and Wood than for the results of Soullier, Mosher (ref. 28), and the present study. Agreement with the results of Ousterhout is not good (see fig. 23), particularly for the effective velocity ratio of 3.3. In this case, the results of Ousterhout represent a significantly more rapid pressure recovery in the wake and also a significant change in the shape of the contours to the side of the jet. The reasons for this are not presently known.

An order-of-magnitude range in both jet diameter and Reynolds number is seen among the experiments shown in table 3. The comparisons between the pressure distributions from the various experimenters indicate that the effect of jet diameter is small when distances are nondimensionalized with the jet diameter. Over the range of Reynolds number used in the experiments, this parameter also appears to have a small effect.

CONCLUSIONS

The results of a wind-tunnel investigation of the turbulent flow of a round subsonic jet of air exhausting perpendicularly through a flat plate into an essentially incompressible subsonic crossflow indicate the following conclusions about the static pressure distribution on the flat plate:

1. The dominant flow parameter for describing the pressure distribution on the plate is the effective velocity ratio. In particular, when distances are based on jet diameters, the pressure distribution does not appear to depend strongly on the jet size for jets up to 12 cm (5 in.) in diameter or on the jet Mach number. There do appear to be small but significant differences in the results of the experiments presented in this report. The parameters causing these secondary effects have not been identified.

2. There are regions of intense turbulence on the plate close to the jet orifice. For an effective velocity ratio of 4 the most severe turbulence is encountered at the point of minimum pressure. The intensity of the turbulence decays rapidly with distance to the side of the jet but persists farther into the wake region. The distribution of turbulence on the plate also appears to be a strong function of effective velocity ratio.

3. Some caution must be used when comparing flat-plate pressure distributions on the basis of contours of constant pressure coefficient. In regions of low pressure gradients, differences on the order of a jet diameter between contours are not unlikely even for the same test conditions.

Langley Research Center,
National Aeronautics and Space Administration,
Hampton, Va., March 31, 1975.

REFERENCES

1. Otis, James H., Jr.: Induced Interference Effects on a Four-Jet VTOL Configuration With Various Wing Planforms in the Transition Speed Range. NASA TN D-1400, 1962.

2. Vogler, Raymond D.: Interference Effects of Single and Multiple Round or Slotted Jets on a VTOL Model in Transition. NASA TN D-2380, 1964.

3. Hickey, David H.; Kirk, Jerry V.; and Hall, Leo P.: Aerodynamic Characteristics of a V/STOL Transport Model With Lift and Lift-Cruise Fan Power Plants. Conference on V/STOL and STOL Aircraft, NASA SP-116, 1966, pp. 81-96.

4. Spreeman, Kenneth P.: Free-Stream Interference Effects on Effectiveness of Control Jets Near the Wing Tip of a VTOL Aircraft Model. NASA TN D-4084, 1967.

5. Margason, Richard J.; and Gentry, Garl L., Jr.: Aerodynamic Characteristics of a Five-Jet VTOL Configuration in the Transition Speed Range. NASA TN D-4812, 1968.

6. Barrack, Jerry P.; and Kirk, Jerry V.: Low-Speed Characteristics of High-Performance Lift-Engine V/STOL Aircraft. [Preprint] 680644, Soc. Automot. Eng., Oct. 1968.

7. Winston, Matthew M.: Wind-Tunnel Data From a 0.16-Scale V/STOL Model With Direct-Lift and Lift-Cruise Jets. NASA TM X-1758, 1969.

8. Carter, Arthur W.: Effects of Jet-Exhaust Location on the Longitudinal Aerodynamic Characteristics of a Jet V/STOL Model. NASA TN D-5333, 1969.

9. Mineck, Raymond E.; and Margason, Richard J.: Pressure Distribution on a Vectored-Thrust V/STOL Fighter in the Transition-Speed Range. NASA TM X-2867, 1974.

10. Callaghan, Edmund E.; and Ruggeri, Robert S.: Investigation of the Penetration of an Air Jet Directed Perpendicularly to an Air Stream. NACA TN 1615, 1948.

11. Ruggeri, Robert S.; Callaghan, Edmund E.; and Bowden, Dean T.: Penetration of Air Jets Issuing from Circular, Square, and Elliptical Orifices Directed Perpendicularly to an Air Stream. NACA TN 2019, 1950.

12. Jordinson, R.: Flow in a Jet Directed Normal to the Wind. R. & M. No. 3074, Brit. A.R.C., 1958.

13. Keffer, J. F.; and Baines, W. D.: The Round Turbulent Jet in a Cross-Wind. J. Fluid Mech., vol. 15, pt. 4, Apr. 1963, pp. 481-497.

14. Margason, Richard J.: The Path of a Jet Directed at Large Angles to a Subsonic Free Stream. NASA TN D-4919, 1968.

15. Thompson, A. M.: The Flow Induced by Jets Exhausting Normally From a Plane Wall Into an Airstream. Ph. D. Thesis, Univ. of London, 1971.

16. Kamotani, Yasuhiro, and Greber, Isaac.: Experiments on a Turbulent Jet in a Cross Flow. AIAA J., vol. 10, no. 11, Nov. 1972, pp. 1425-1429.

17. Vogler, Raymond D.: Surface Pressure Distribution Induced on a Flat Plate by a Cold Air Jet Issuing Perpendicularly From the Plate and Normal to a Low-Speed Free-Stream Flow. NASA TN D-1629, 1963.

18. Bradbury, L. J. S.; and Wood, M. N.: The Static Pressure Distribution Around a Circular Jet Exhausting Normally From a Plane Wall Into an Airstream. C.P. No. 822, Brit. A.R.C., 1965.

19. Gelb, G. H.; and Martin, W. A.: An Experimental Investigation of the Flow Field About a Subsonic Jet Exhausting Into a Quiescent and a Low Velocity Air Stream. Can. Aeronaut. & Space J., vol. 12, no. 8, Oct. 1966, pp. 333-342.

20. Wu, J. C.; McMahon, H. M.; Mosher, D. K.; and Wright, M. A.: Experimental and Analytical Investigations of Jets Exhausting Into a Deflecting Stream. J. Aircraft, vol. 7, no. 1, Jan.-Feb. 1970, pp. 44-51.

21. Soullier, A.: Testing at S1.MA for Basic Investigations on Jet Interactions. Distribution of Pressures and Velocities in the Jet Using the Ideal Standard Nozzle (in Unheated State). NASA TT F-14072, 1972.

22. Soullier, A.: Testing at S1.MA for Basic Investigations on Jet Interactions Distribution of Pressures Around the Jet Orifice. NASA TT F-14066, 1972.

23. Ousterhout, Donald S.: An Experimental Investigation of a Cold Jet Emitting From a Body of Revolution Into a Subsonic Free Stream. NASA CR-2089, 1972.

24. Harms, L.: Experimental Investigation of the Flow Field of a Hot Turbulent Jet With Lateral Flow. Part II. NASA TT F-15706, 1974.

25. Fearn, Richard; and Weston, Robert P.: Vorticity Associated With a Jet in a Cross Flow. AIAA J., vol. 12, no. 12, Dec. 1974, pp. 1666-1671.

26. Margason, Richard J.; and Fearn, Richard: Jet-Wake Characteristics and Their Induced Aerodynamic Effects on V/STOL Aircraft in Transition Flight. Analysis of a Jet in a Subsonic Crosswind, NASA SP-218, 1969, pp. 1-18.

27. Smith, Richard H.; and Wang, Chi-Teh: Contracting Cones Giving Uniform Throat Speed. Jour. Aero. Sci., vol. 11, no. 4, Oct. 1944, pp. 356-360.

28. Mosher, David Kenneth: An Experimental Investigation of a Turbulent Jet in a Cross Flow. Ph. D. Thesis, Georgia Inst. Technol., 1970.

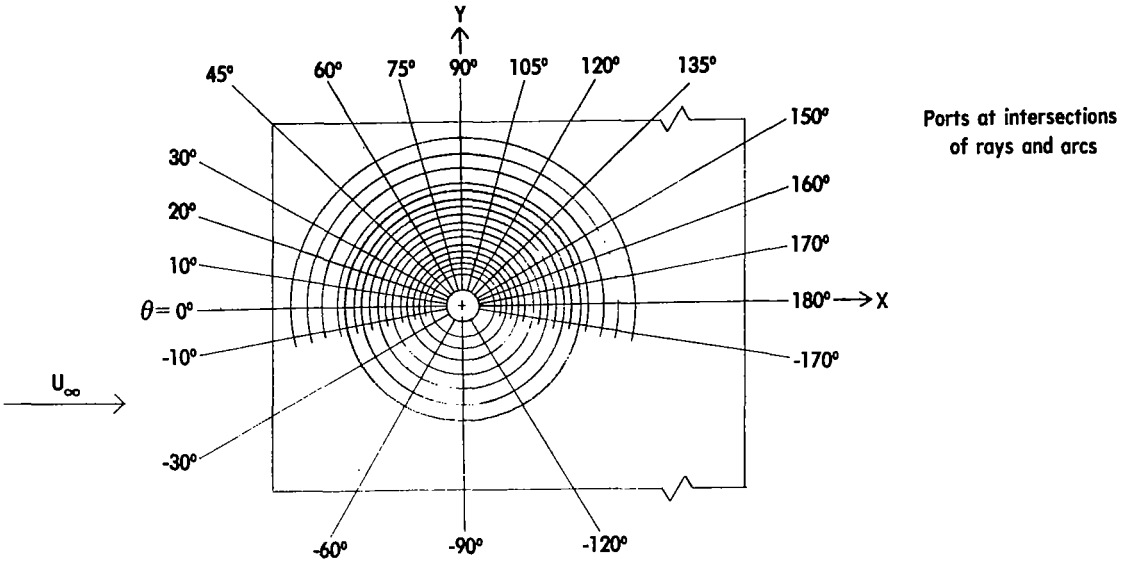

(a) Pressure-port layout for $r/D \geq 1$.

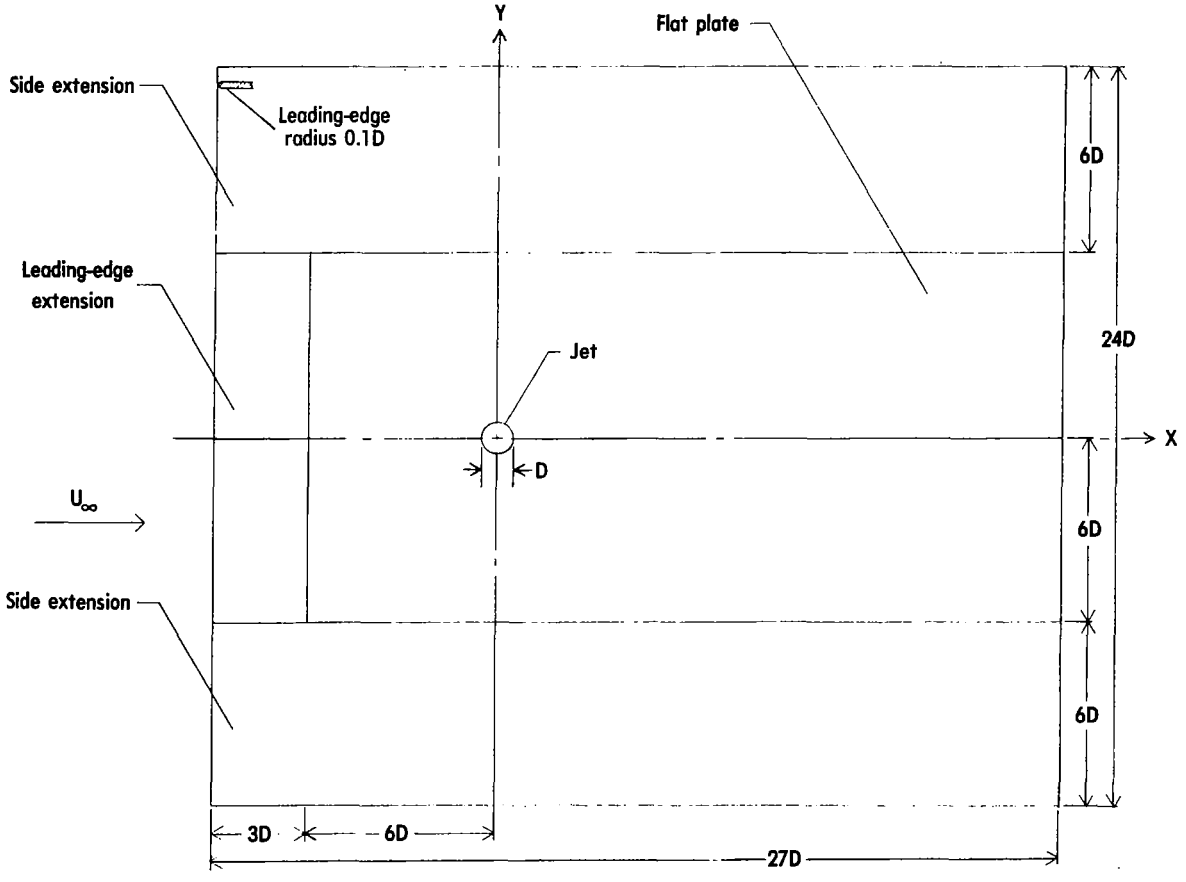

(b) Original flat plate and extensions.

Figure 1.- Pressure-port locations and details of the flat plate.

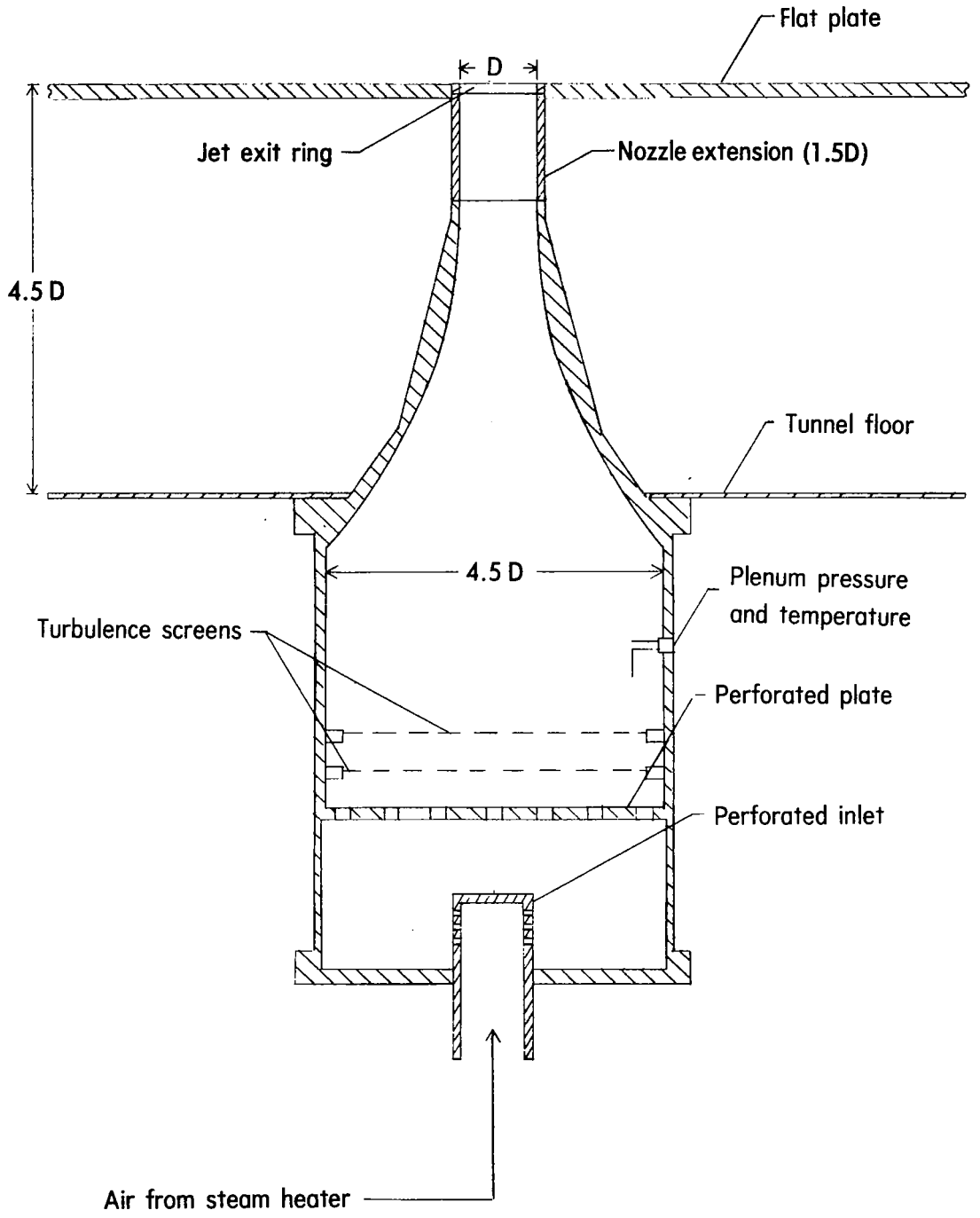

Figure 2.- Jet nozzle and plenum for plate 4.5D above tunnel floor.
D = 10.16 cm (4.0 in.).

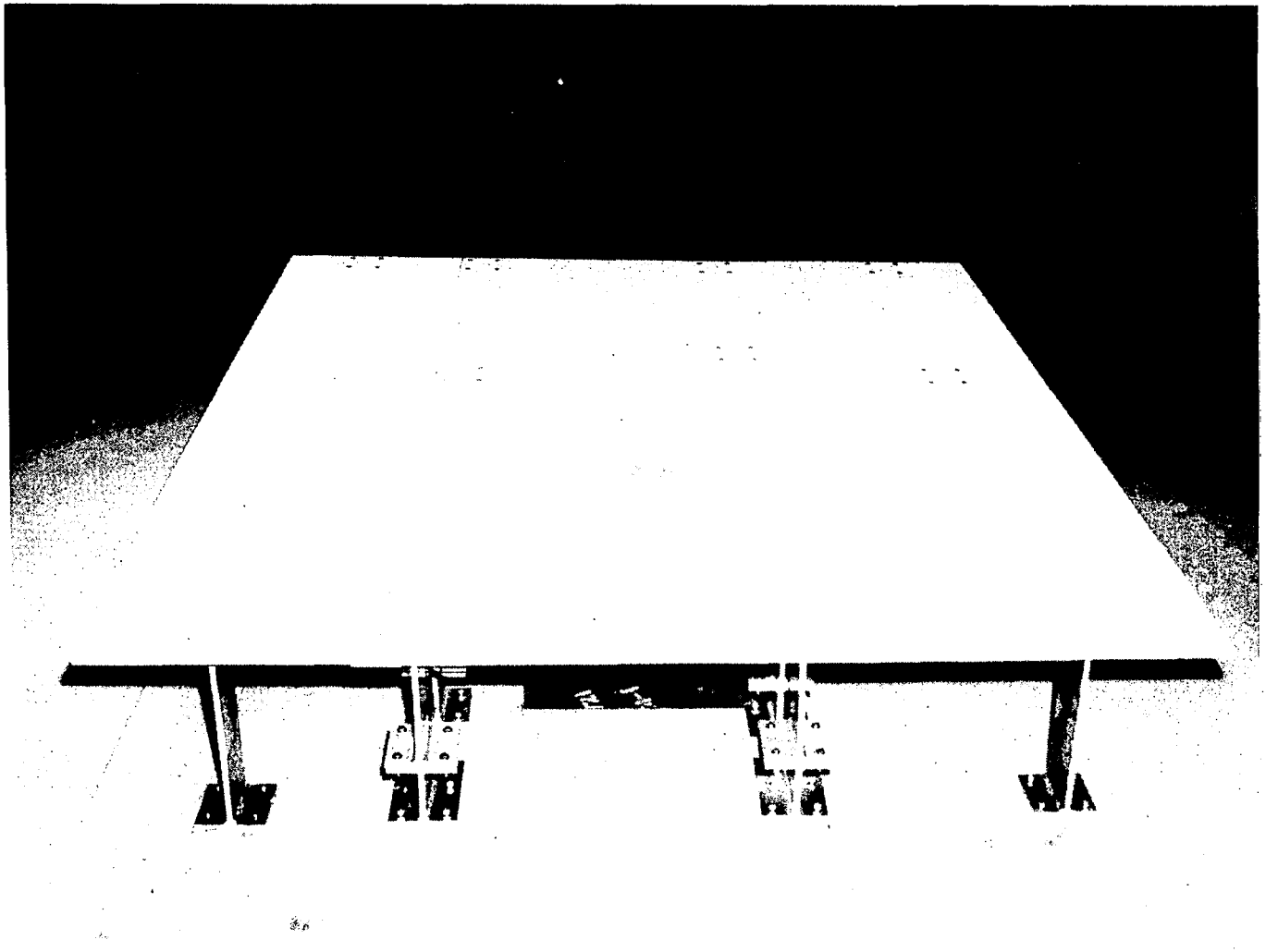

L-72-4893

Figure 3.- View of flat plate in V/STOL tunnel showing jet orifice.

θ (deg) \ r/D	.58	.62	.66	.70	.75	.80	.90	1.00	1.20	1.40	1.60	1.80	2.00
0	.72	.68	.56	.49	.51	.52	.48	.46	.36	.30	.26	.22	.19
10	.57	.60	.51	.47	.48	.48	.45	.42	.34	.28	.25	.22	.19
20	.52	.46	.40	.39	.38	.40	.41	.37	.31	.26	.22	.20	.17
30	.34	.30	.24	.23	.27	.28	.30	.29	.25	.20	.19	.17	.15
45	-.12	-.11	-.07	-.07	-.04	.01	.09	.09	.14	.14	.14	.10	.11
60	-.57	-.60	-.60	-.55	-.41	-.30	-.21	-.10	-.03	.01	.03	.03	.04
75	-1.33	-1.44	-1.15	-1.33	-.87	-.75	-.54	-.38	-.21	-.12	-.08	-.06	-.03
90	-2.44	-2.12	-1.89	-1.62	-1.36	-1.15	-.89	-.65	-.40	-.30	-.20	-.14	-.13
105	-2.72	-2.51	-2.08	-1.91	-1.53	-1.50	-1.20	-.84	-.58	-.44	-.35	-.27	-.22
120	-2.64	-1.75	-1.46	-1.86	-1.40	-1.43	-1.05	-1.01	-.77	-.57	-.46	-.41	-.33
135	-1.89	-1.84	-1.77	-1.53	-1.17	-1.32	-1.22	-.86	-.83	-.71	-.72	-.47	-.48
150	-1.70	-1.40	-1.24	-1.15	-1.16	-1.16	-.93	-.83	-.96	-.73	-.68	-.53	-.55
160	-1.60	-1.39	-1.21	-1.30	-1.07	-1.25	-.92	-.83	-.83	-.72	-.65	-.58	-.48
170	-1.74	-1.74	-1.33	-1.18	-1.15	-1.12	-.95	-.91	-.80	-.74	-.65	-.62	-.61
180	-1.38	-1.72	-1.57	-1.38	-1.15	-1.18	-1.09	-1.08	-.94	-.87	-.74	-.66	-.53
-170	-1.93	-1.65	-1.74	-1.62	-1.42	-1.42	-1.27	-1.05	-1.04	-.91	-.70	-.78	-.56
-120		-3.92		-2.69		-2.10		-1.31		-.61		-.42	
-90		-2.39		-1.90		-1.29		-.72		-.27		-.13	
-60		-.57		-.37		-.27		-.08		.06		.06	
-30		.44		.32		.35		.33		.24		.20	
-10	.71	.66	.54	.48	.49	.49	.49	.45	.36	.30	.25	.22	.20

θ (deg) \ r/D	2.25	2.50	2.75	3.00	3.25	3.50	3.75	4.00	4.50	5.00	5.50	6.00	7.00
0	.16	.14	.12	.11	.10	.10	.09	.06	.06	.06	.04		
10	.16	.15	.12	.11	.10	.08	.08	.08	.06	.05	.05		
20	.15	.13	.11	.10	.09	.08	.09	.07	.06	.05	.04		
30	.14	.13	.11	.09	.08	.07	.07	.07	.05	.05	.04	.03	
45	.09	.08	.07	.07	.06	.06	.05	.06	.04	.04	.02	.03	-.00
60	.04	.04	.04	.03	.04	.03	.03	.04	.02	.02	.02	.02	
75	-.02	-.01	.00	-.01	-.00	-.00	-.00	.03	.01	.01	.01	.01	
90	-.09	-.09	-.06	-.04	-.04	-.03	-.02	-.03	-.02	-.01	-.01		
105	-.13	-.14	-.11	-.10	-.08	-.07	-.06	-.05	-.03	-.03	-.02	-.02	
120	-.27	-.23	-.19	-.14	-.13	-.11	-.09	-.08	-.06	-.04	-.03	-.02	
135	-.36	-.28	-.23	-.18	-.17	-.15	-.09	-.08	-.06	-.04	-.04	-.02	-.02
150	-.33	-.23	-.24	-.18	-.15	-.11	-.10	-.08	-.03	-.03	-.02		
160	-.36	-.32	-.22	-.15	-.12	-.11	-.04	-.04	-.02	-.01	0.00		
170	-.47	-.39	-.34	-.22	-.15	-.13	-.07	-.05	-.03	-.01	-.02		
180	-.44	-.37	-.23	-.24	-.13	-.15	-.12	-.08	-.04	-.04	-.02	-.02	.00
-170	-.41	-.37	-.29	-.23	-.18	-.13	-.14	-.07	-.03	-.03			
-120	-.29		-.20		-.13		-.13						
-90	-.08		-.05		-.04		-.12						
-60	.06		.05		.04		.01						
-30	.13		.11		.09		.06						
-10	.17	.14	.12	.11	.09	.09	.06	.07	.06	.05			

(a) C_p values.

Figure 4.- Pressure distribution on flat plate. $R = 2.2$; $M_j = 0.39$.

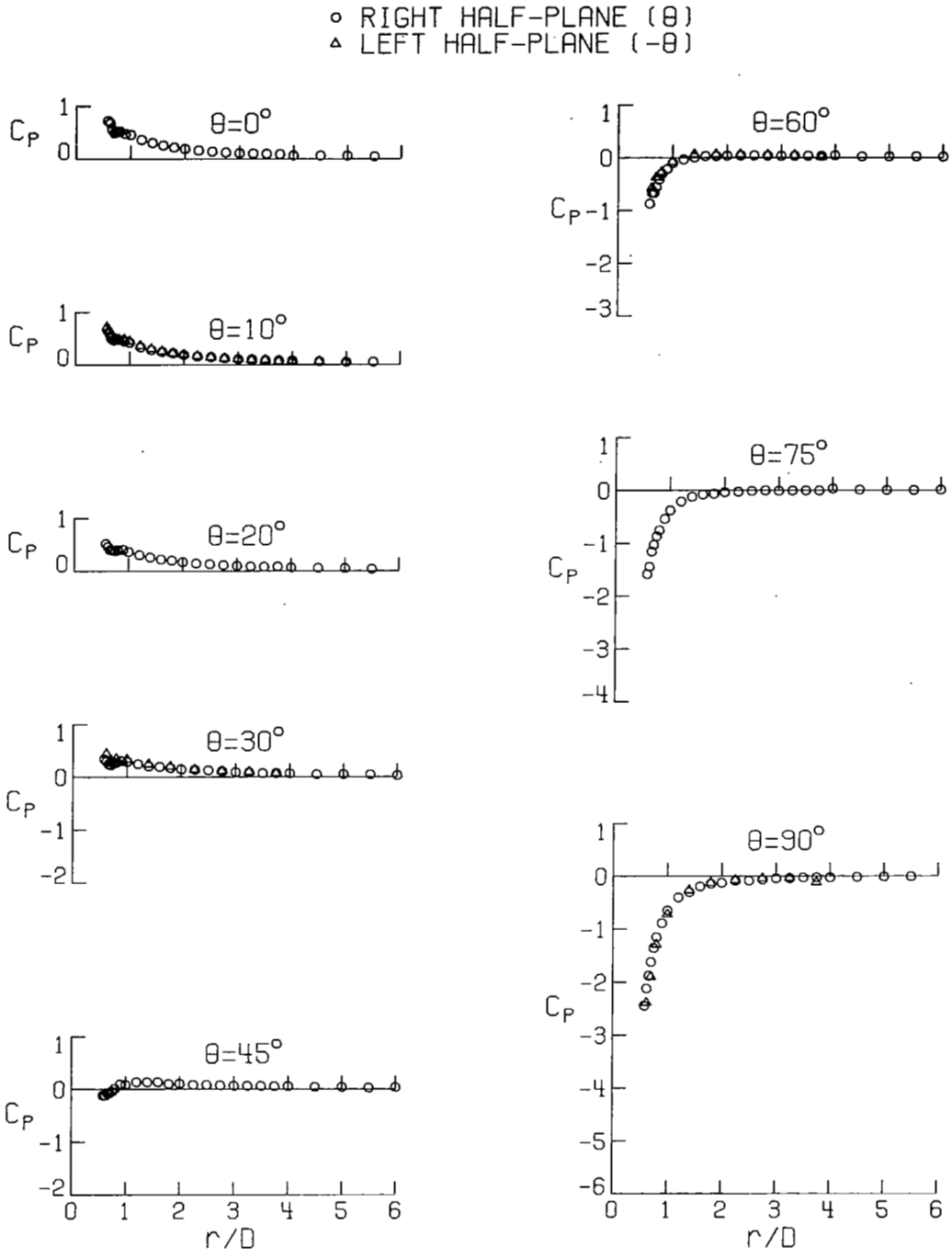

(b) Pressure distribution on rays.

Figure 4.- Continued.

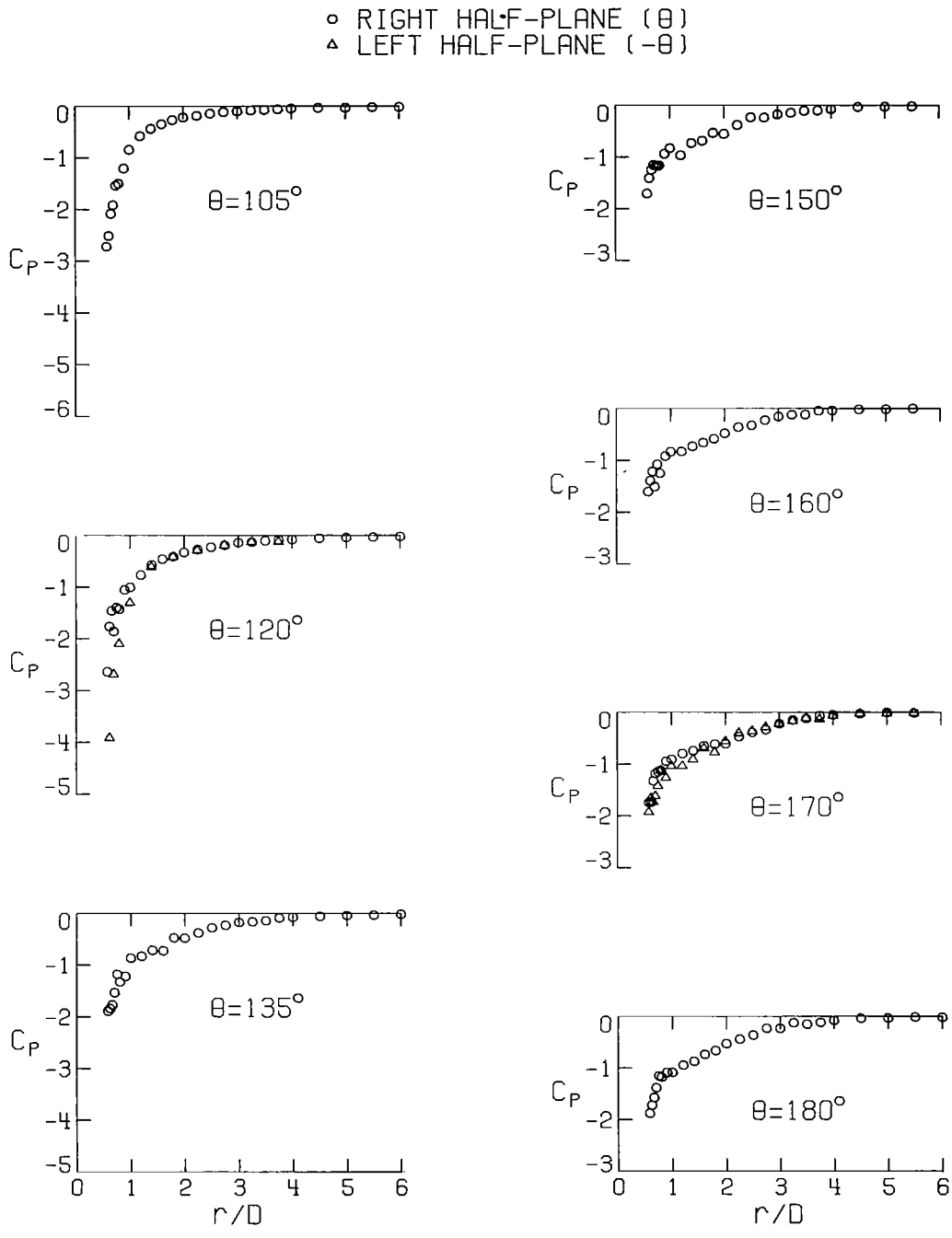

(b) Concluded.

Figure 4.- Continued.

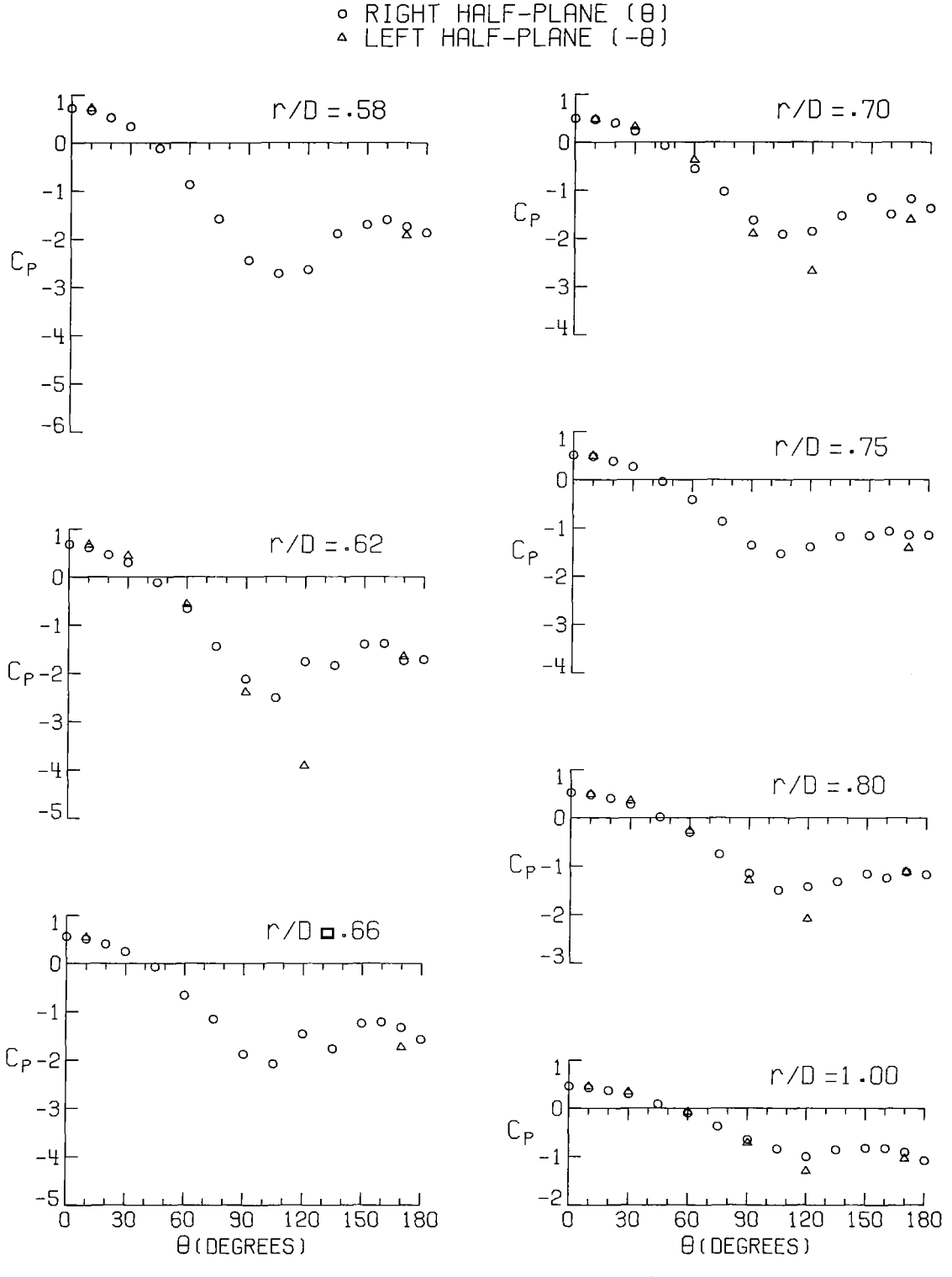

(c) Pressure distribution on circles.

Figure 4.- Continued.

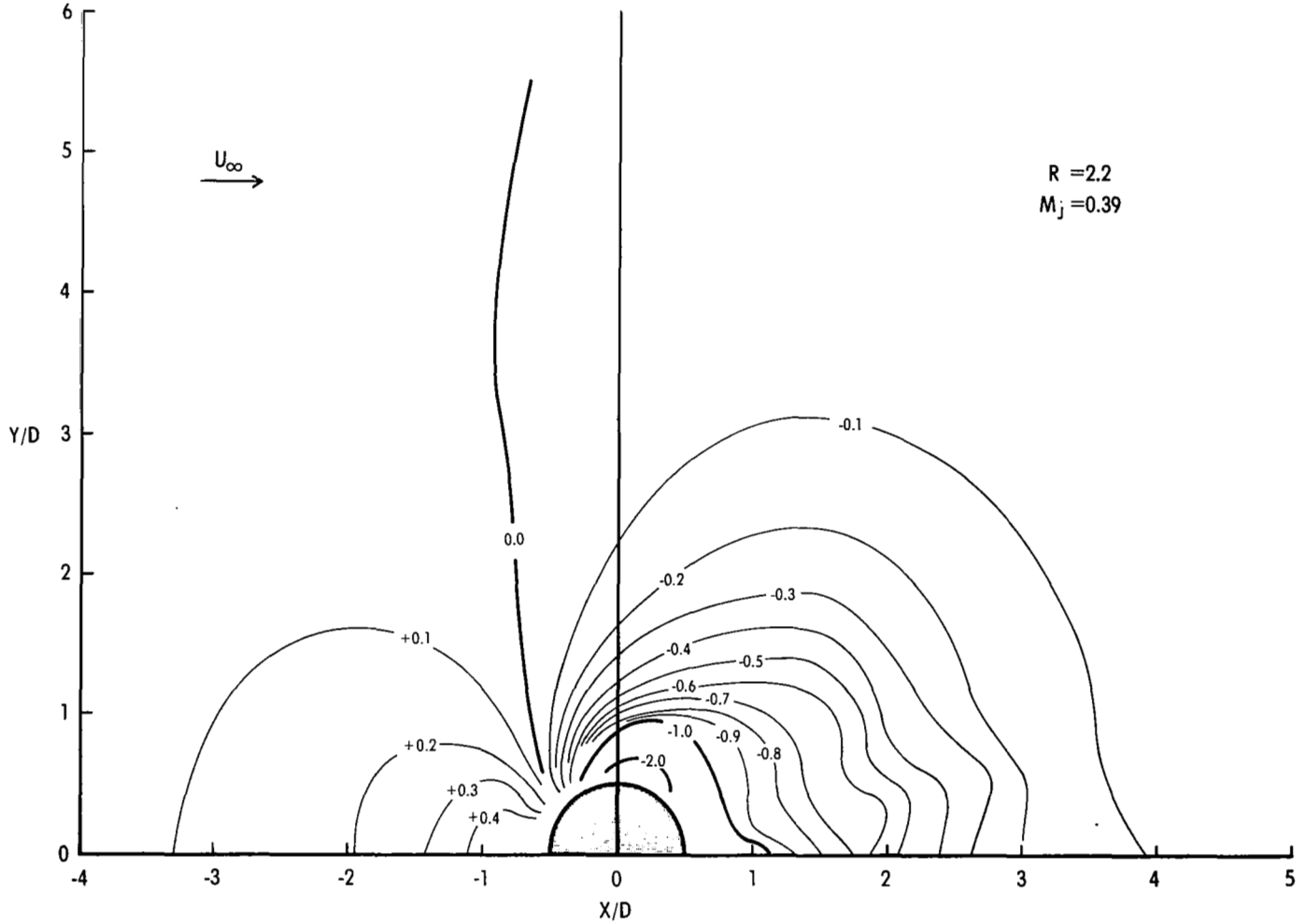

(d) Contours of constant C_p.

Figure 4.- Concluded.

θ (deg) \ r/D	.58	.62	.66	.70	.75	.80	.90	1.00	1.20	1.40	1.60	1.80	2.00
0	.60	.54	.49	.48	.49	.48	.43	.39	.32	.25	.22	.19	.16
10	.60	.53	.45	.45	.44	.46	.41	.37	.30	.24	.22	.18	.17
20	.44	.35	.30	.35	.34	.33	.32	.31	.24	.21	.18	.14	.14
30	.13	.10	.11	.15	.17	.17	.18	.20	.18	.15	.13	.13	.11
45	-.52	-.41	-.37	-.31	-.22	-.16	-.05	-.01	.03	.04	.05	.04	.05
60	-1.51	-1.31	-1.05	-.97	-.73	-.64	-.43	-.31	-.18	-.11	-.06	-.06	-.04
75	-2.46	-2.08	-1.84	-1.61	-1.38	-1.17	-.89	-.65	-.44	-.31	-.20	-.16	-.14
90	-3.53	-3.12	-2.72	-2.47	-2.04	-1.72	-1.35	-1.05	-.67	-.50	-.37	-.30	-.24
105	-3.94	-3.54	-3.17	-2.96	-2.58	-2.15	-1.60	-1.39	-.98	-.68	-.55	-.44	-.36
120	-3.59	-3.52	-3.23	-2.89	-2.74	-2.28	-2.11	-1.61	-1.11	-.92	-.71	-.57	-.53
135	-3.29	-2.59	-2.86	-2.47	-2.27	-2.11	-1.57	-1.50	-1.29	-.99	-.86	-.70	-.57
150	-2.41	-2.47	-2.13	-1.81	-1.68	-1.79	-1.39	-1.04	-1.01	-.92	-.67	-.74	-.55
160	-2.16	-1.94	-1.68	-1.97	-1.53	-1.42	-1.23	-.98	-.81	-.76	-.71	-.58	-.56
170	-1.84	-1.83	-1.67	-1.56	-1.35	-1.21	-.99	-.92	-.76	-.69	-.53	-.56	-.44
180	-1.80	-1.67	-1.68	-1.53	-1.47	-1.31	-1.13	-.93	-.80	-.64	-.68	-.52	-.38
-170	-1.87	-1.98	-1.67	-1.68	-1.43	-1.41	-1.22	-1.04	-.84	-.68	-.67	-.45	-.38
-120		-4.44		-3.46		-2.73		-1.79		-.98		-.65	
-90		-3.43		-2.64		-1.90		-1.07		-.52		-.30	
-60		-1.10		-.81		-.58		-.29		-.10		-.04	
-30		.30		.21		.27		.23		.16		.13	
-10	.60	.54	.49	.47	.46	.46	.41	.37	.31	.26	.21	.18	.16

θ (deg) \ r/D	2.25	2.50	2.75	3.00	3.25	3.50	3.75	4.00	4.50	5.00	5.50	6.00	7.00
0	.14	.12	.10	.08	.09	.07	.06	.04	.05	.04	.02		
10	.12	.12	.10	.08	.08	.07	.05	.05	.04	.04	.04		
20	.12	.09	.08	.07	.07	.06	.05	.05	.03	.04	.02		
30	.10	.08	.08	.06	.06	.05	.04	.05	.03	.02	.03	.00	
45	.04	.04	.05	.03	.02	.02	.02	.01	.02	.01	.02	.00	-.05
60	-.02	-.01	.00	-.00	-.01	-.00	.00	-.00	-.00	-.01	.00	.00	
75	-.09	-.08	-.06	-.05	-.05	-.03	-.03	-.03	-.03	-.02	-.00	-.02	
90	-.14	-.13	-.13	-.11	-.10	-.04	-.07	-.06	-.05	-.04	-.04		
105	-.24	-.23	-.19	-.17	-.15	-.13	-.11	-.10	-.08	-.06	-.05	-.05	
120	-.40	-.33	-.28	-.23	-.19	-.18	-.15	-.12	-.11	-.09	-.06	-.06	
135	-.47	-.41	-.31	-.29	-.24	-.20	-.18	-.16	-.12	-.09	-.08	-.07	-.04
150	-.48	-.41	-.33	-.28	-.22	-.22	-.17	-.13	-.11	-.08	-.07		
160	-.32	-.35	-.23	-.20	-.16	-.12	-.11	-.10	-.06	-.05	-.04		
170	-.38	-.32	-.26	-.18	-.09	-.09	-.10	-.08	-.04	-.02	-.02		
180	-.33	-.28	-.35	-.16	-.11	-.16	-.11	-.04	-.05	-.01	-.02	.00	-.02
-170	-.40	-.31	-.19	-.17	-.15	-.08	-.09	-.05	-.03	-.02			
-120	-.41		-.29		-.20		-.11						
-90	-.19		-.12		-.09		-.07						
-60	-.02		-.00		-.00		-.02						
-30	.10		.07		.06		.03						
-10	.15	.12	.10	.09	.07	.07	.04	.05	.05	.02			

(a) C_p values.

Figure 5.- Pressure distribution on flat plate. R = 2.8; M_j = 0.44.

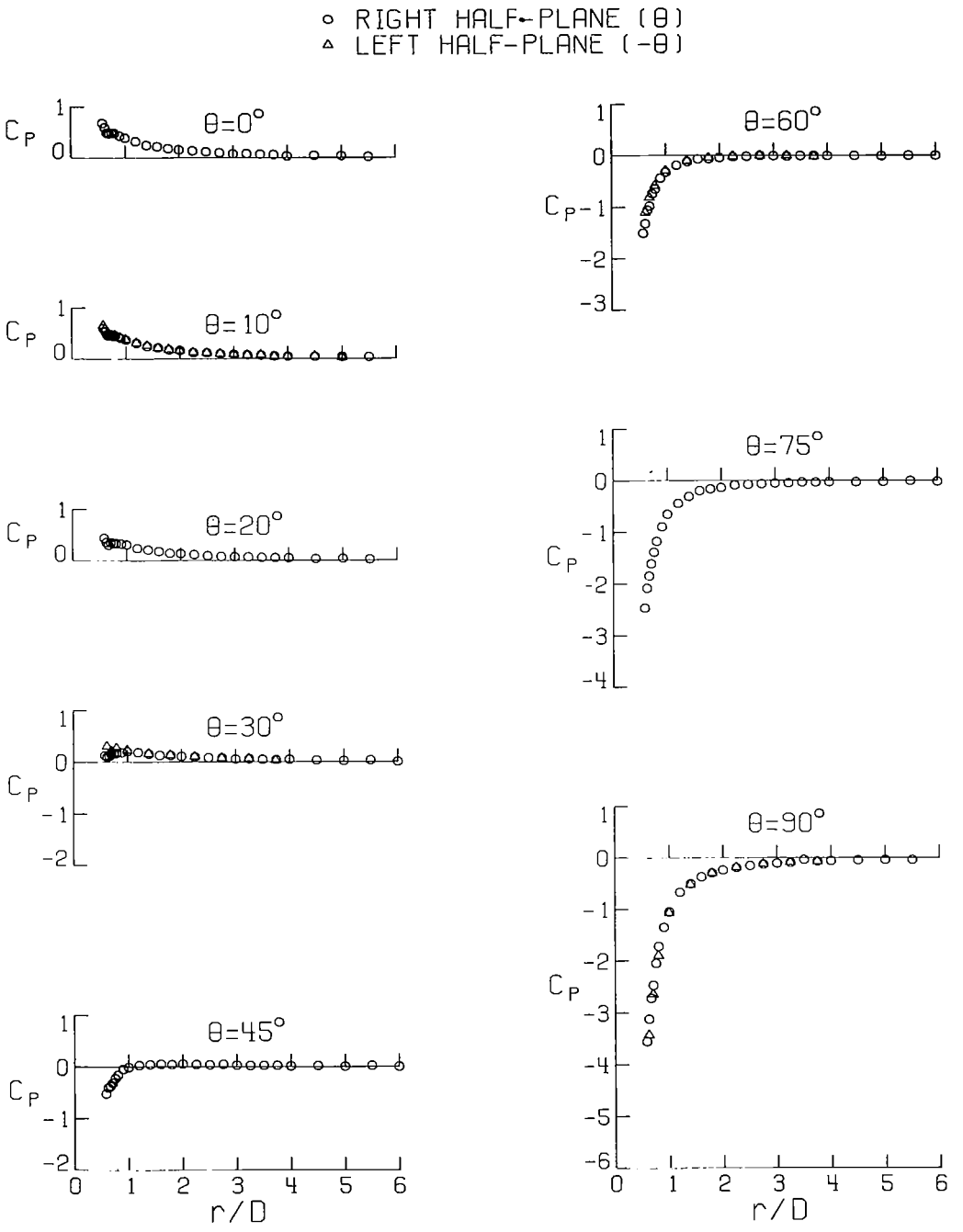

(b) Pressure distribution on rays.

Figure 5.- Continued.

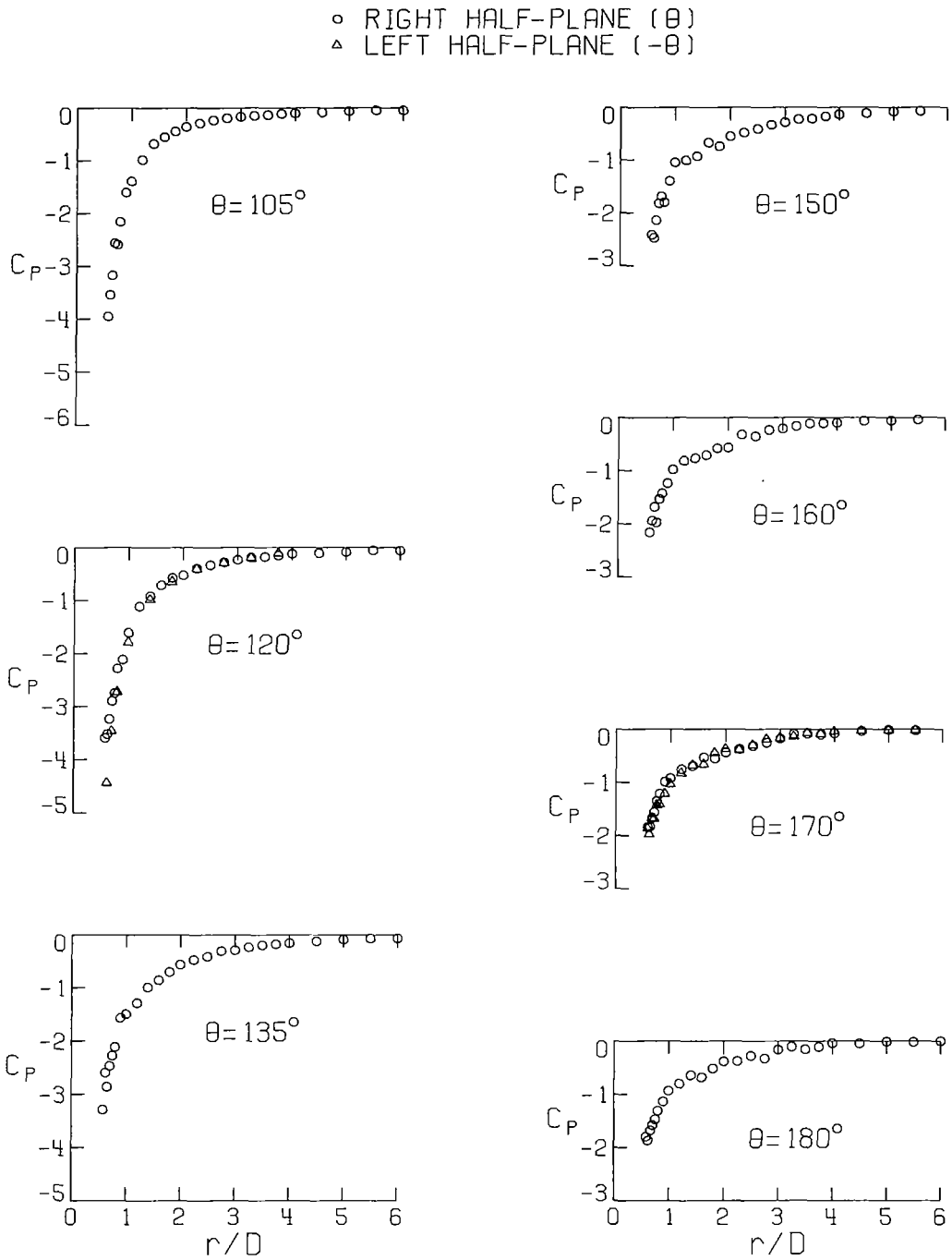

(b) Concluded.

Figure 5.- Continued.

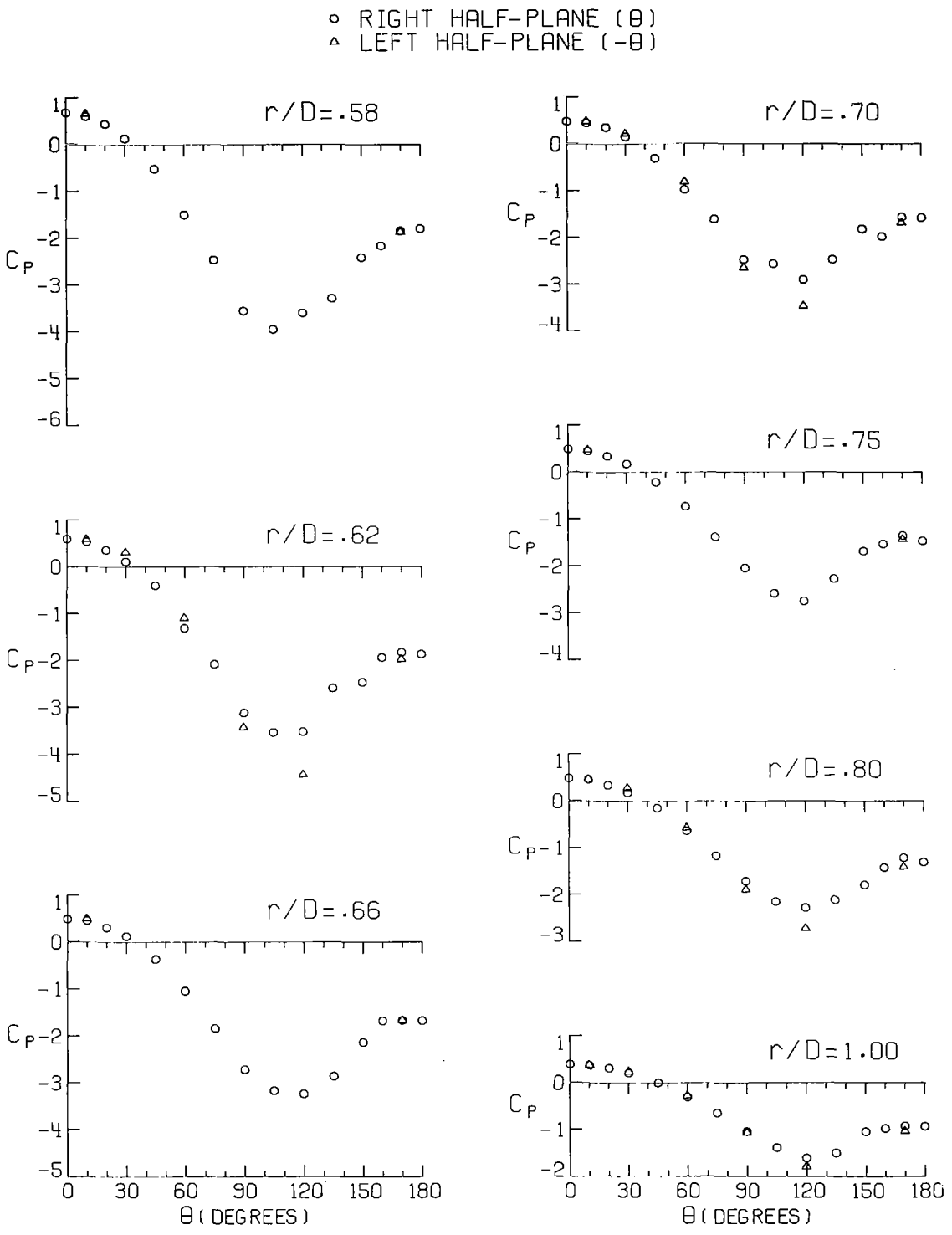

(c) Pressure distribution on circles.

Figure 5.- Continued.

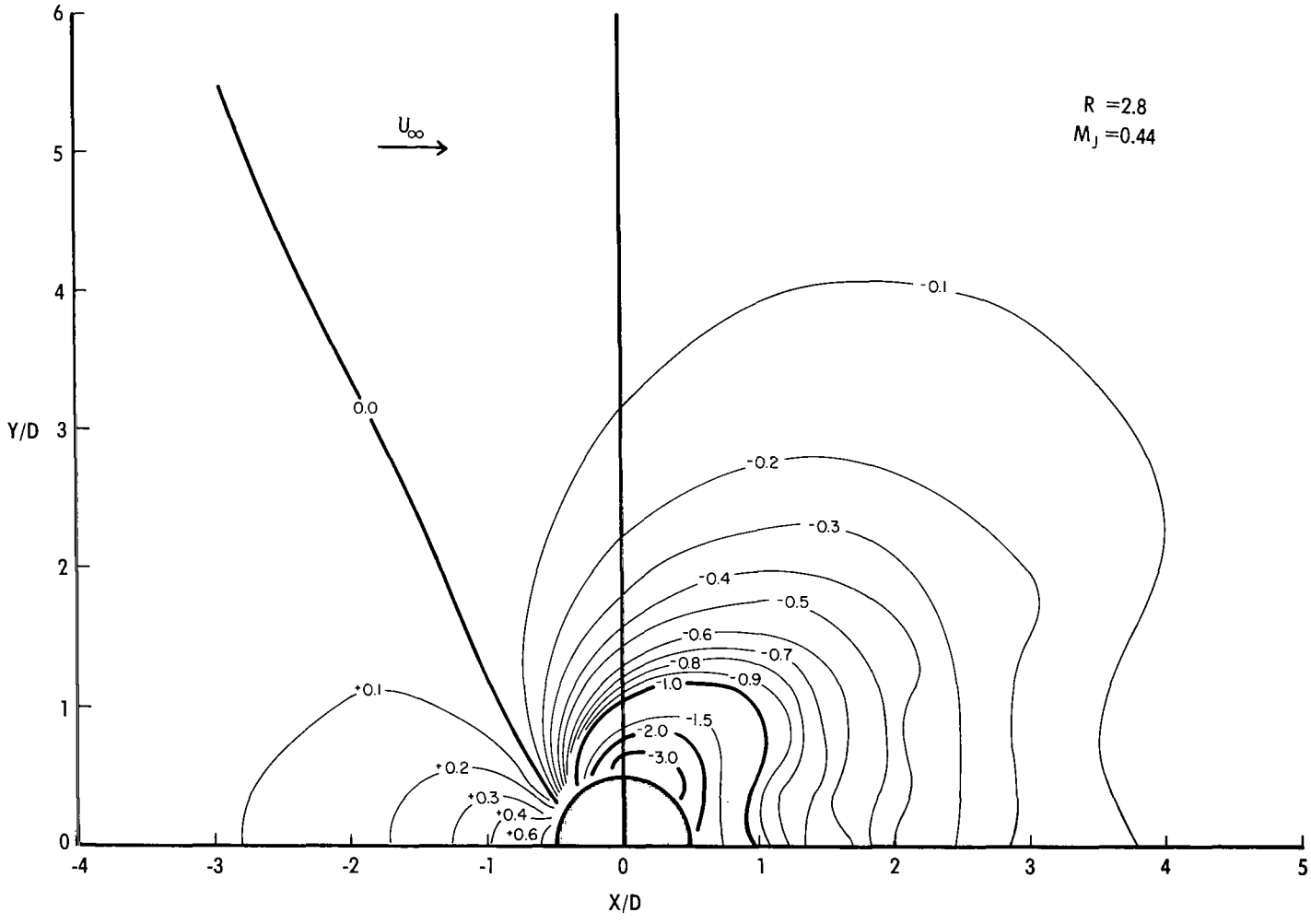

(d) Contours of constant C_p.

Figure 5.- Concluded.

θ (deg) \ r/D	.58	.62	.66	.70	.75	.80	.90	1.00	1.20	1.40	1.60	1.80	2.00
0	.71	.60	.51	.49	.49	.47	.40	.33	.26	.21	.16	.14	.12
10	.59	.47	.40	.42	.40	.40	.35	.28	.22	.18	.14	.13	.11
20	.33	.27	.20	.23	.25	.28	.24	.23	.18	.12	.12	.09	.09
30	-.03	-.10	-.04	-.03	.00	.02	.05	.07	.07	.05	.06	.05	.05
45	-1.03	-.87	-.74	-.60	-.54	-.43	-.31	-.26	-.16	-.11	-.06	-.06	-.03
60	-2.21	-1.95	-1.69	-1.52	-1.23	-1.00	-.84	-.65	-.43	-.32	-.24	-.18	-.14
75	-3.03	-2.92	-2.56	-2.27	-1.88	-1.76	-1.35	-1.10	-.76	-.55	-.41	-.34	-.28
90	-4.17	-3.81	-3.21	-3.00	-2.51		-1.77	-1.50	-1.08	-.82	-.60	-.49	-.41
105	-4.32	-3.86	-3.44	-3.23	-2.94		-2.03	-1.79	-1.26	-.98	-.77	-.61	-.50
120	-3.64	-3.39	-3.17	-2.95	-2.75		-2.01	-1.85	-1.39	-1.12	-.84	-.73	-.60
135	-3.04	-2.78	-2.90	-2.40	-2.47		-1.95	-1.62	-1.24	-.96	-.76	-.65	-.56
150	-2.77	-2.54	-2.55	-2.31	-2.24	-2.00	-1.80	-1.47	-1.20	-.91	-.69	-.63	-.54
160	-2.69	-2.50	-2.49	-2.25	-2.23	-2.01	-1.80	-1.53	-1.17	-1.00	-.78	-.67	-.58
170	-2.26	-2.43	-2.48	-2.34	-2.22	-2.01	-1.75	-1.37	-1.19	-.88	-.86	-.86	-.61
180	-2.10	-2.23	-2.13	-2.34	-2.08	-1.99	-1.89	-1.46	-1.22	-1.22	-.94	-.82	-.77
-170	-1.98	-2.16	-2.21	-2.26	-2.38	-2.01	-1.77	-1.54	-1.31	-1.05	-.78	-.71	-.76
-120		-3.24		-2.85		-2.03		-1.67		-1.07		-.66	
-90		-4.02		-3.22		-2.03		-1.50		-.84		-.51	
-60		-1.66		-1.26		-.98		-.59		-.31		-.18	
-30		.11		.06		.13		.12		.08		.06	
-10	.70	.54	.49	.44	.47	.43	.38	.32	.25	.19	.15	.12	.12

θ (deg) \ r/D	2.25	2.50	2.75	3.00	3.25	3.50	3.75	4.00	4.50	5.00	5.50	6.00	7.00
0	.10	.07	.07	.07	.06	.06	.05	.05	.03	.04	.04		
10	.10	.07	.08	.06	.06	.06	.04	.05	.03	.04	.03		
20	.08	.06	.06	.05	.05	.05	.04	.04	.02	.03	.02		
30	.04	.04	.05	.03	.04	.04	.02	.03	.01	.02	.02	.03	
45	-.02	-.03	-.01	-.01	.00	.01	.01	.02	-.01	-.00	.01	-.00	-.01
60	-.11	-.08	-.07	-.07	-.05	-.04	-.03	-.01	-.02	-.02	-.01	-.02	
75	-.22	-.18	-.13	-.13	-.10	-.08	-.06	-.04	-.05	-.03	-.03	-.03	
90	-.31	-.27	-.21	-.19	-.15	-.11	-.13	-.08	-.06	-.07	-.05		
105	-.43	-.36	-.29	-.24	-.22	-.18	-.15	-.13	-.06	-.08	-.07	-.07	
120	-.49	-.37	-.32	-.28	-.24	-.20	-.18	-.15	-.14	-.09	-.08	-.07	
135	-.46	-.37	-.32	-.30	-.22	-.19	-.19	-.13	-.13	-.09	-.08	-.08	-.05
150	-.44	-.35	-.26	-.24	-.20	-.14	-.16	-.10	-.10	-.06	-.04		
160	-.46	-.37	-.33	-.22	-.23	-.15	-.15	-.09	-.09	-.03	-.05		
170	-.55	-.56	-.37	-.39	-.27	-.33	-.26	-.23	-.17	-.14	-.16		
180	-.74	-.55	-.47	-.50	-.42	-.43	-.43	-.31	-.35	-.30	-.33	-.30	-.12
-170	-.64	-.56	-.48	-.41	-.39	-.32	-.29	-.24	-.18	-.15			
-120	-.48		-.32		-.24		-.20						
-90	-.34		-.22		-.15		-.12						
-60	-.12		-.07		-.05		-.04						
-30	.04		.05		.03		.02						
-10	.08	.08	.07	.06	.06	.04	.06	.04	.02	.05			

(a) C_p values.

Figure 6.- Pressure distribution on flat plate. R = 3.9; M_j = 0.75.

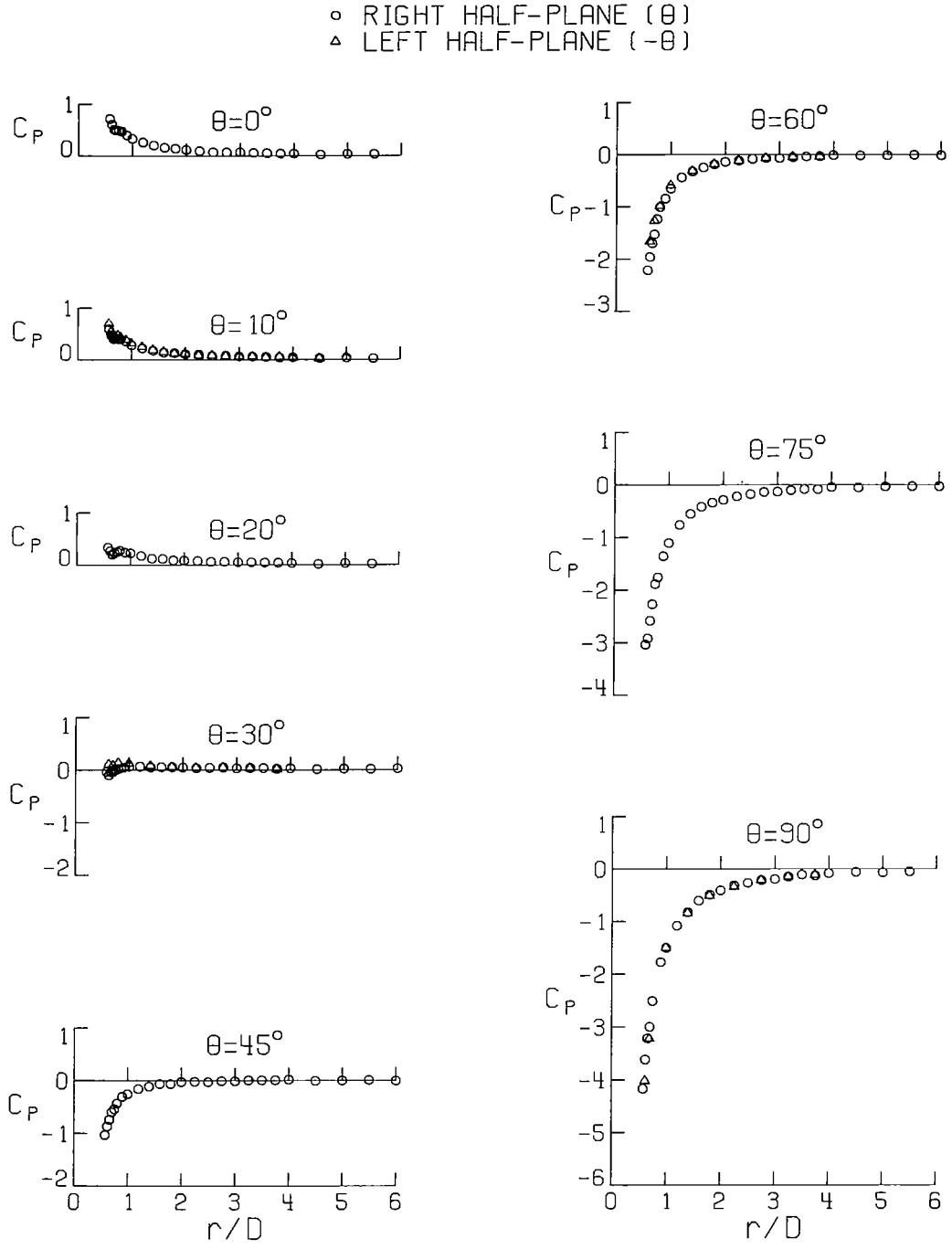

(b) Pressure distribution on rays.

Figure 6.- Continued.

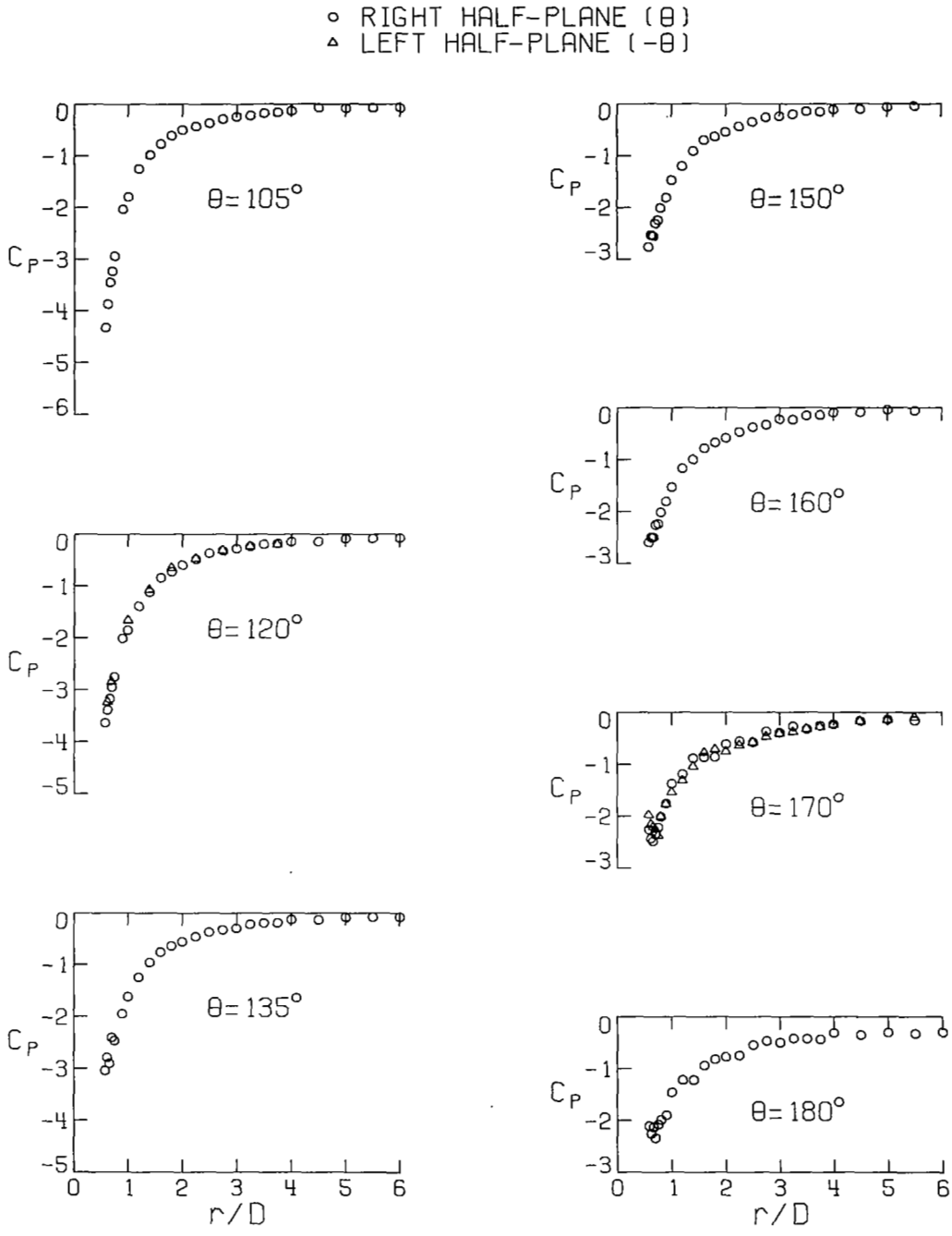

(b) Concluded.

Figure 6.- Continued.

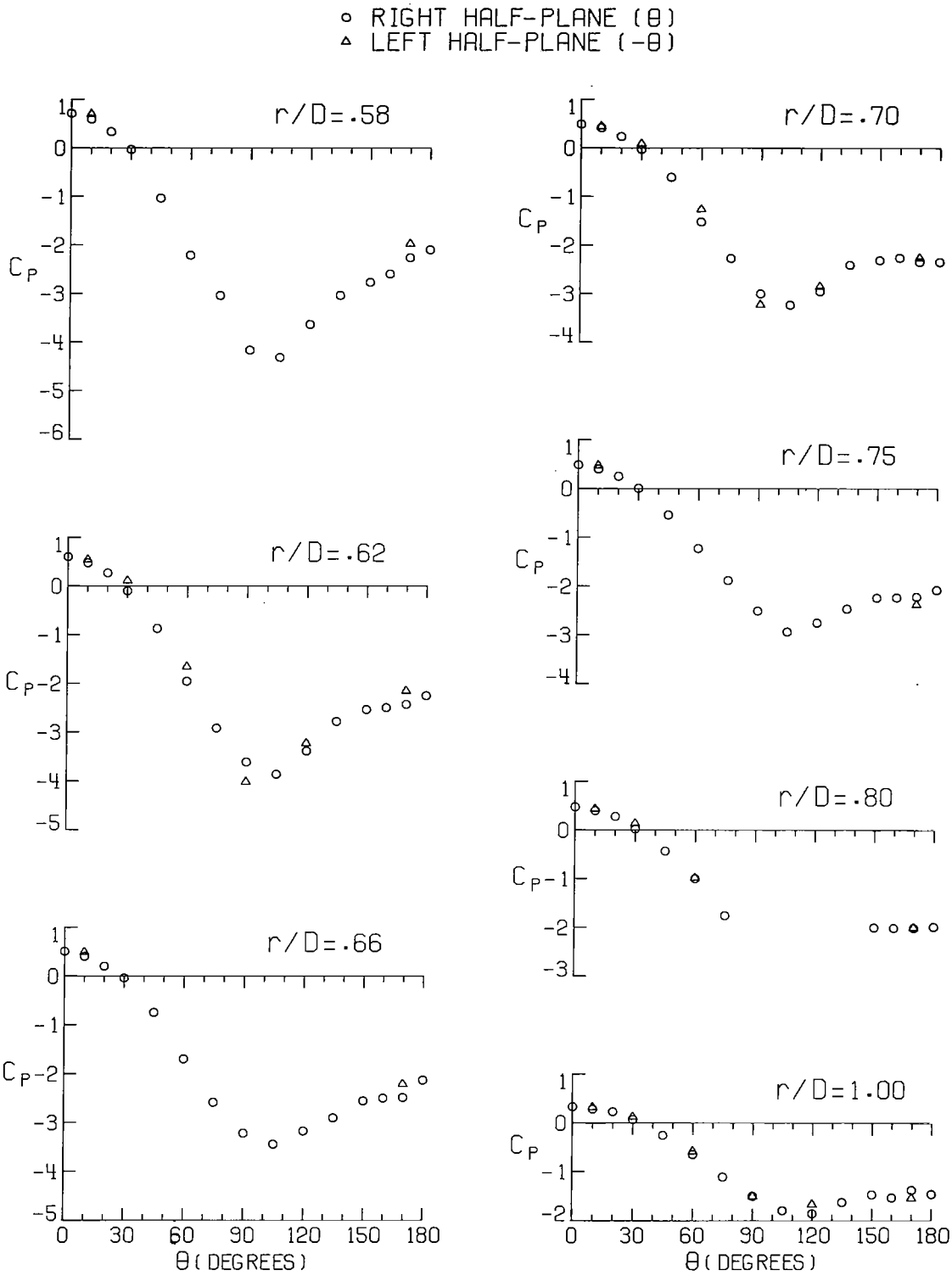

(c) Pressure distribution on circles.

Figure 6.- Continued.

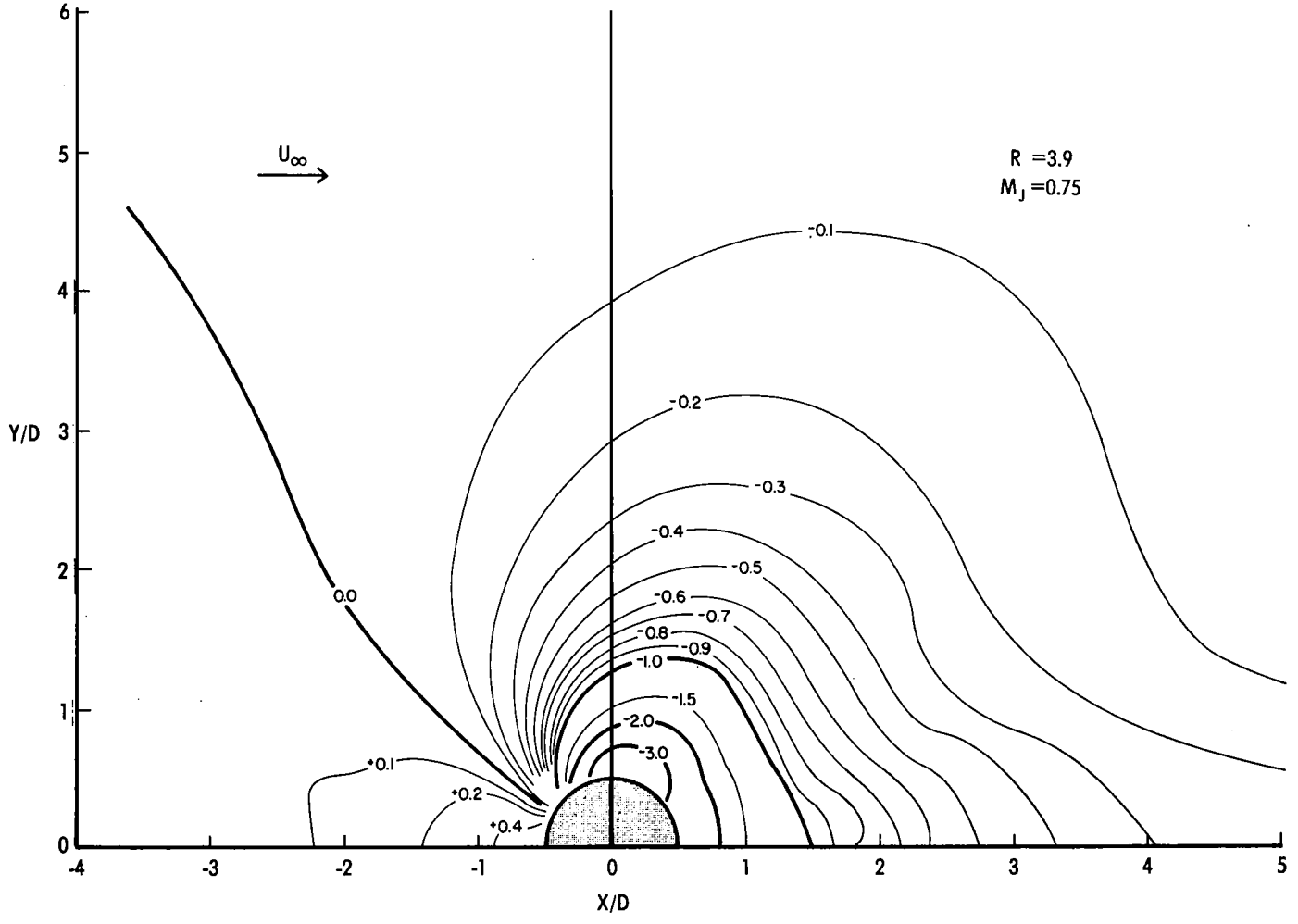

(d) Contours of constant C_p.

Figure 6.- Concluded.

θ (deg) \ r/D	.55	.62	.66	.70	.75	.80	.90	1.00	1.20	1.40	1.60	1.80	2.00
0	.57	.51	.48	.47	.45	.40	.32	.26	.18	.13	.08	.07	.05
10	.51	.42	.36	.36	.37	.34	.28	.22	.15	.09	.07	.05	.04
20	.15	.15	.13	.12	.16	.15	.13	.09	.07	.04	.02	.02	.01
30	-.34	-.32	-.28	-.20	-.13	-.13	-.08	-.07	-.07	-.07	-.06	-.05	-.03
45	-1.51	-1.34	-1.09	-.99	-.87	-.72	-.54	-.48	-.34	-.26	-.22	-.18	-.16
60	-2.37	-2.50	-2.25	-1.84	-1.60	-1.48	-1.16	-.95	-.71	-.53	-.45	-.32	-.29
75	-3.69	-3.24	-3.03	-2.82	-2.35	-2.11	-1.63	-1.46	-1.05	-.81	-.65	-.54	-.46
90	-4.35	-3.91	-3.61	-3.41	-2.81	-2.20	-2.14	-1.82	-1.36	-1.07	-.86	-.67	-.59
105	-4.03	-3.66	-3.43	-3.20	-2.67	-2.20	-2.10	-1.82	-1.50	-1.20	-.97	-.75	-.74
120	-3.25	-2.87	-2.75	-2.37	-2.52	-2.07	-1.86	-1.78	-1.28	-1.06	-.93	-.77	-.66
135	-2.36	-2.54	-2.42	-2.22	-2.02	-1.81	-1.62	-1.47	-1.05	-.91	-.72	-.63	-.48
150	-2.14	-2.07	-2.12	-2.10	-1.90	-1.67	-1.46	-1.30	-1.01	-.82	-.68	-.50	-.37
160	-1.87	-2.03	-2.03	-1.88	-1.81	-1.74	-1.50	-1.30	-.99	-.73	-.58	-.51	-.44
170	-1.57	-1.69	-1.84	-1.83	-1.77	-1.68	-1.43	-1.22	-1.01	-.67	-.62	-.48	-.39
180	-1.56	-1.62	-1.72	-1.95	-1.74	-1.67	-1.32	-1.17	-.92	-.83	-.71	-.52	-.51
-170	-1.52	-1.62	-1.77	-1.82	-1.74	-1.68	-1.41	-1.16	-.90	-.78	-.54	-.52	-.44
-120		-2.96		-2.63		-2.20		-1.77		-1.08		-.75	
-90		-4.22		-3.71		-2.20		-1.96		-1.09		-.70	
-60		-2.25		-1.78		-1.30		-.89		-.51		-.34	
-30		-.08		-.09		.01		-.01		-.05		-.03	
-10	.56	.49	.43	.42	.42	.39	.31	.23	.16	.11	.07	.06	.05

θ (deg) \ r/D	2.25	2.50	2.75	3.00	3.25	3.50	3.75	4.00	4.50	5.00	5.50	6.00	7.00
0	.05	.03	.03	.04	.03	.02	.02	.00	.02	.02	.02		
10	.04	.02	.03	.02	.02	.03	.03	.02	.02	.03	.02		
20	.01	.01	.00	.01	.02	.01	.01	.03	.03	.02	.01		
30	-.04	-.03	-.03	-.01	-.01	-.00	.00	.01	-.00	.00	.00	.01	
45	-.13	-.10	-.09	-.08	-.06	-.05	-.05	-.02	-.02	-.02	-.00	-.01	-.03
60	-.24	-.21	-.17	-.13	-.13	-.10	-.08	-.08	-.03	-.04	-.03	-.02	
75	-.37	-.29	-.25	-.22	-.18	-.16	-.14	-.12	-.05	-.08	-.06	-.05	
90	-.49	-.40	-.33	-.28	-.27	-.22	-.20	-.18	-.13	-.11	-.09		
105	-.53	-.49	-.40	-.36	-.30	-.25	-.25	-.20	-.16	-.13	-.11	-.09	
120	-.54	-.51	-.38	-.35	-.29	-.28	-.24	-.21	-.17	-.14	-.12	-.10	
135	-.45	-.39	-.35	-.30	-.26	-.20	-.18	-.19	-.16	-.11	-.10	-.08	-.06
150	-.33	-.32	-.23	-.19	-.16	-.14	-.12	-.09	-.07	-.06	-.03		
160	-.30	-.29	-.24	-.20	-.15	-.14	-.12	-.11	-.06	-.05	-.04		
170	-.35	-.39	-.38	-.21	-.25	-.23	-.17	-.22	-.18	-.14	-.11		
180	-.40	-.39	-.29	-.40	-.31	-.26	-.26	-.19	-.18	-.23	-.24	-.14	-.08
-170	-.40	-.34	-.31	-.23	-.27	-.30	-.14	-.14	-.09	-.09			
-120	-.56		-.44		-.32		-.25						
-90	-.50		-.36		-.26		-.19						
-60	-.24		-.17		-.13		-.10						
-30	-.02		-.02		-.01		-.03						
-10	.03	.03	.03	.02	.02	.03	.00	.03	.01	.03			

(a) C_p values.

Figure 7.- Pressure distribution on flat plate. R = 5.1; M_j = 0.95.

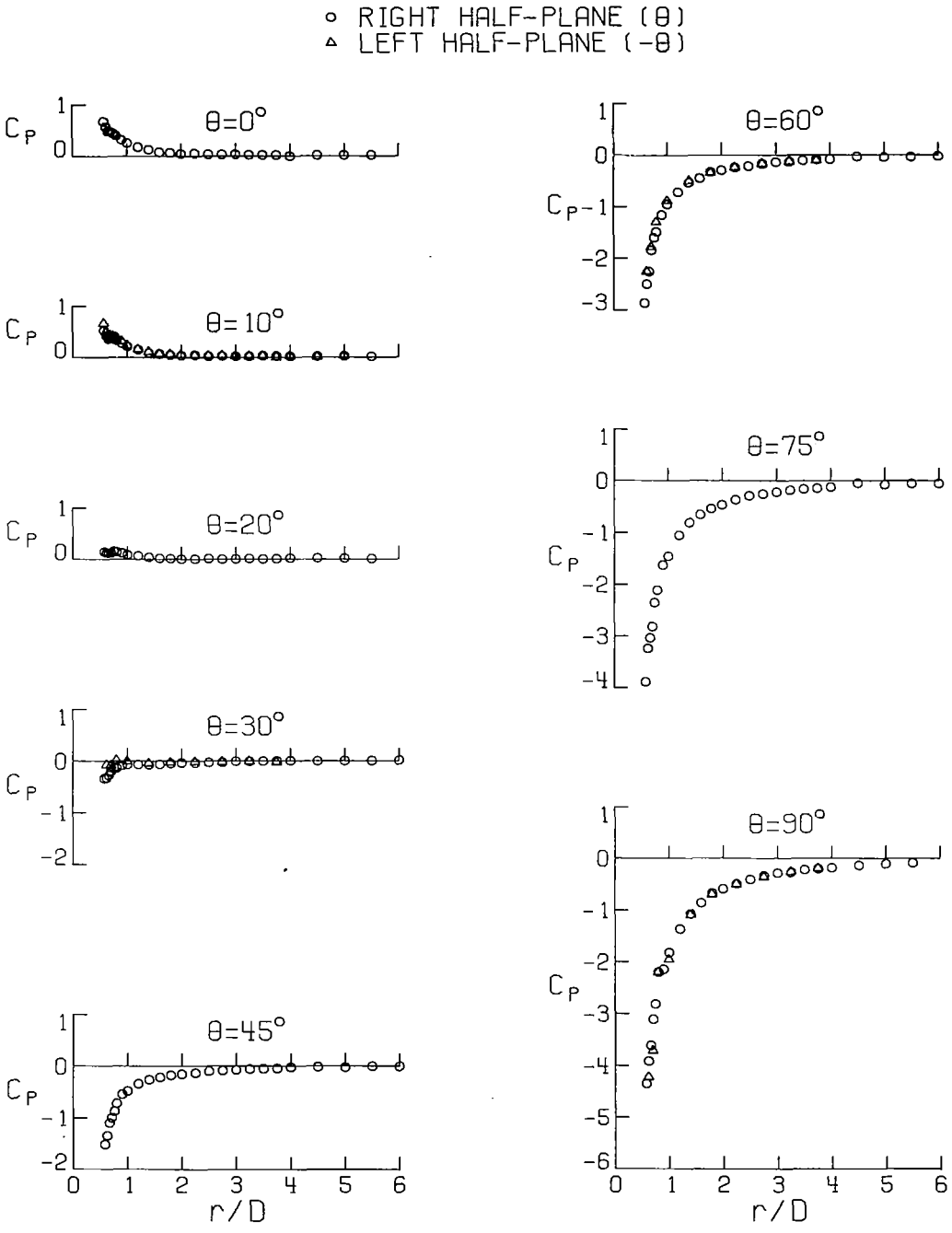

(b) Pressure distribution on rays.

Figure 7.- Continued.

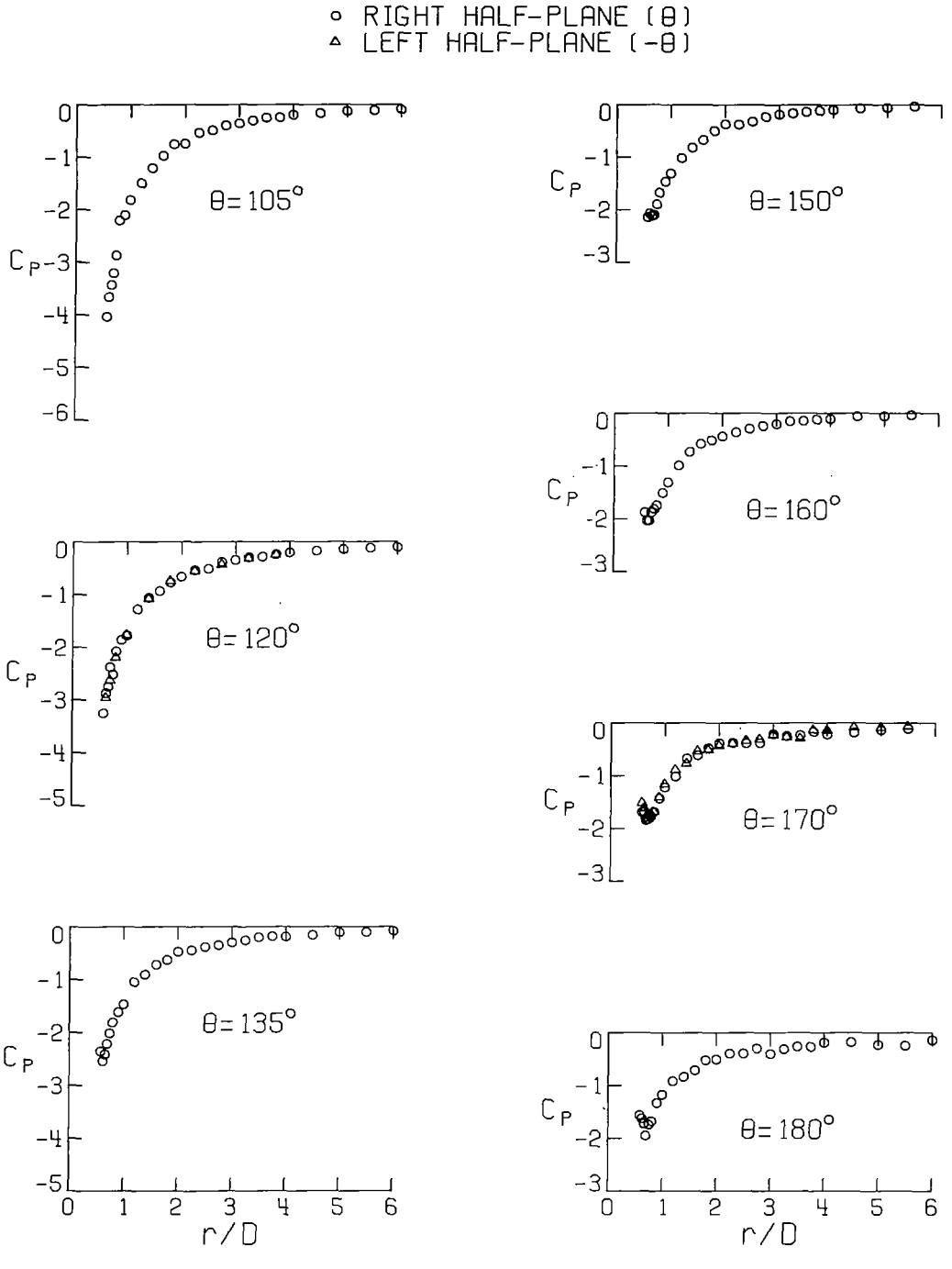

(b) Concluded.

Figure 7.- Continued.

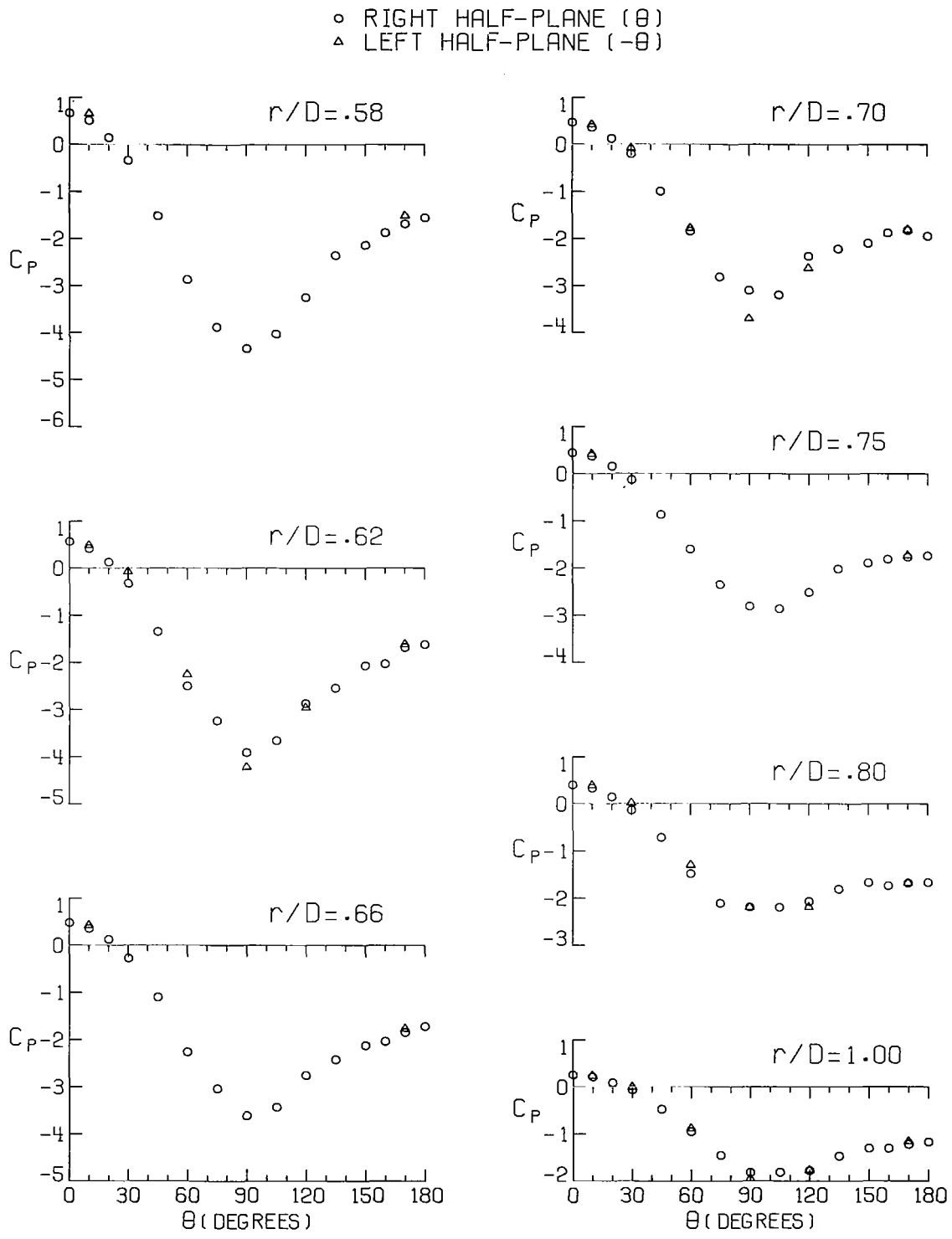

(c) Pressure distribution on circles.

Figure 7.- Continued.

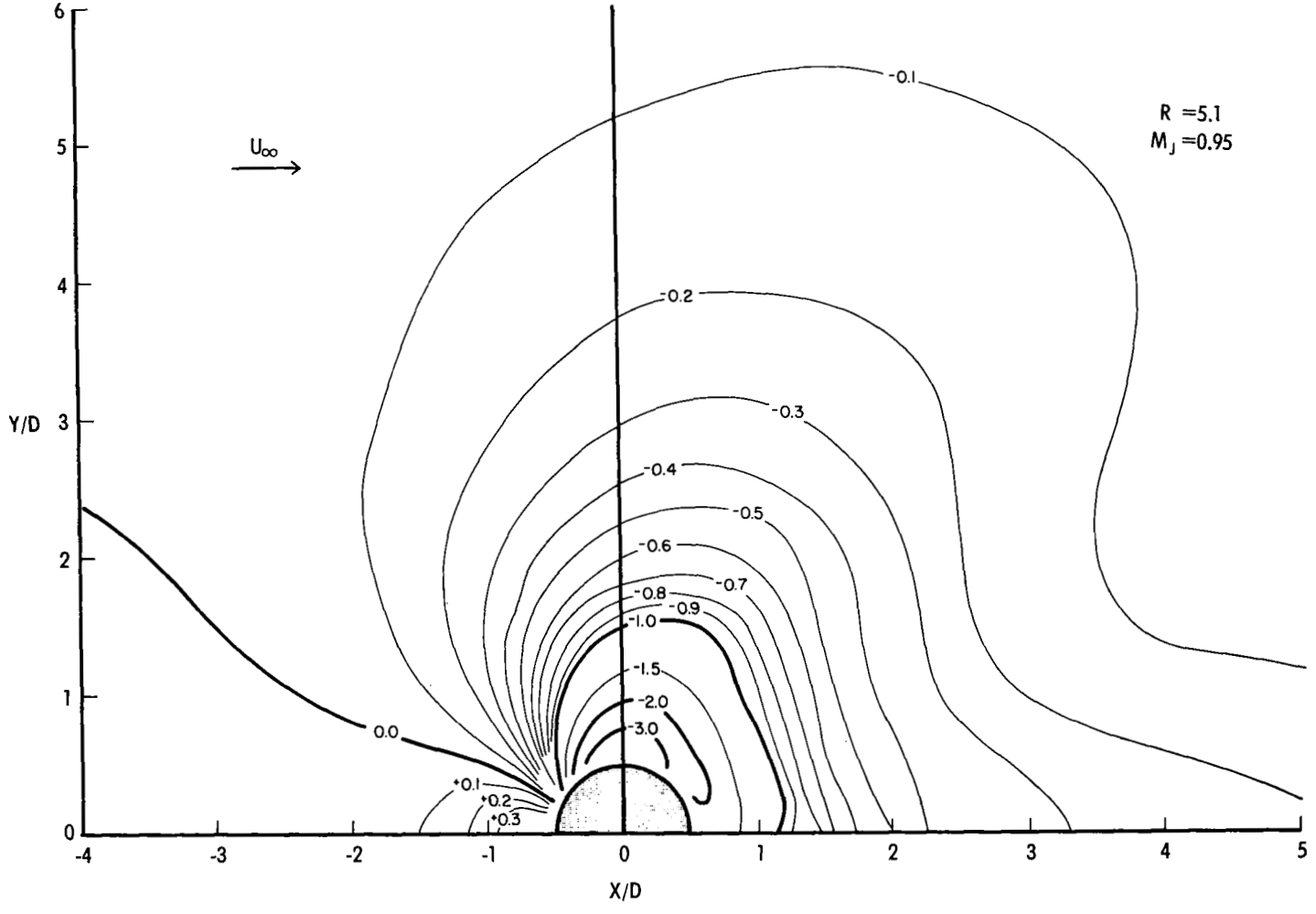

(d) Contours of constant C_p.

Figure 7.- Concluded.

θ (deg) \ r/D	.58	.62	.66	.70	.75	.80	.90	1.00	1.20	1.40	1.60	1.80	2.00
0	.59	.59	.47	.39	.36	.33	.24	.18	.08	.02	.02	-.01	-.02
10	.43	.39	.33	.28	.25	.26	.18	.13	.04	.00	-.01	-.02	-.03
20	.05	.10	.07	.05	.04	.05	.05	-.00	-.05	-.07	-.07	-.08	-.08
30	-.52	-.42	-.32	-.35	-.29	-.24	-.24	-.21	-.20	-.19	-.17	-.15	-.13
45	-1.74	-1.51	-1.34	-1.18	-1.05	-.92	-.74	-.61	-.48	-.42	-.33	-.28	-.25
60	-3.13	-2.67	-2.36	-2.31	-1.96	-1.75	-1.28	-1.06	-.82	-.71	-.54	-.46	-.39
75	-4.16	-3.45	-2.92	-2.95	-2.71	-2.38	-1.86	-1.65	-1.18	-.95	-.75	-.65	-.54
90	-4.74	-3.64	-3.62	-3.26	-2.87	-2.58	-2.18	-1.86	-1.43	-1.08	-.93	-.83	-.69
105	-3.89	-3.66	-3.23	-3.00	-2.56	-2.42	-2.25	-1.83	-1.47	-1.16	-1.05	-.89	-.75
120	-2.65	-2.59	-2.52	-2.52	-2.13	-2.19	-1.81	-1.52	-1.27	-1.09	-.89	-.74	-.72
135	-2.40	-2.00	-1.97	-1.98	-1.97	-1.69	-1.52	-1.17	-.95	-.82	-.68	-.56	-.52
150	-1.86	-1.93	-1.76	-1.88	-1.63	-1.58	-1.32	-1.22	-.92	-.68	-.57	-.44	-.38
160	-1.63	-1.71	-1.78	-1.82	-1.58	-1.49	-1.22	-1.04	-.73	-.65	-.54	-.40	-.37
170	-1.40	-1.57	-1.64	-1.51	-1.57	-1.45	-1.29	-1.03	-.83	-.64	-.43	-.42	-.42
180	-1.35	-1.39	-1.61	-1.57	-1.52	-1.47	-1.32	-1.09	-.74	-.67	-.49	-.38	-.39
-170	-1.46	-1.51	-1.59	-1.62	-1.56	-1.48	-1.37	-1.03	-.86	-.59	-.53	-.50	-.37
-120		-2.92		-2.16		-2.20		-1.66		-1.17		-.86	
-90		-4.44		-3.75		-2.88		-1.96		-1.21		-.83	
-60		-2.48		-2.04		-1.59		-1.09		-.67		-.47	
-30		-.15		-.18		-.13		-.14		-.14		-.12	
-10	.61	.48	.36	.38	.34	.30	.21	.15	.05	.01	-.01	-.02	-.03

θ (deg) \ r/D	2.25	2.50	2.75	3.00	3.25	3.50	3.75	4.00	4.50	5.00	5.50	6.00	7.00
0	-.03	-.03	-.02	-.02	-.02	-.01	-.01	-.02	-.01	-.01	-.01		
10	-.04	-.03	-.03	-.03	-.03	-.02	-.02	-.02	-.02	-.01	.01		
20	-.07	-.06	-.06	-.06	-.04	-.04	-.03	-.04	-.03	-.01	-.01		
30	-.11	-.10	-.08	-.09	-.07	-.06	-.05	-.05	-.04	-.03	-.01	.00	
45	-.21	-.18	-.16	-.14	-.12	-.10	-.11	-.09	-.07	-.04	-.03	-.03	-.04
60	-.34	-.30	-.25	-.22	-.18	-.17	-.15	-.12	-.08	-.09	-.06	-.05	
75	-.47	-.41	-.34	-.30	-.26	-.23	-.20	-.16	-.10	-.11	-.10	-.08	
90	-.59	-.51	-.44	-.38	-.32	-.27	-.25	-.21	-.20	-.15	-.12		
105	-.63	-.53	-.47	-.42	-.37	-.32	-.31	-.25	-.22	-.17	-.15	-.12	
120	-.52	-.55	-.45	-.38	-.35	-.31	-.27	-.22	-.20	-.17	-.15	-.12	
135	-.48	-.33	-.32	-.25	-.24	-.26	-.19	-.21	-.14	-.13	-.10	-.10	-.08
150	-.31	-.25	-.22	-.15	-.15	-.11	-.08	-.10	-.08	-.06	-.04		
160	-.38	-.21	-.17	-.17	-.13	-.15	-.07	-.10	-.06	-.04	-.03		
170	-.30	-.24	-.19	-.19	-.18	-.12	-.20	-.13	-.10	-.06	-.04		
180	-.32	-.31	-.23	-.19	-.18	-.18	-.23	-.20	-.15	-.09	-.07	-.10	-.13
-170	-.38	-.27	-.20	-.19	-.14	-.12	-.14	-.15	-.09	-.09			
-120	-.61		-.45		-.37		-.26						
-90	-.61		-.45		-.35		-.26						
-60	-.36		-.24		-.19		-.25						
-30	-.11		-.09		-.06		-.04						
-10	-.04	-.02	-.04	-.03	-.03	-.02	-.01	-.01	-.02	-.01			

(a) C_p values.

Figure 8.- Pressure distribution on flat plate. R = 6.1; M_j = 0.94.

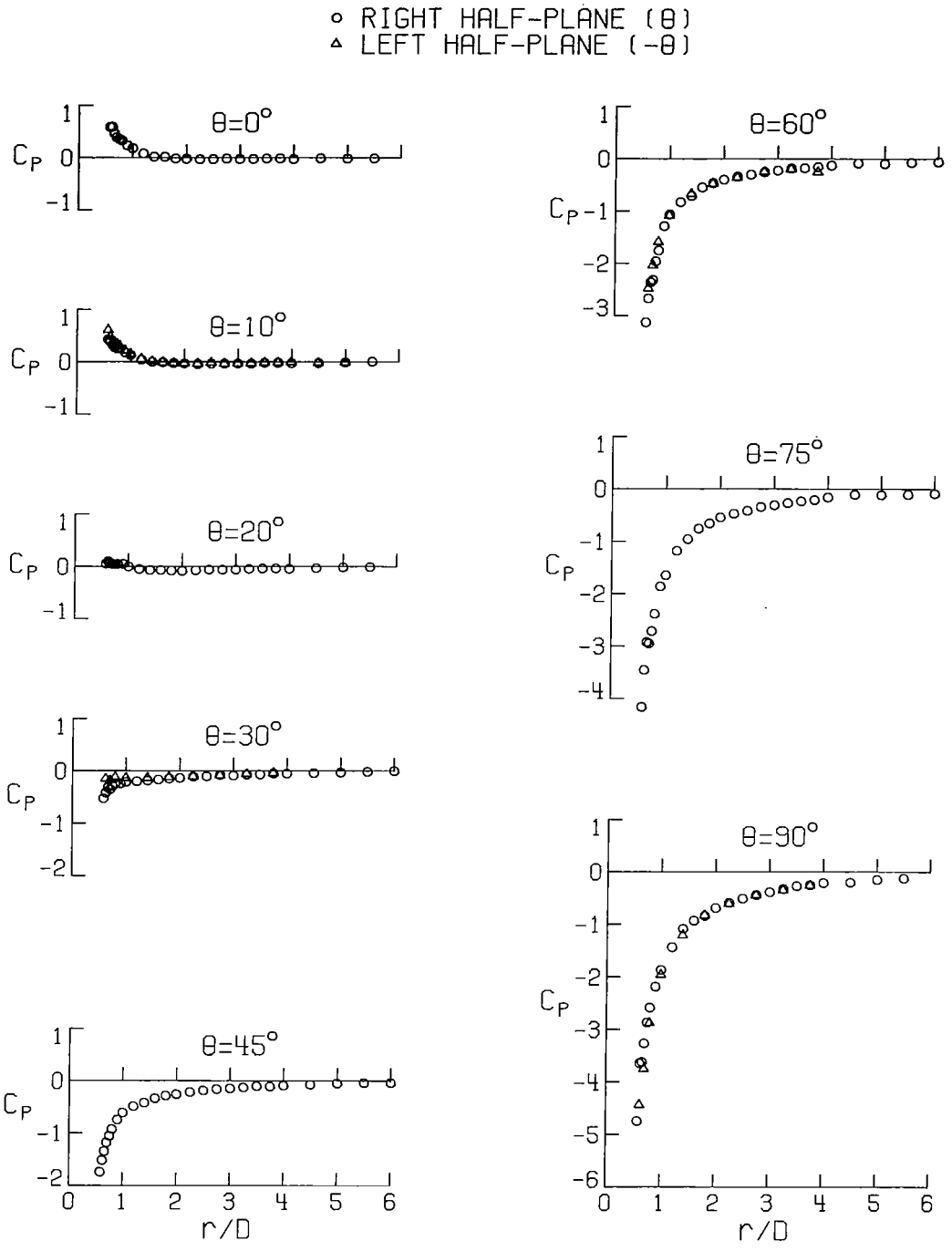

(b) Pressure distribution on rays.

Figure 8.- Continued.

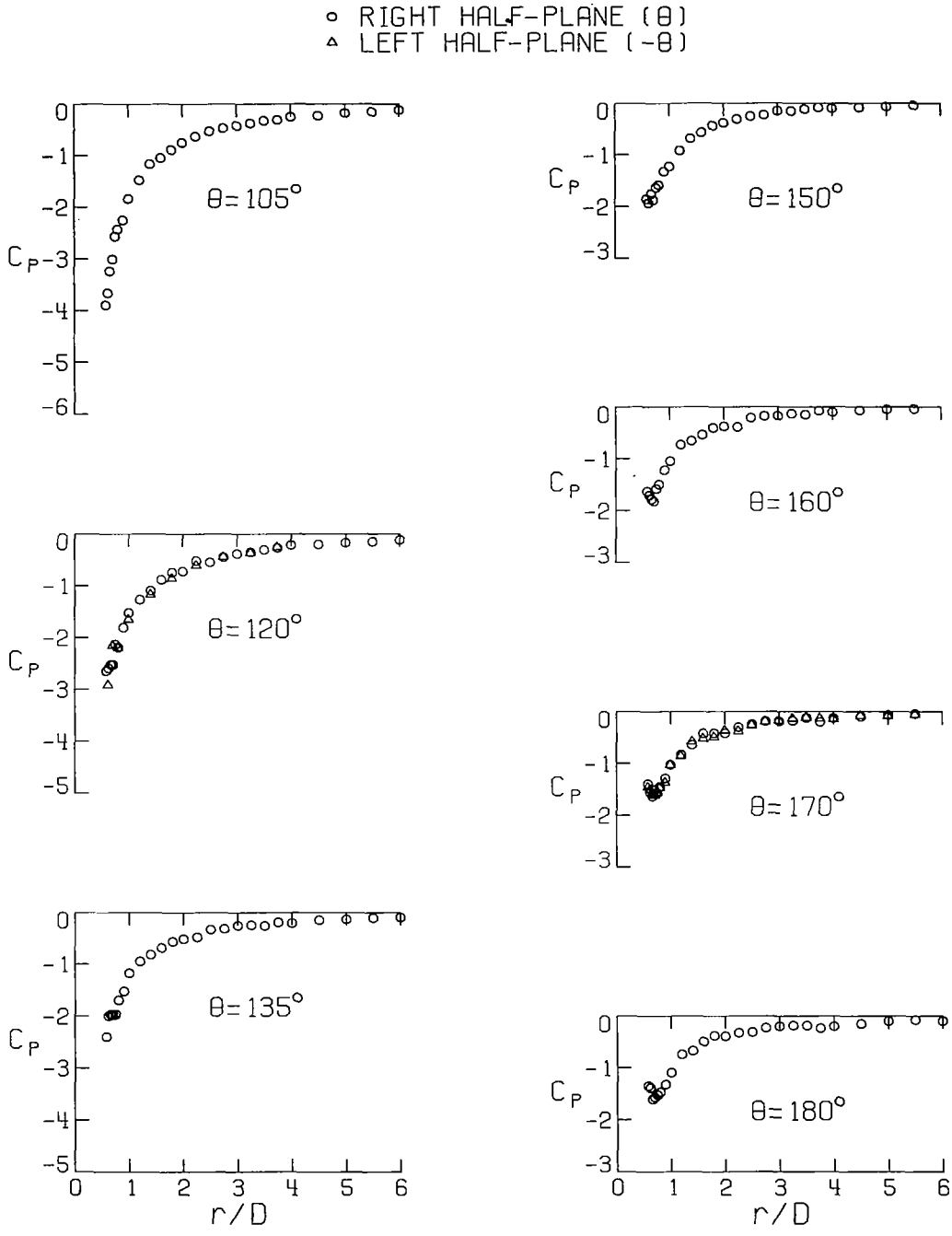

(b) Concluded.

Figure 8.- Continued.

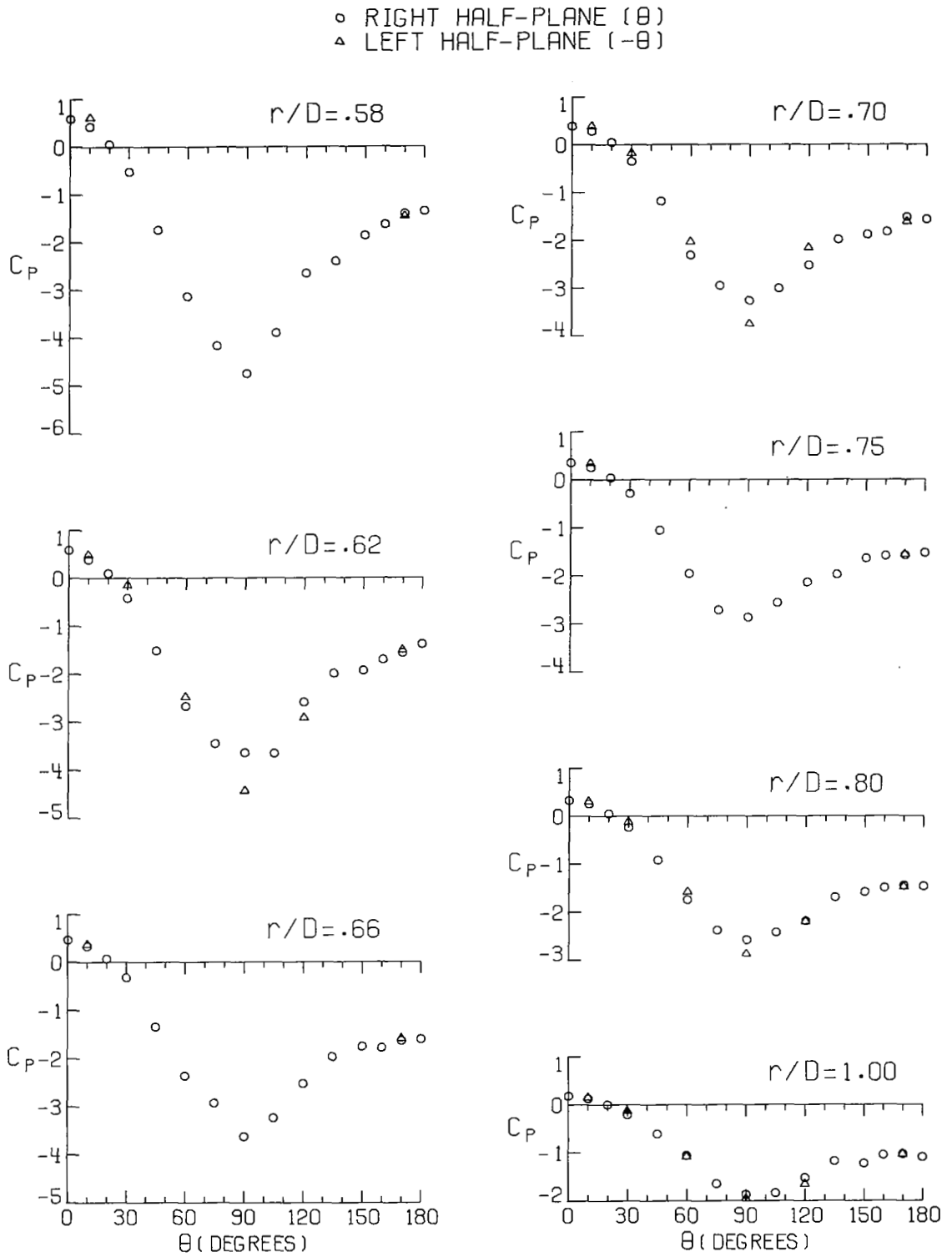

(c) Pressure distribution on circles.

Figure 8.- Continued.

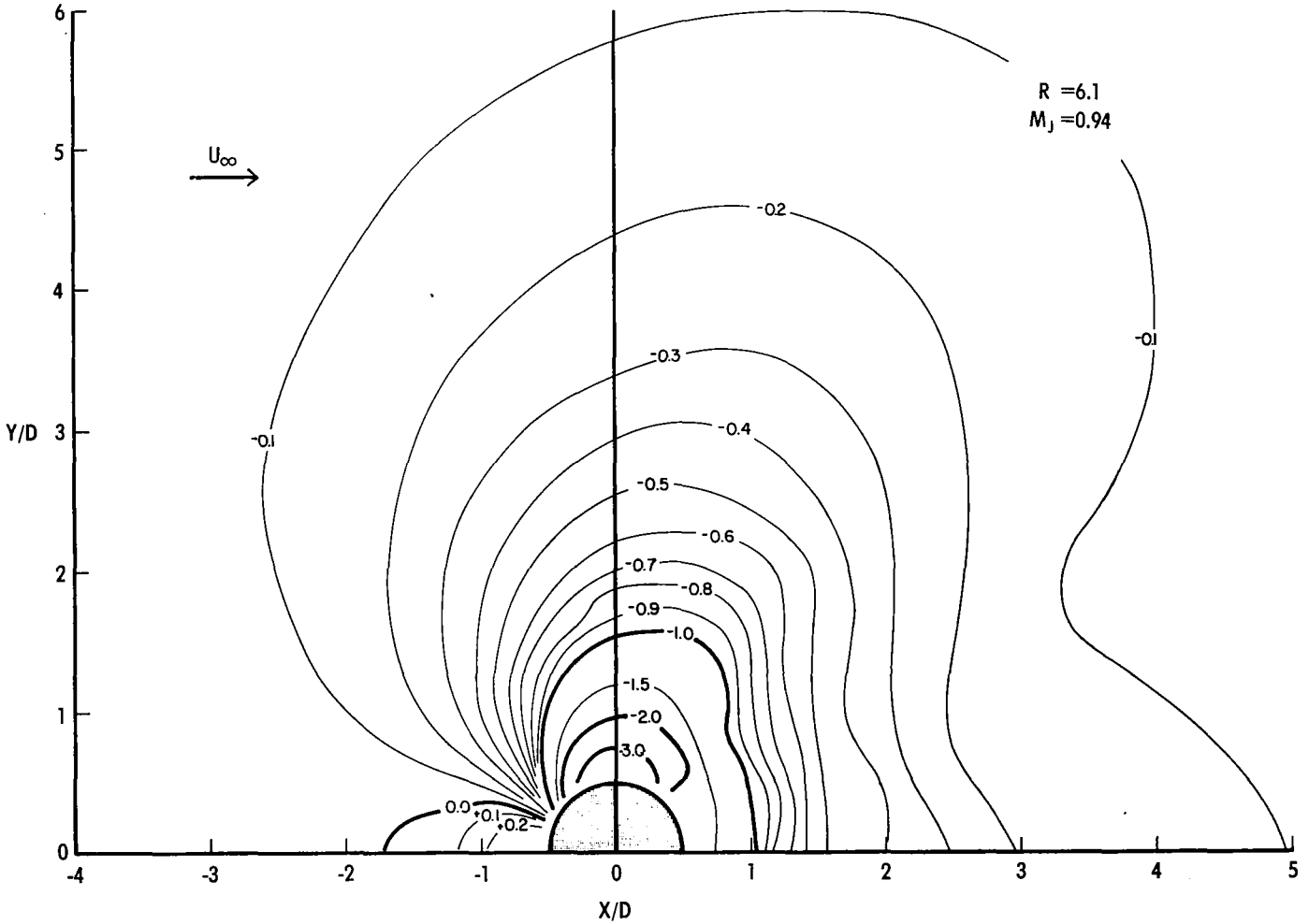

(d) Contours of constant C_p.

Figure 8.- Concluded.

θ (deg) \ r/D	.58	.62	.66	.70	.75	.80	.90	1.00	1.20	1.40	1.60	1.80	2.00
0	.47	.40	.39	.31	.28	.29	.18	.12	.01	-.04	-.07	-.08	-.09
10	.32	.27	.28	.20	.18	.20	.12	.06	-.02	-.06	-.09	-.10	-.10
20	-.08	-.04	-.03	-.04	-.03	.01	-.05	-.08	-.13	-.14	-.15	-.14	-.14
30	-.64	-.75	-.48	-.51	-.42	-.39	-.29	-.30	-.27	-.29	-.26	-.22	-.21
45	-2.08	-1.71	-1.49	-1.42	-1.32	-.96	-.82	-.74	-.59	-.50	-.43	-.38	-.32
60	-3.10	-2.68	-2.51	-2.25	-2.00	-1.74	-1.45	-1.16	-.88	-.75	-.62	-.57	-.47
75	-3.94	-3.46	-2.98	-2.76	-2.44	-2.25	-1.90	-1.65	-1.31	-.98	-.85	-.76	-.65
90	-4.20	-3.82	-3.48	-3.05	-2.67	-2.40	-2.23	-1.79	-1.44	-1.19	-1.04	-.80	-.70
105	-3.17	-3.01	-2.98	-2.98	-2.52	-2.43	-1.77	-1.71	-1.40	-1.08	-1.00	-.91	-.78
120	-2.72	-2.48	-2.21	-2.06	-1.83	-1.87	-1.69	-1.30	-1.21	-.89	-.79	-.69	-.66
135	-2.10	-1.97	-1.81	-1.67	-1.62	-1.53	-1.30	-1.22	-.84	-.70	-.63	-.62	-.44
150	-1.70	-1.80	-1.60	-1.74	-1.49	-1.25	-1.23	-1.15	-.79	-.65	-.52	-.49	-.40
160	-1.40	-1.53	-1.62	-1.55	-1.47	-1.35	-1.17	-.86	-.67	-.52	-.40	-.35	-.31
170	-1.26	-1.31	-1.43	-1.47	-1.43	-1.24	-1.09	-.92	-.68	-.53	-.41	-.36	-.34
180	-1.27	-1.33	-1.38	-1.43	-1.35	-1.30	-1.16	-.91	-.65	-.52	-.41	-.35	-.29
-170	-1.35	-1.42	-1.45	-1.45	-1.36	-1.22	-1.08	-.95	-.66	-.49	-.40	-.35	-.25
-120		-2.23		-2.15		-1.88		-1.36		-.98		-.85	
-90		-3.97		-3.69		-2.86		-1.93		-1.28		-.85	
-60		-2.64		-2.00		-1.66		-1.21		-.73		-.56	
-30		-.30		-.23		-.10		-.19		-.20		-.19	
-10	.47	.36	.30	.32	.29	.23	.17	.09	-.01	-.05	-.08	-.10	-.11

θ (deg) \ r/D	2.25	2.50	2.75	3.00	3.25	3.50	3.75	4.00	4.50	5.00	5.50	6.00	7.00
0	-.09	-.09	-.08	-.09	-.07	-.07	-.06	-.07	-.06	-.03	-.02		
10	-.10	-.10	-.09	-.08	-.07	-.08	-.06	-.08	-.06	-.04	-.03		
20	-.13	-.12	-.12	-.11	-.10	-.09	-.07	-.09	-.07	-.04	-.05		
30	-.19	-.16	-.15	-.14	-.12	-.11	-.10	-.09	-.08	-.05	-.06	.01	
45	-.29	-.25	-.22	-.19	-.17	-.16	-.14	-.13	-.10	-.09	-.08	-.04	-.05
60	-.44	-.36	-.32	-.28	-.26	-.22	-.20	-.16	-.12	-.11	-.10	-.06	
75	-.56	-.47	-.43	-.36	-.30	-.28	-.26	-.20	-.14	-.16	-.13	-.09	
90	-.63	-.56	-.49	-.43	-.38	-.32	-.31	-.25	-.23	-.19	-.16		
105	-.56	-.57	-.48	-.43	-.40	-.38	-.33	-.29	-.24	-.21	-.18	-.14	
120	-.54	-.50	-.44	-.38	-.35	-.35	-.29	-.26	-.22	-.21	-.16	-.12	
135	-.41	-.36	-.34	-.26	-.28	-.21	-.21	-.16	-.14	-.13	-.13	-.08	-.09
150	-.26	-.26	-.19	-.16	-.13	-.10	-.10	-.08	-.04	-.05	-.05		
160	-.24	-.17	-.22	-.15	-.14	-.07	-.08	-.05	-.06	-.05	-.04		
170	-.25	-.23	-.18	-.16	-.15	-.11	-.08	-.07	-.07	-.01	-.04		
180	-.29	-.21	-.21	-.15	-.10	-.11	-.13	-.09	-.08	-.07	-.04	-.09	-.08
-170	-.25	-.23	-.20	-.17	-.12	-.09	-.11	-.03	-.09	-.03			
-120	-.59		-.46		-.41		-.31						
-90	-.66		-.49		-.39		-.32						
-60	-.40		-.32		-.24		-.20						
-30	-.17		-.15		-.12		-.10						
-10	-.10	-.09	-.09	-.08	-.08	-.07	-.08	-.07	-.04	-.04			

(a) C_p values.

Figure 9.- Pressure distribution on flat plate. R = 7.0; M_j = 0.94.

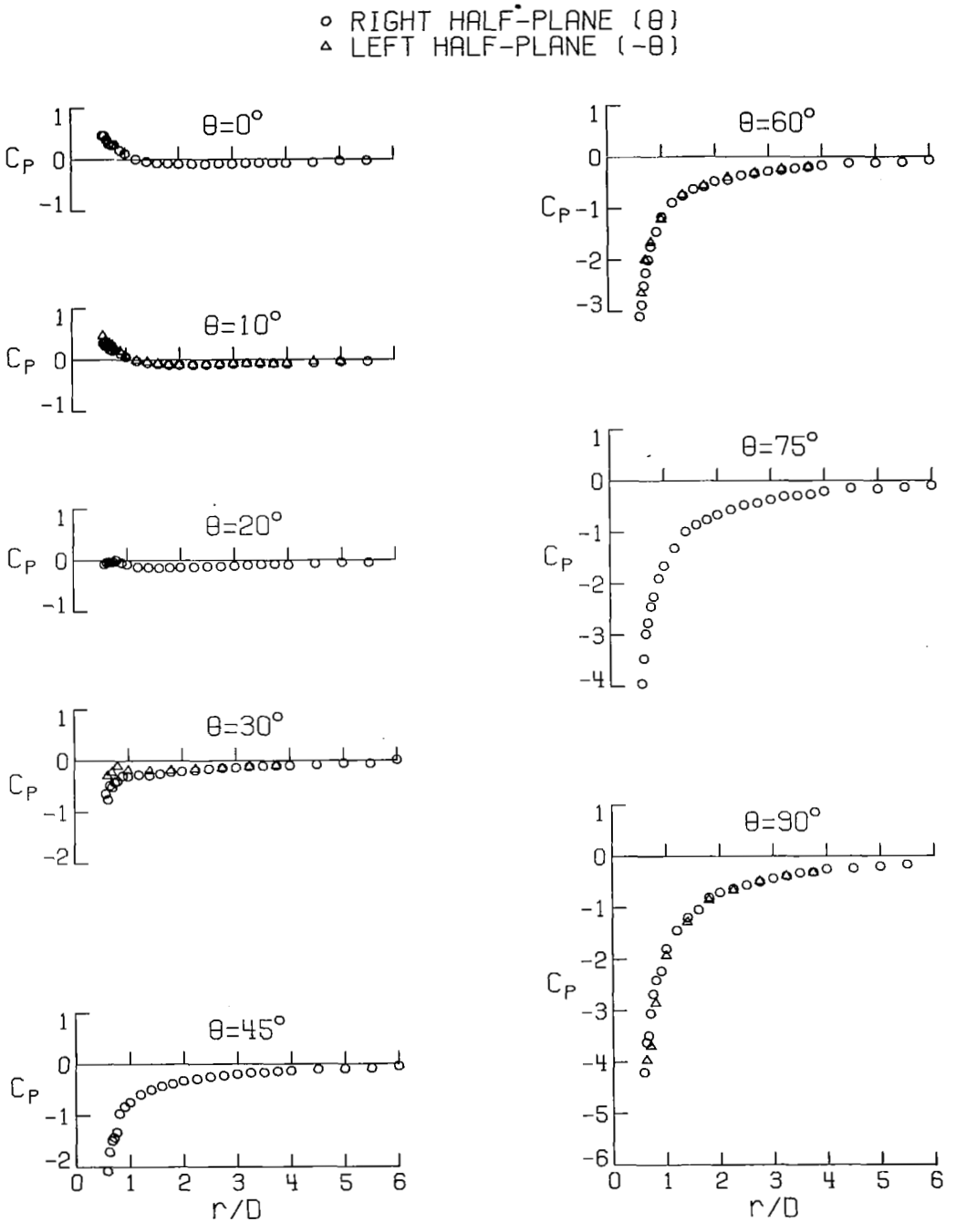

(b) Pressure distribution on rays.

Figure 9.- Continued.

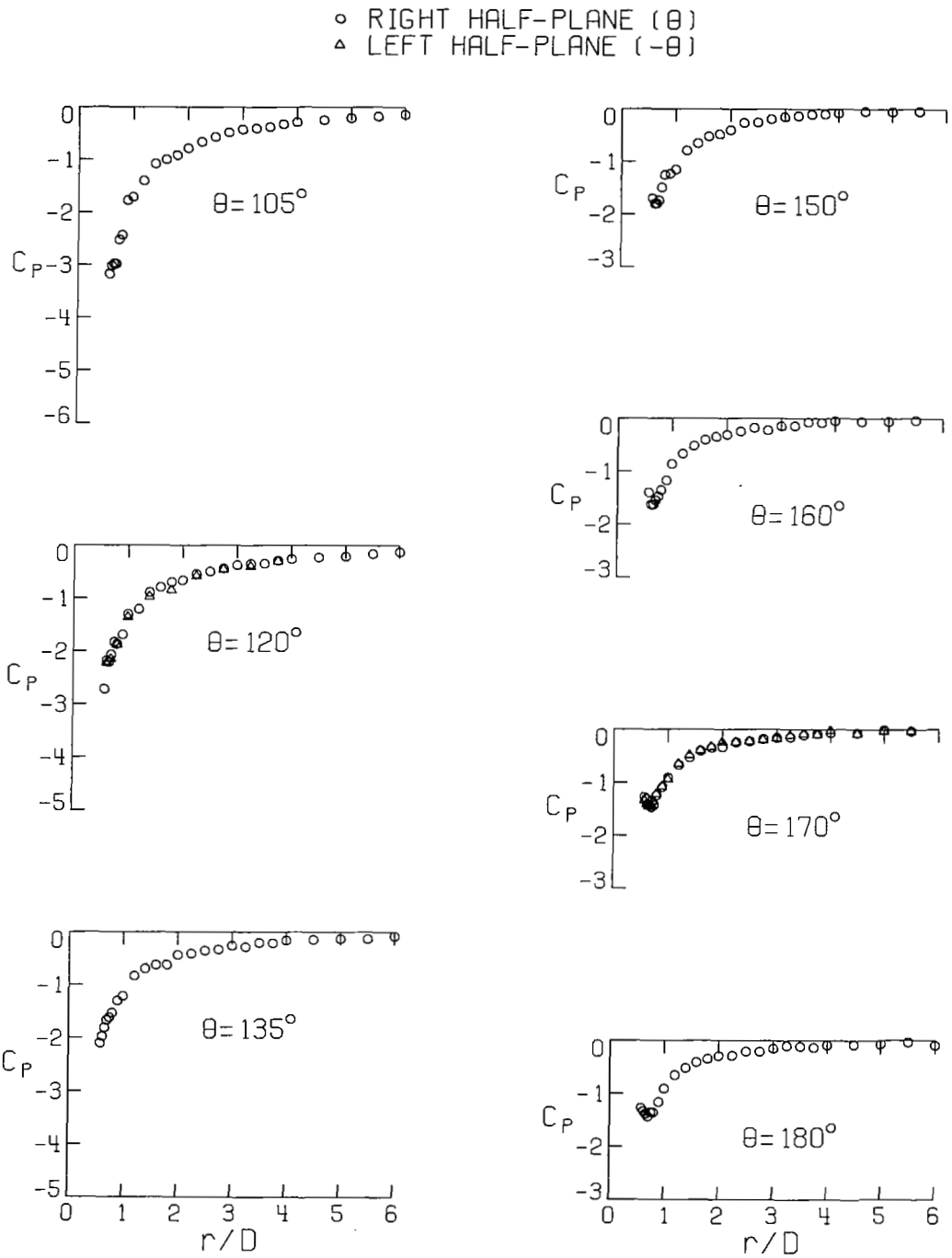

(b) Concluded.

Figure 9.- Continued.

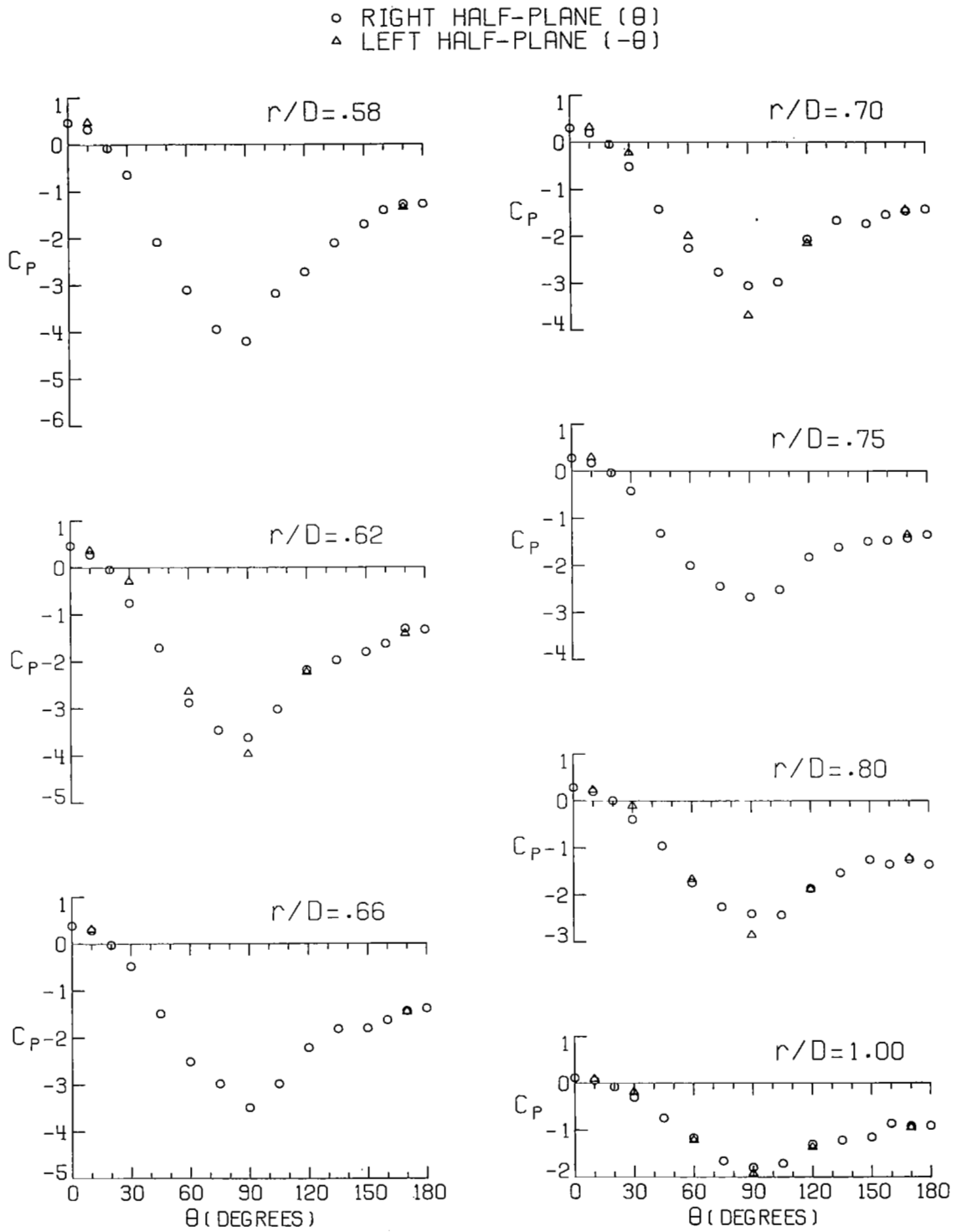

(c) Pressure distribution on circles.

Figure 9.- Continued.

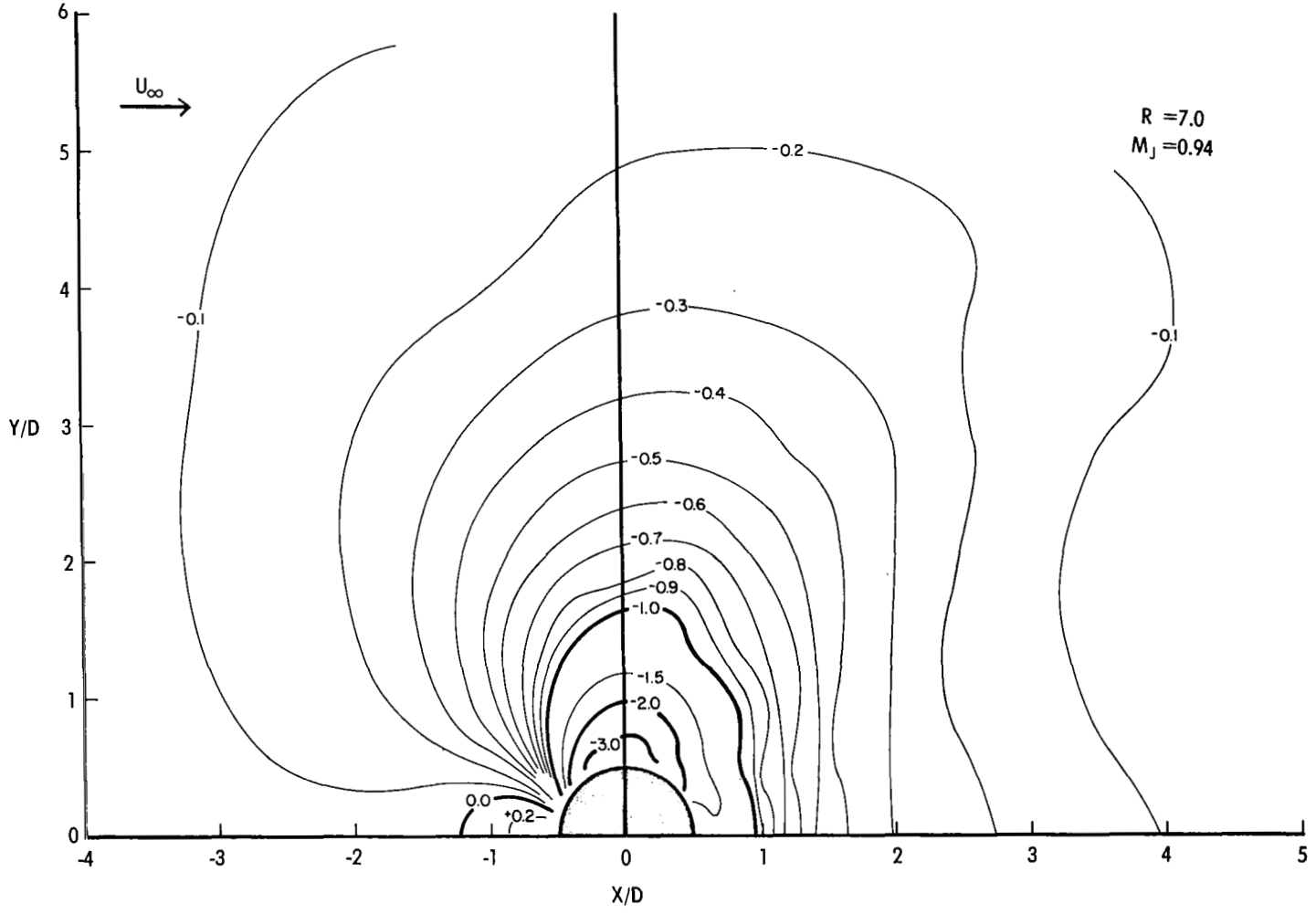

(d) Contours of constant C_p.

Figure 9.- Concluded.

θ (deg) \ r/D	.58	.62	.66	.70	.75	.80	.90	1.00	1.20	1.40	1.60	1.80	2.00
0	.47	.44	.40	.30	.27	.22	.14	.06	-.04	-.08	-.12	-.14	-.13
10	.29	.34	.24	.20	.14	.12	.07	.00	-.06	-.12	-.14	-.15	-.14
20	-.16	-.07	-.03	-.16	-.07	-.10	-.08	-.14	-.15	-.19	-.20	-.20	-.20
30	-.82	-.61	-.50	-.51	-.45	-.50	-.38	-.33	-.33	-.34	-.32	-.26	-.25
45	-2.24	-1.65	-1.42	-1.22	-1.35	-.98	-.80	-.76	-.54	-.58	-.45	-.42	-.38
60	-2.39	-2.48	-2.31	-2.13	-2.13	-1.63	-1.42	-1.16	-.95	-.74	-.72	-.62	-.53
75	-3.48	-2.98	-2.77	-2.46	-2.22	-2.22	-1.94	-1.41	-1.23	-.96	-.81	-.73	-.72
90	-3.85	-2.89	-2.66	-2.43	-2.43	-2.21	-1.88	-1.56	-1.31	-1.02	-.92	-.84	-.71
105	-2.84	-2.54	-2.30	-2.50	-2.02	-1.96	-1.81	-1.43	-1.11	-1.09	-.90	-.93	-.67
120	-1.91	-1.98	-1.84	-1.43	-1.80	-1.49	-1.70	-1.16	-.90	-.67	-.61	-.61	-.62
135	-1.69	-1.69	-1.60	-1.56	-1.24	-1.41	-1.05	-1.16	-.72	-.63	-.49	-.49	-.38
150	-1.47	-1.76	-1.61	-1.58	-1.26	-1.09	-1.08	-.95	-.74	-.53	-.49	-.40	-.30
160	-1.14	-1.36	-1.43	-1.31	-1.19	-1.10	-1.02	-.78	-.54	-.42	-.31	-.35	-.26
170	-1.19	-1.24	-1.18	-1.20	-1.14	-1.14	-.94	-.79	-.56	-.43	-.38	-.27	-.19
180	-1.07	-1.22	-1.19	-1.21	-1.17	-1.16	-.93	-.81	-.56	-.46	-.36	-.29	-.27
-170	-1.29	-1.11	-1.18	-1.29	-1.22	-1.21	-.94	-.76	-.55	-.37	-.32	-.30	-.30
-120		-2.05		-1.65		-1.54		-1.07		-.94		-.66	
-90		-3.41		-3.31		-2.76		-1.74		-1.18		-.90	
-60		-2.30		-2.00		-1.54		-1.05		-.72		-.56	
-30		-.35		-.23		-.22		-.26		-.22		-.25	
-10	.46	.39	.30	.28	.24	.18	.11	.01	-.05	-.10	-.13	-.13	-.15

θ (deg) \ r/D	2.25	2.50	2.75	3.00	3.25	3.50	3.75	4.00	4.50	5.00	5.50	6.00	7.00
0	-.13	-.13	-.12	-.11	-.10	-.10	-.09	-.10	-.07	-.06	-.05		
10	-.14	-.14	-.13	-.12	-.12	-.11	-.10	-.10	-.07	-.06	-.05		
20	-.18	-.16	-.17	-.14	-.13	-.12	-.11	-.11	-.06	-.07	-.07		
30	-.21	-.21	-.18	-.18	-.16	-.14	-.13	-.12	-.07	-.08	-.08	-.07	
45	-.34	-.28	-.28	-.24	-.21	-.18	-.17	-.15	-.10	-.11	-.10	-.09	-.01
60	-.47	-.40	-.35	-.32	-.30	-.27	-.23	-.19	-.11	-.14	-.12	-.10	
75	-.56	-.49	-.43	-.40	-.35	-.31	-.28	-.20	-.24	-.18	-.15	-.13	
90	-.58	-.54	-.49	-.48	-.39	-.37	-.32	-.27	-.25	-.22	-.17		
105	-.59	-.54	-.43	-.41	-.42	-.39	-.31	-.29	-.25	-.22	-.20	-.16	
120	-.46	-.42	-.36	-.36	-.34	-.32	-.28	-.22	-.22	-.21	-.17	-.16	
135	-.36	-.27	-.30	-.24	-.25	-.22	-.17	-.15	-.16	-.12	-.11	-.08	-.08
150	-.26	-.20	-.15	-.17	-.13	-.14	-.07	-.07	-.04	-.04	-.06		
160	-.24	-.17	-.19	-.14	-.08	-.08	-.08	-.07	-.04	-.03	-.01		
170	-.25	-.18	-.17	-.20	-.11	-.09	-.08	-.04	-.06	-.04	-.02		
180	-.26	-.20	-.18	-.16	-.16	-.11	-.08	-.09	-.16	-.03	-.02	-.06	.01
-170	-.23	-.20	-.17	-.19	-.08	-.13	-.10	-.06	.01	-.02			
-120	-.47		-.48		-.41		-.24						
-90	-.63		-.54		-.43		-.34						
-60	-.44		-.36		-.28		-.24						
-30	-.20		-.19		-.15		-.14						
-10	-.13	-.13	-.12	-.12	-.12	-.10	-.11	-.09	-.05	-.05			

(a) C_p values.

Figure 10.- Pressure distribution on flat plate. R = 8.0; M_j = 0.93.

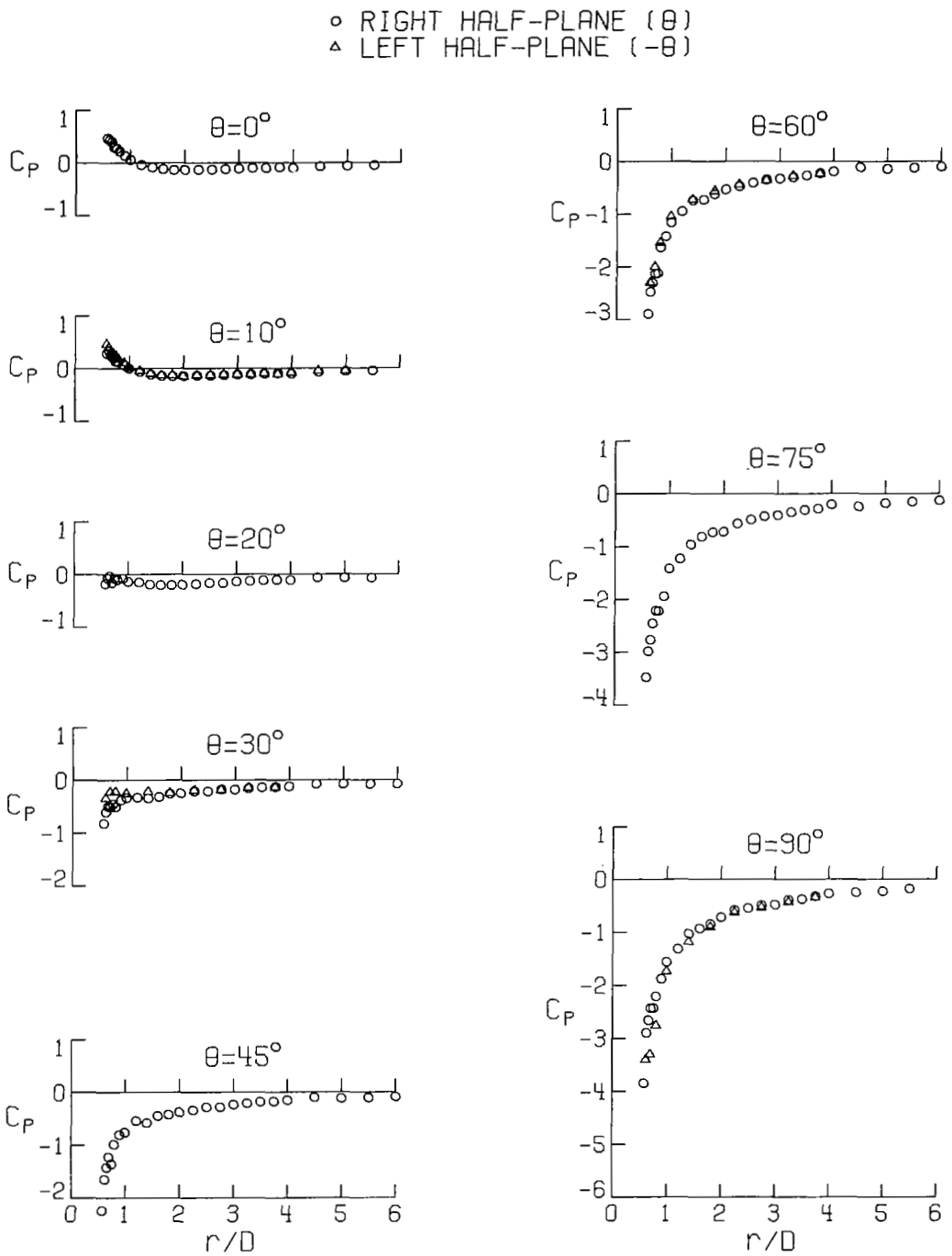

(b) Pressure distribution on rays.

Figure 10.- Continued.

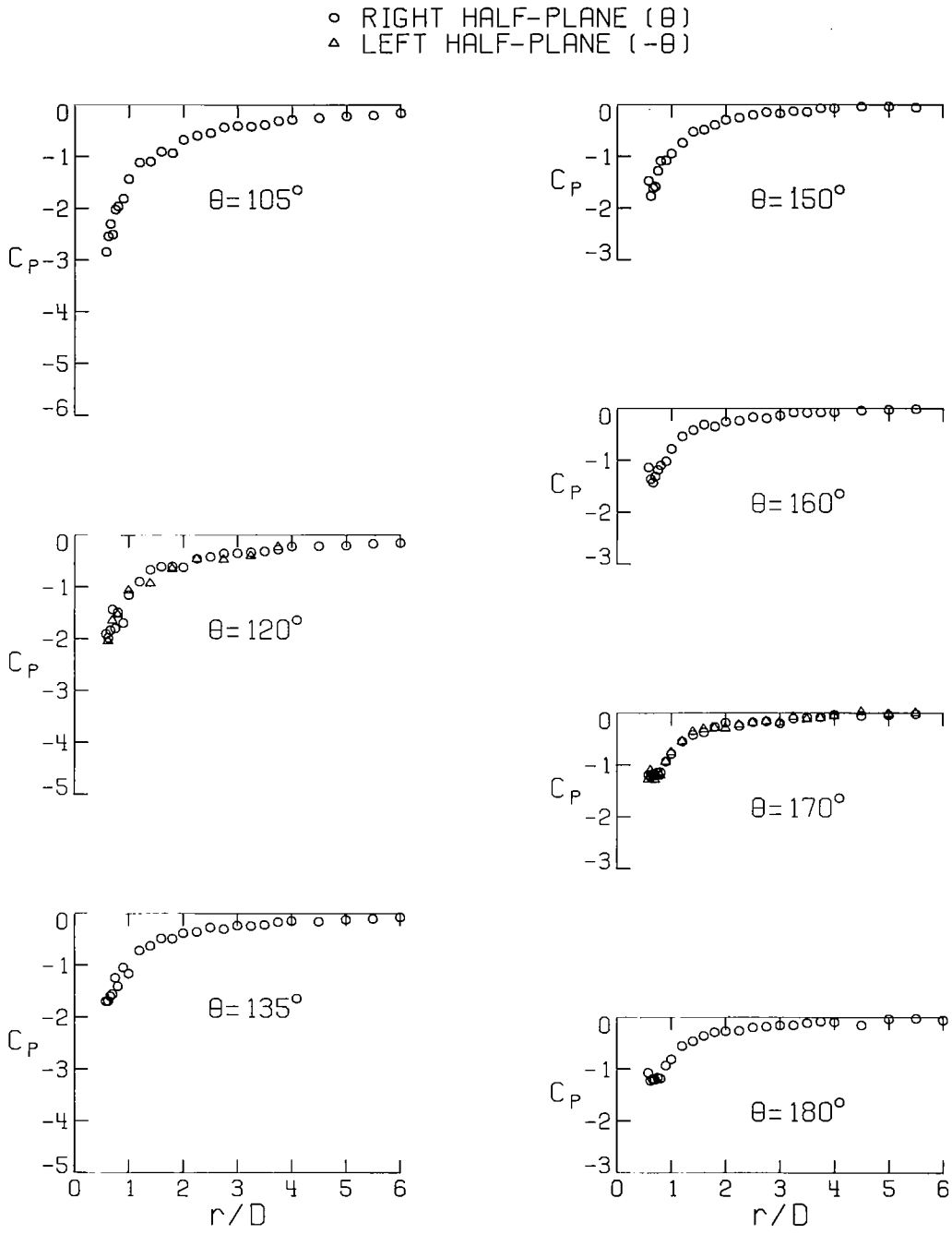

(b) Concluded.

Figure 10.- Continued.

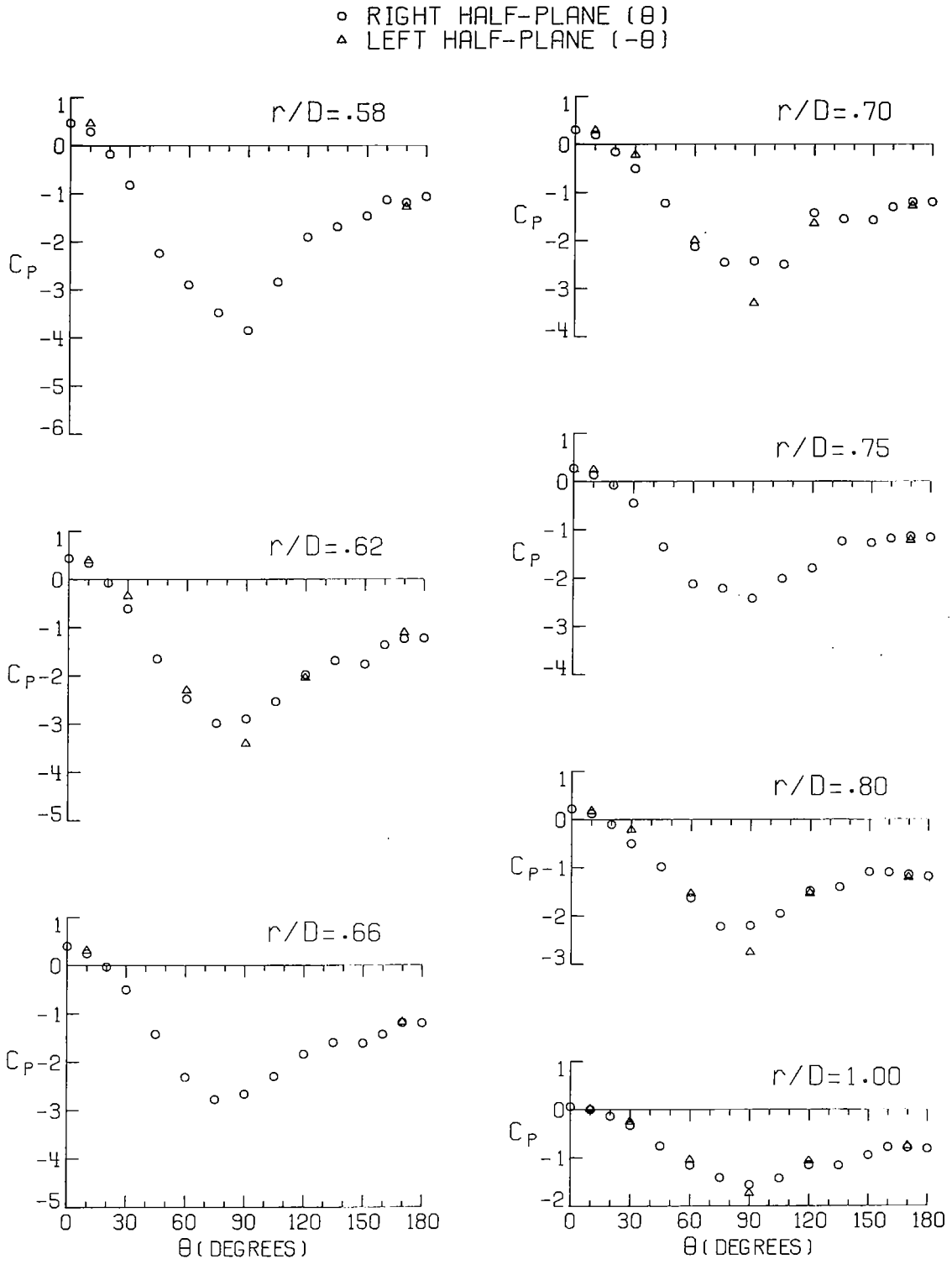

(c) Pressure distribution on circles.

Figure 10.- Continued.

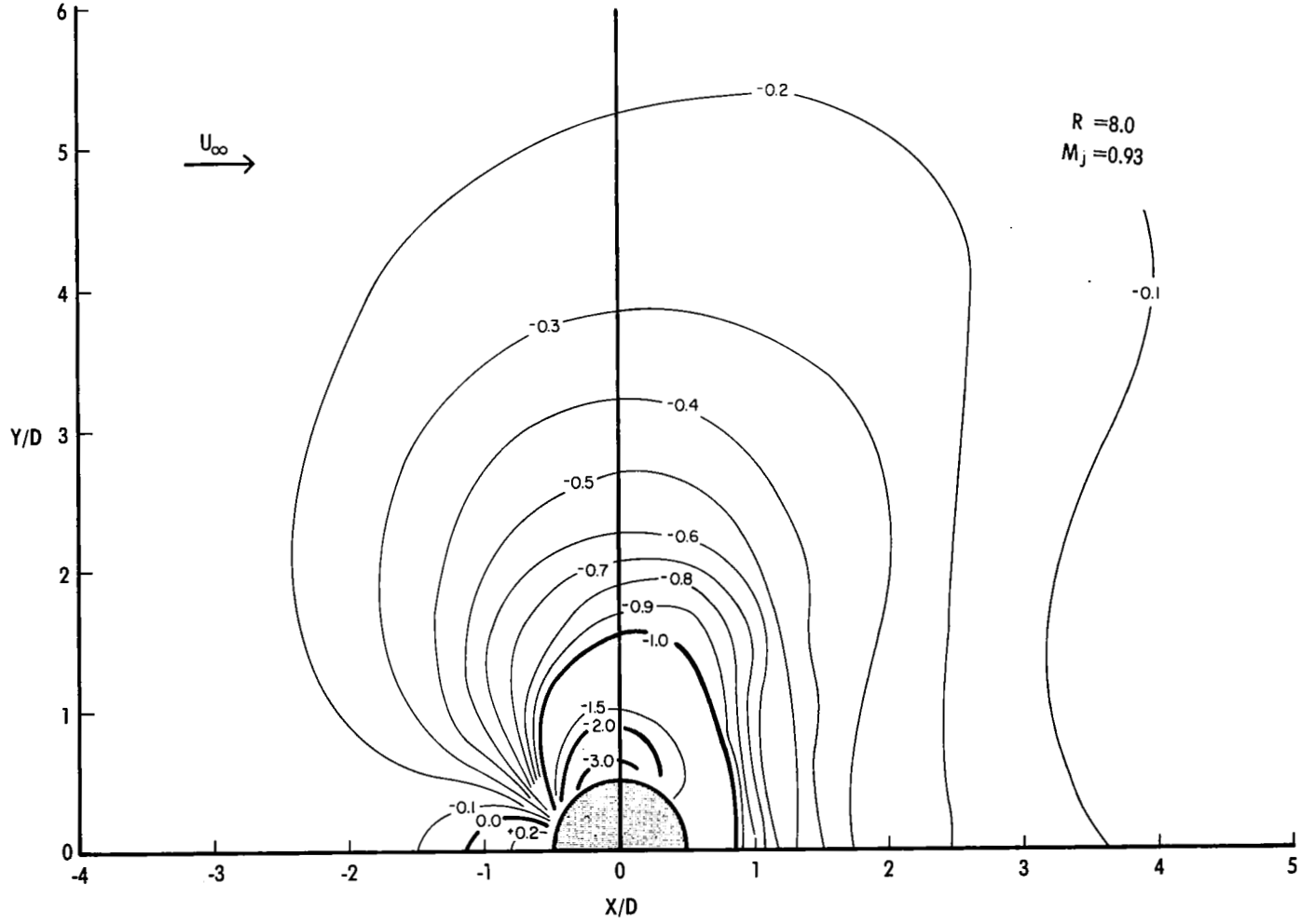

(d) Contours of constant C_p.

Figure 10.- Concluded.

θ (deg) \ r/D	.58	.62	.66	.70	.75	.80	.90	1.00	1.20	1.40	1.60	1.80	2.00
0	.41	.40	.34	.26	.21	.19	.09	.01	-.09	-.14	-.17	-.18	-.17
10	.29	.22	.25	.16	.08	.06	-.01	-.07	-.10	-.18	-.19	-.19	-.17
20	-.19	.01	-.13	-.13	-.17	-.10	-.16	-.20	-.23	-.22	-.23	-.21	-.24
30	-.70	-.53	-.54	-.35	-.39	-.39	-.32	-.37	-.31	-.35	-.33	-.28	-.29
45	-1.69	-1.34	-1.33	-1.34	-1.16	-.90	-.73	-.75	-.61	-.45	-.47	-.40	-.42
60	-2.49	-2.35	-2.06	-1.92	-1.40	-1.47	-1.16	-1.23	-.82	-.75	-.63	-.52	-.54
75	-3.13	-2.74	-2.74	-2.09	-2.11	-1.68	-1.40	-1.25	-1.00	-.82	-.61	-.73	-.59
90	-2.78	-2.85	-2.28	-2.32	-1.95	-1.67	-1.75	-1.36	-.94	-.89	-.79	-.73	-.57
105	-2.10	-2.03	-2.03	-1.54	-1.53	-1.56	-1.35	-1.06	-.95	-.61	-.73	-.72	-.60
120	-1.81	-1.37	-1.22	-1.43	-.97	-1.30	-1.31	-.91	-.74	-.75	-.46	-.52	-.38
135	-1.50	-1.27	-1.25	-1.16	-1.36	-1.09	-1.06	-.89	-.68	-.55	-.40	-.30	-.25
150	-1.09	-.96	-1.28	-1.16	-1.05	-.71	-.76	-.76	-.50	-.42	-.32	-.28	-.23
160	-.83	-1.17	-.98	-.85	-1.01	-.84	-.66	-.54	-.36	-.32	-.22	-.22	-.19
170	-.37	-.97	-1.01	-.85	-.93	-.83	-.73	-.56	-.34	-.31	-.21	-.19	-.17
180	-.84	-.93	-.94	-.96	-1.00	-.91	-.74	-.54	-.40	-.33	-.23	-.18	-.13
-170	-1.01	-.96	-.98	-1.03	-.97	-.89	-.82	-.64	-.39	-.30	-.28	-.16	-.17
-120		-1.75		-1.83		-1.70		-1.09		-.77		-.70	
-90		-3.20		-2.78		-2.19		-1.48		-.97		-.69	
-60		-2.80		-1.99		-1.61		-1.02		-.69		-.56	
-30		-.34		-.35		-.30		-.34		-.32		-.28	
-10	.39	.31	.27	.25	.19	.13	.06	.00	-.10	-.15	-.18	-.17	-.21

θ (deg) \ r/D	2.25	2.50	2.75	3.00	3.25	3.50	3.75	4.00	4.50	5.00	5.50	6.00	7.00
0	-.19	-.19	-.18	-.16	-.14	-.14	-.14	-.32	-.09	-.10	-.10		
10	-.21	-.20	-.18	-.18	-.17	-.14	-.15	-.31	-.10	-.11	-.09		
20	-.23	-.23	-.20	-.20	-.17	-.16	-.15	-.29	-.11	-.11	-.10		
30	-.28	-.24	-.22	-.23	-.20	-.20	-.19	-.29	-.12	-.12	-.11	-.08	
45	-.36	-.36	-.30	-.29	-.27	-.24	-.23	-.28	-.14	-.16	-.12	-.09	-.01
60	-.45	-.43	-.31	-.32	-.31	-.26	-.27	-.28	-.19	-.17	-.15	-.14	
75	-.48	-.50	-.42	-.38	-.33	-.31	-.30	-.29	-.21	-.21	-.18	-.16	
90	-.54	-.49	-.45	-.34	-.39	-.40	-.35	-.29	-.21	-.21	-.20		
105	-.54	-.51	-.38	-.41	-.32	-.29	-.27	-.30	-.21	-.20	-.17	-.18	
120	-.45	-.30	-.33	-.29	-.25	-.28	-.24	-.29	-.19	-.16	-.14	-.11	
135	-.25	-.26	-.16	-.19	-.16	-.15	-.12	-.10	-.06	-.09	-.07	-.11	-.06
150	-.20	-.16	-.17	-.09	-.10	-.14	-.07	-.08	-.04	-.03	-.00		
160	-.18	-.15	-.13	-.12	-.10	-.12	-.10	-.10	-.02	-.01	-.01		
170	-.19	-.16	-.11	-.12	-.04	-.04	-.03	-.08	.01	-.04	-.01		
180	-.13	-.09	-.12	-.07	-.13	-.11	-.14	-.05	-.01	-.06	-.06	-.03	.00
-170	-.14	-.21	-.08	-.15	-.07	-.11	-.03	-.09	.04	-.02			
-120	-.35		-.36		-.34		-.29						
-90	-.55		-.45		-.39		-.43						
-60	-.47		-.39		-.35		-.40						
-30	-.25		-.24		-.20		-.35						
-10	-.19	-.19	-.17	-.17	-.16	-.16	-.33	-.12	-.05	-.09			

(a) C_p values.

Figure 11.- Pressure distribution on flat plate. R = 10.0; M_j = 0.93.

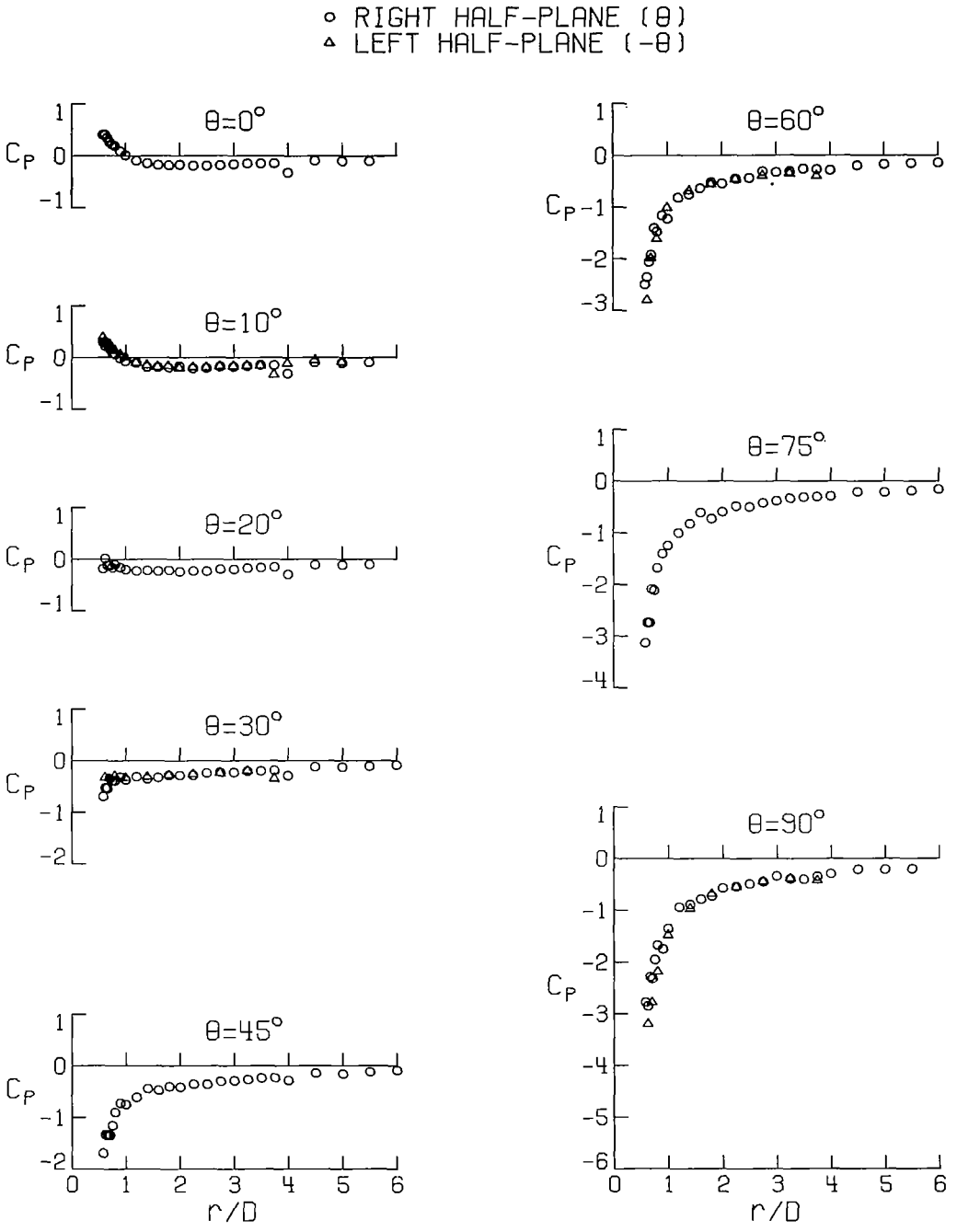

(b) Pressure distribution on rays.

Figure 11.- Continued.

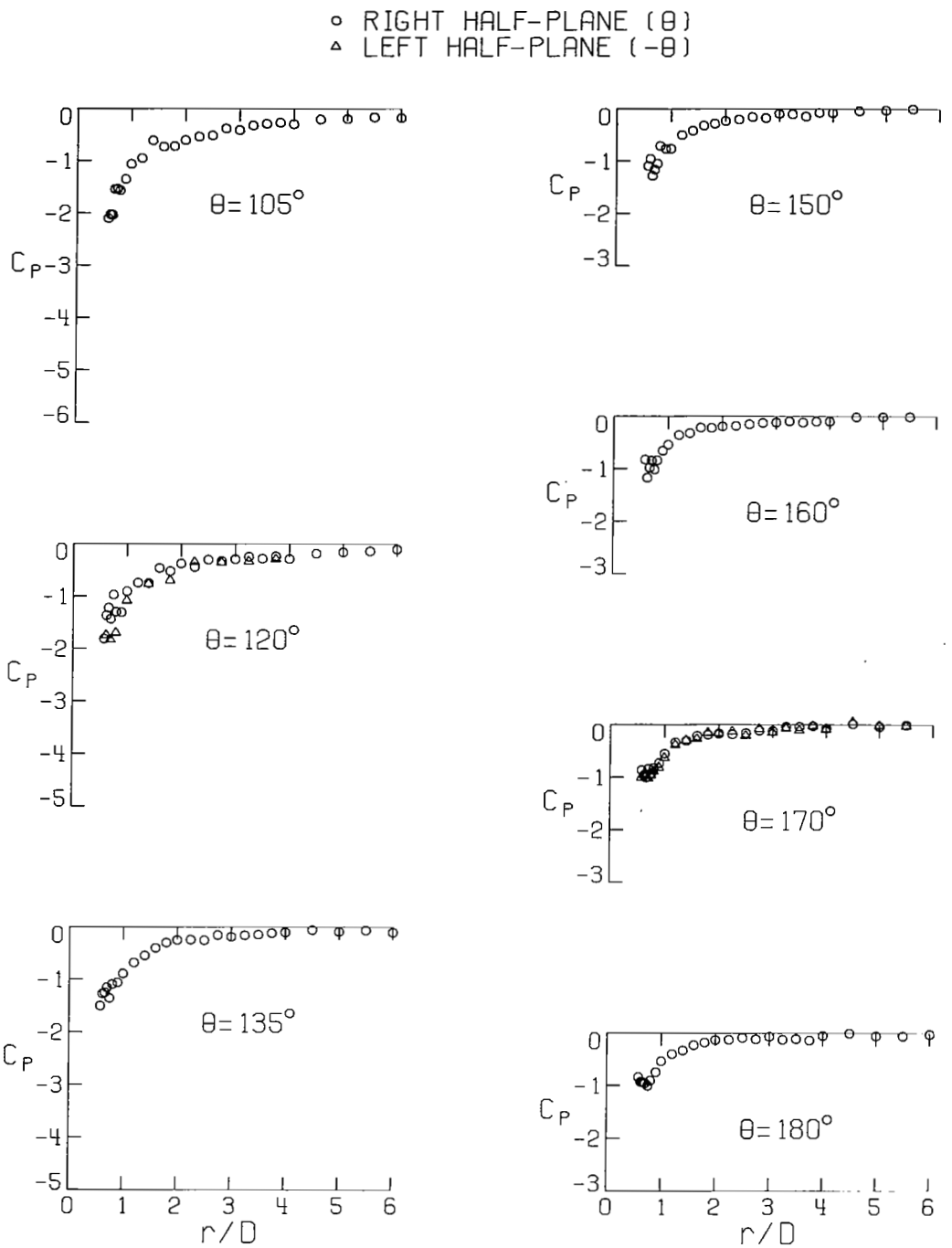

(b) Concluded.

Figure 11.- Continued.

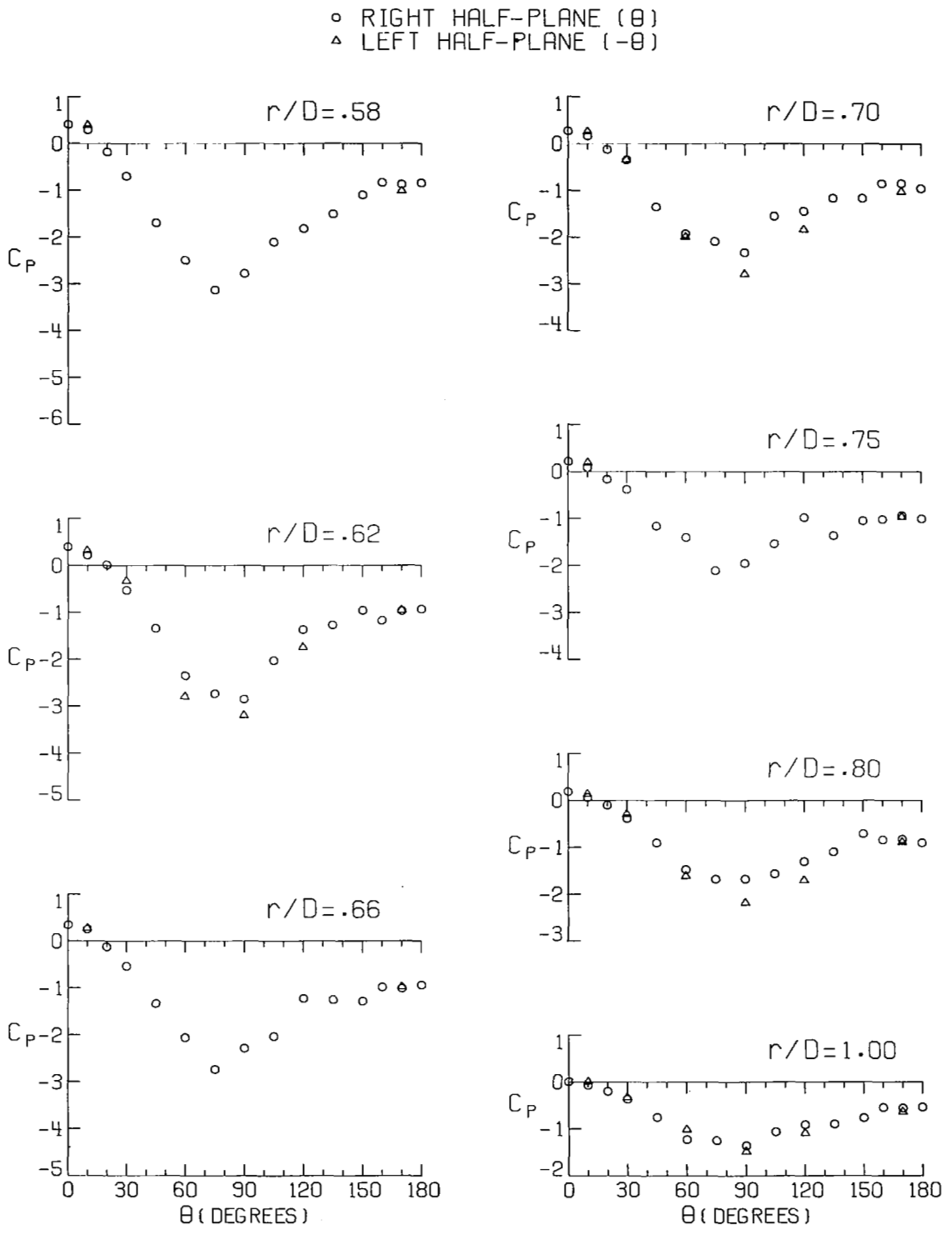

(c) Pressure distribution on circles.

Figure 11.- Continued.

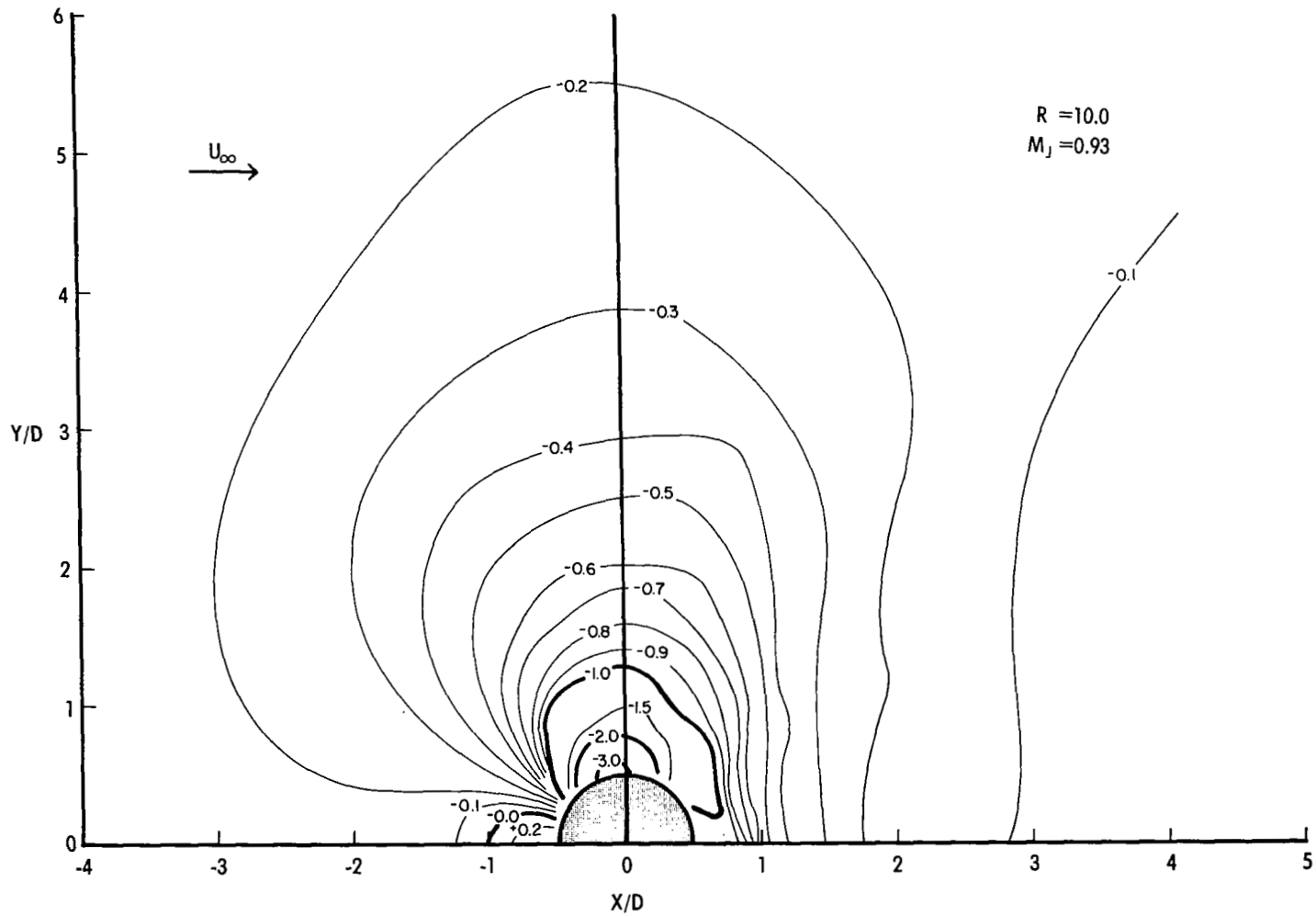

(d) Contours of constant C_p.

Figure 11.- Concluded.

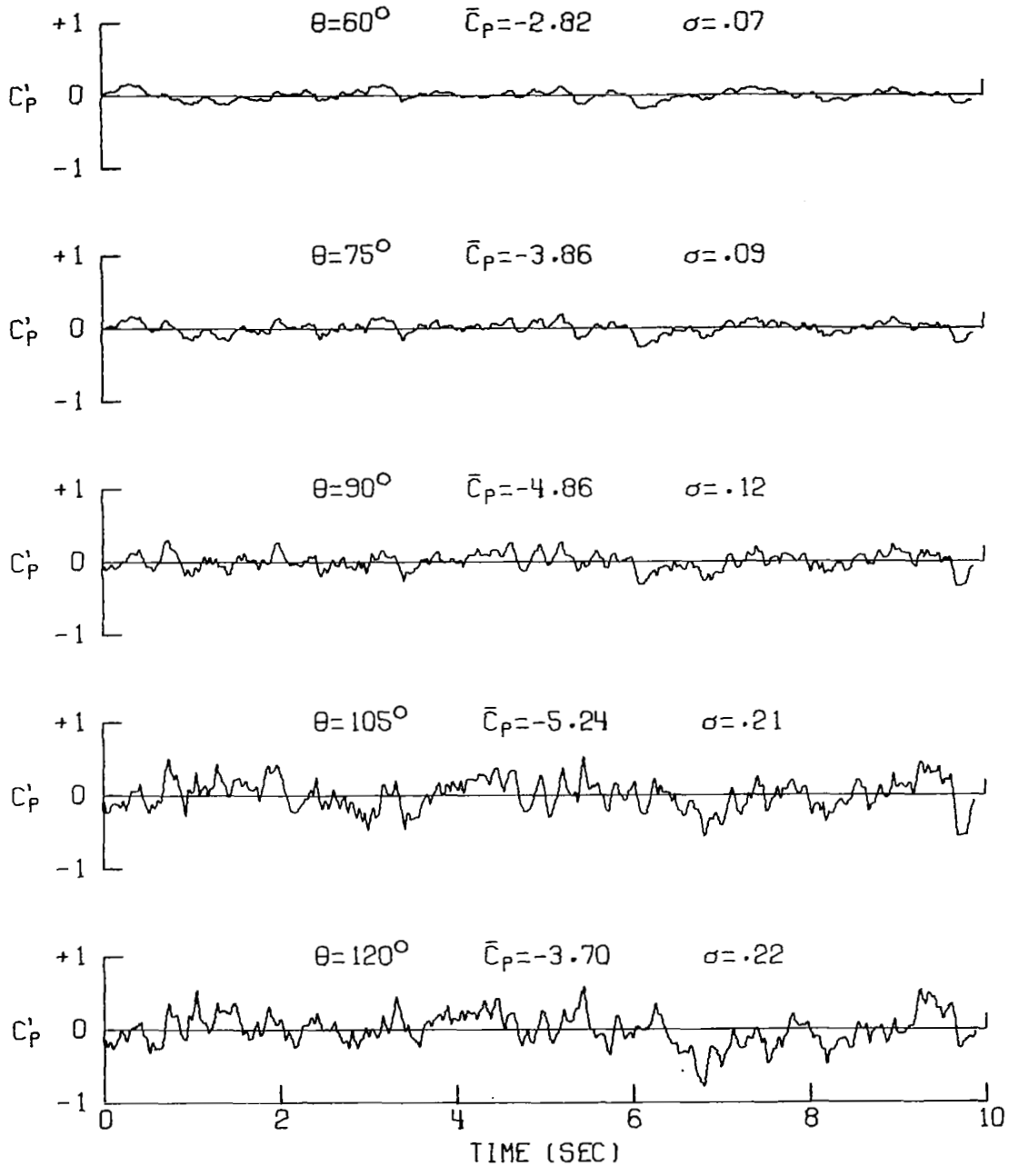

(a) Pressure ports at r/D = 0.58.

Figure 12.- Time variation of C_p with pressure-transducer output filtered. R = 4.1; M_j = 0.48.

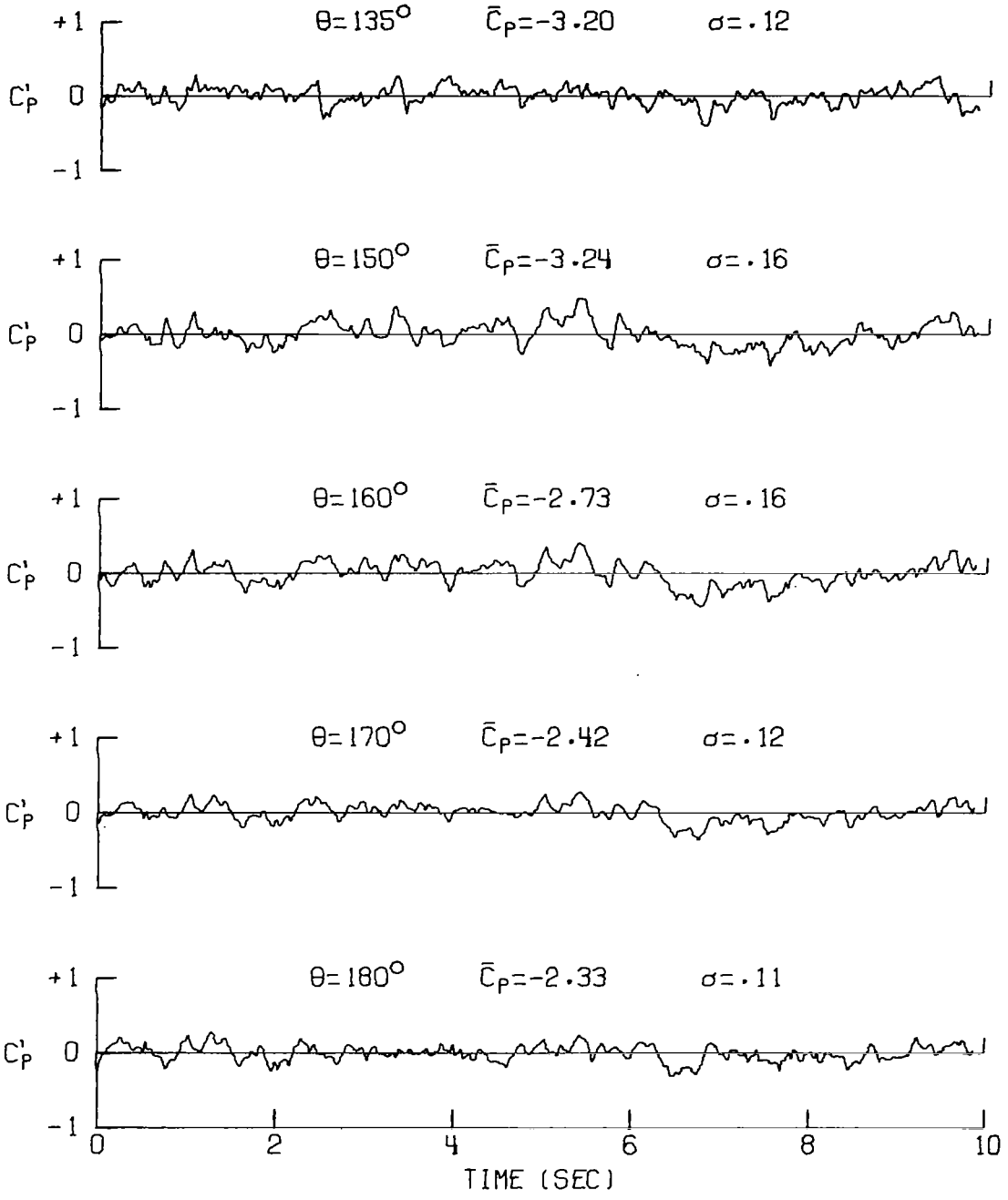

(a) Concluded.

Figure 12.- Continued.

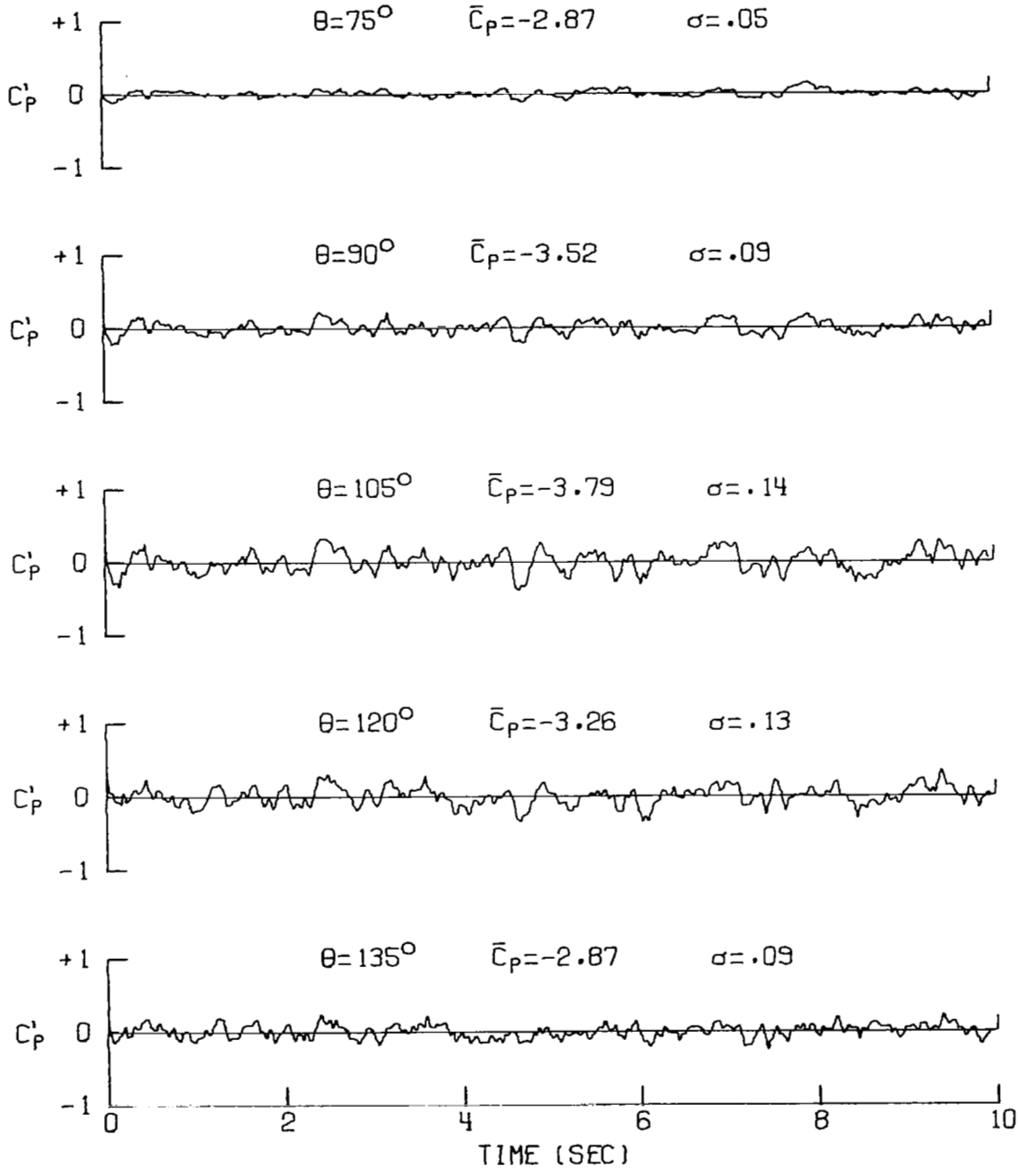

(b) Pressure ports at r/D = 0.70.

Figure 12.- Continued.

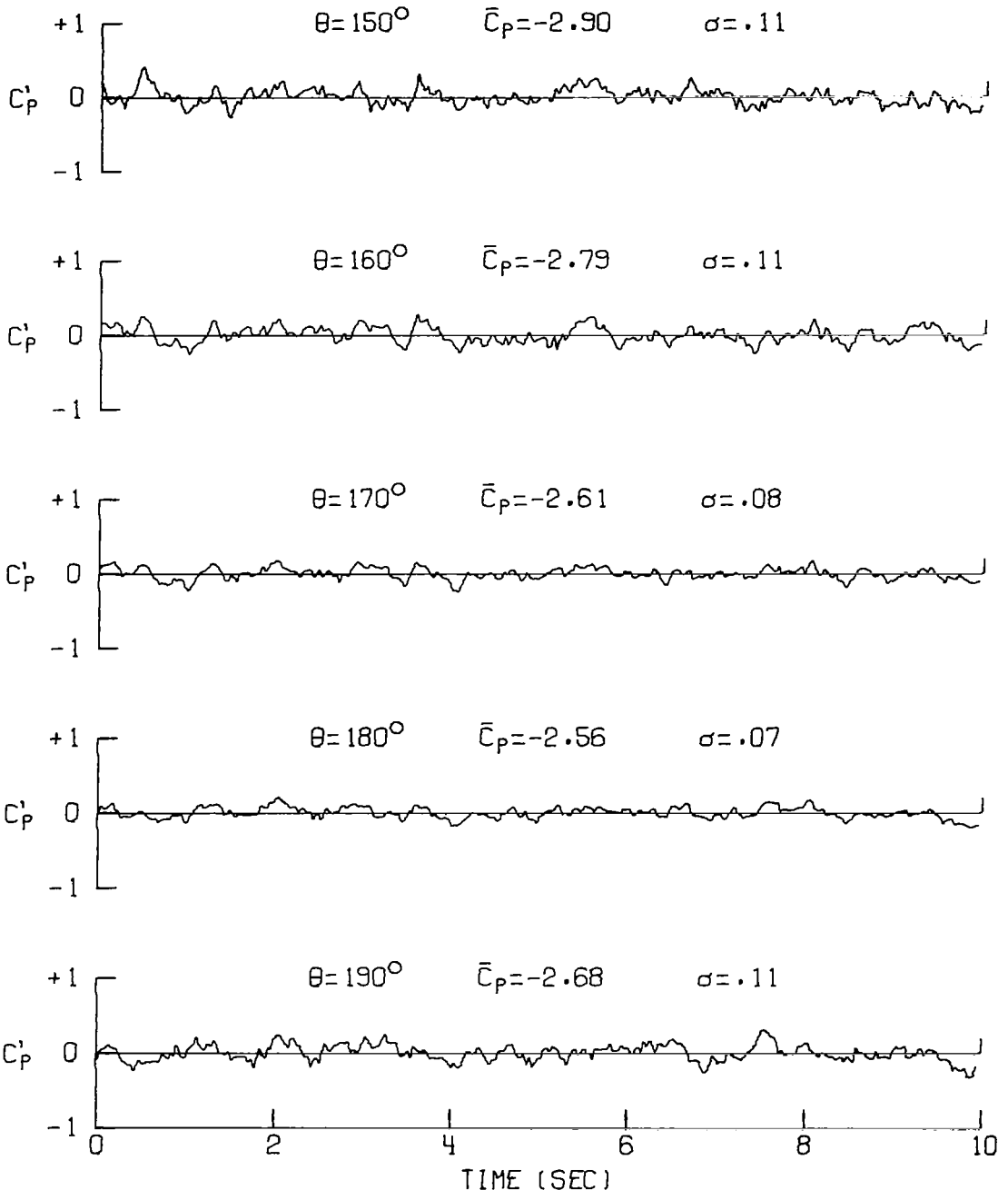

(b) Concluded.

Figure 12.- Continued.

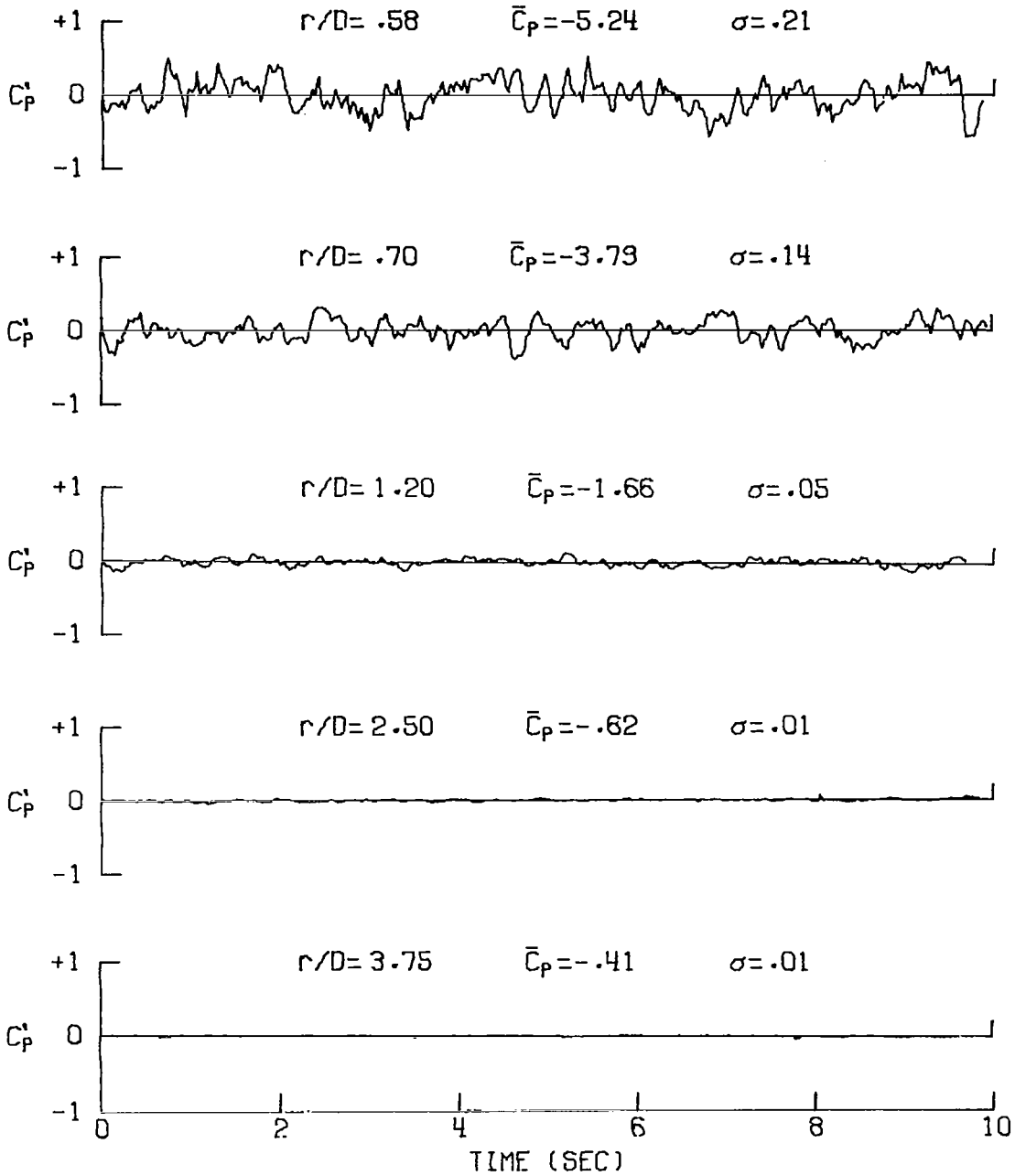

(c) Pressure ports at $\theta = 105^{o}$.

Figure 12.- Continued.

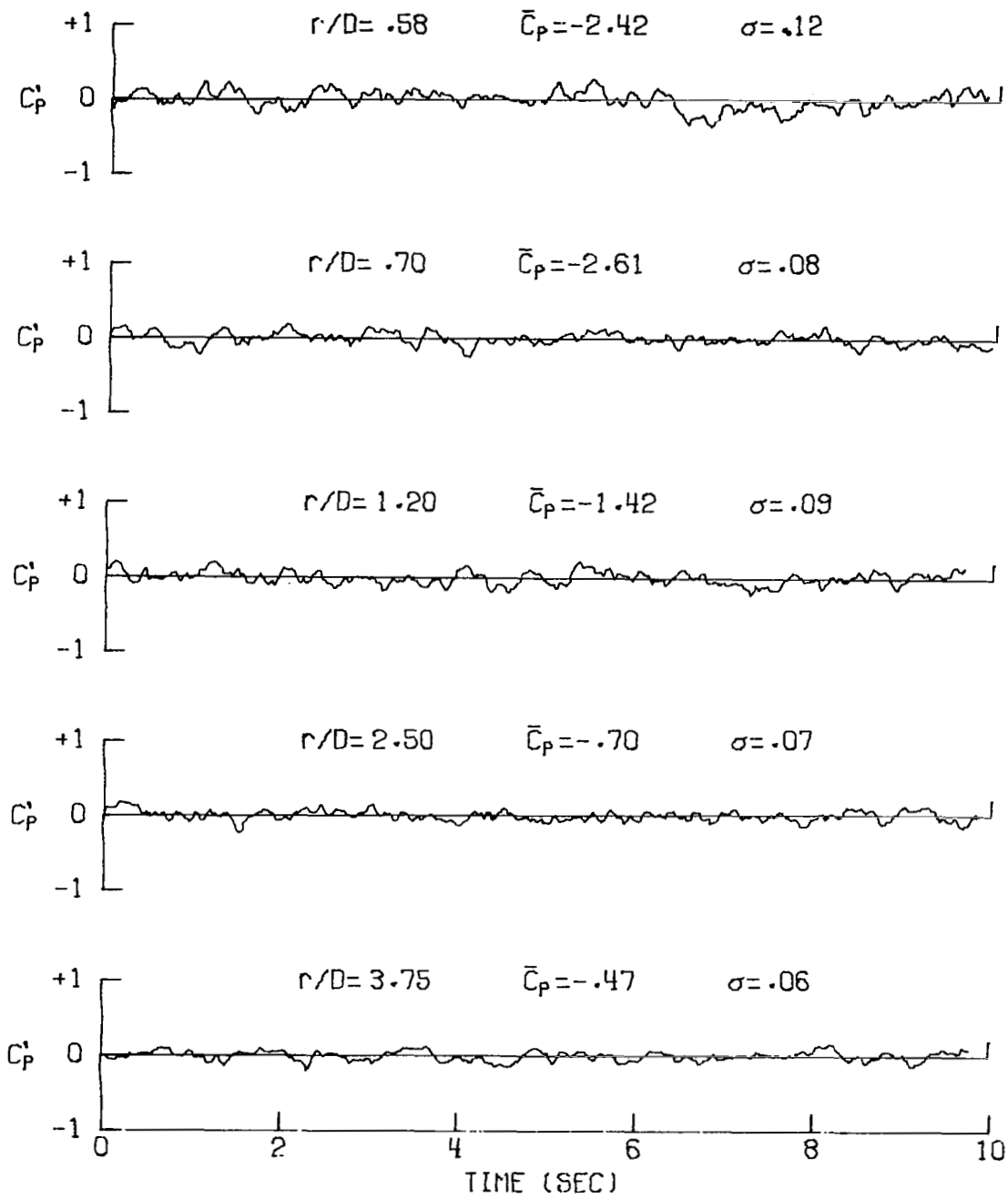

(d) Pressure ports at $\theta = 170^{o}$.

Figure 12.- Concluded.

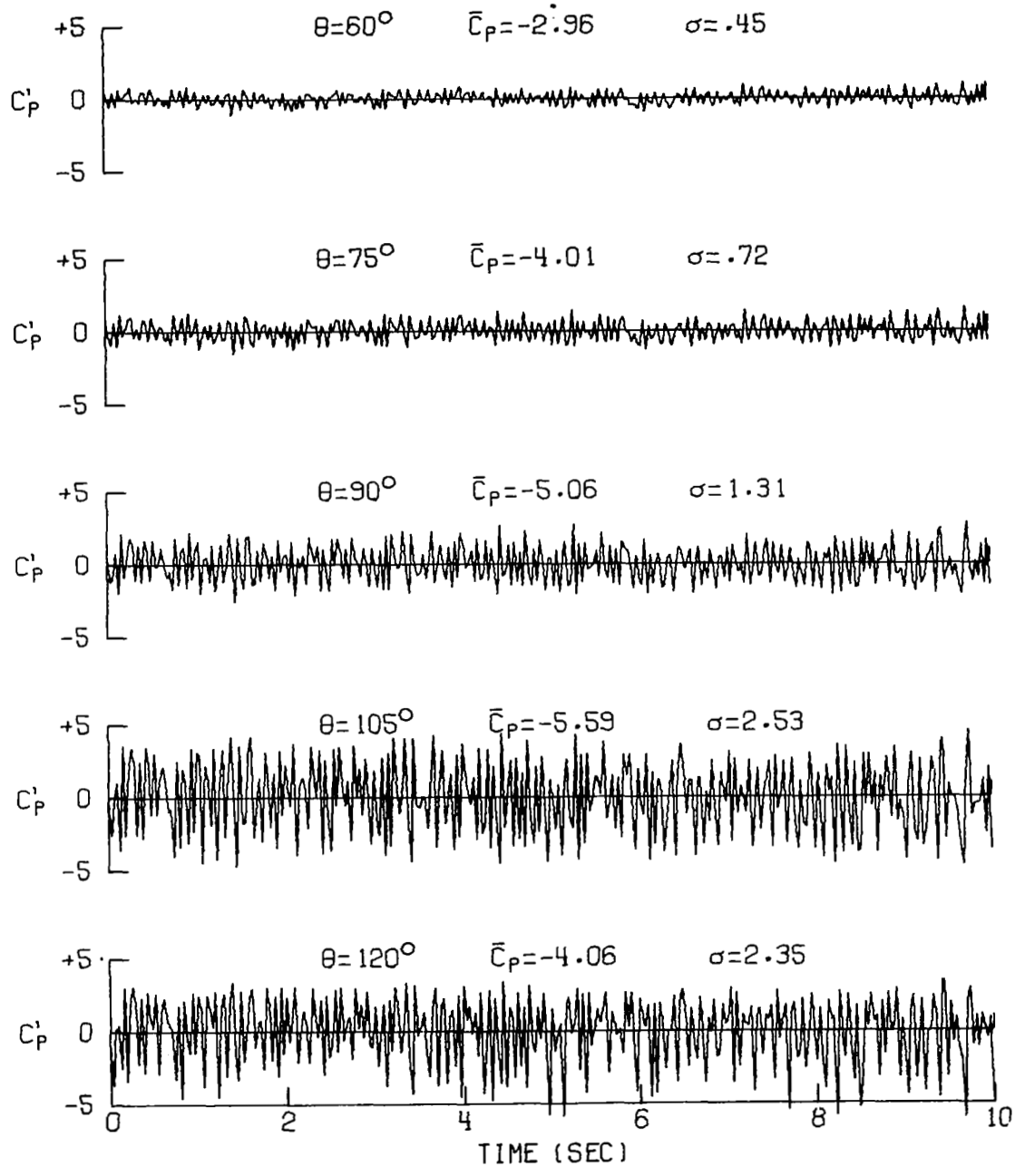

(a) Pressure ports at r/D = 0.58.

Figure 13.- Time variation of C_p with pressure-transducer output not filtered. R = 4.1; M_j = 0.48.

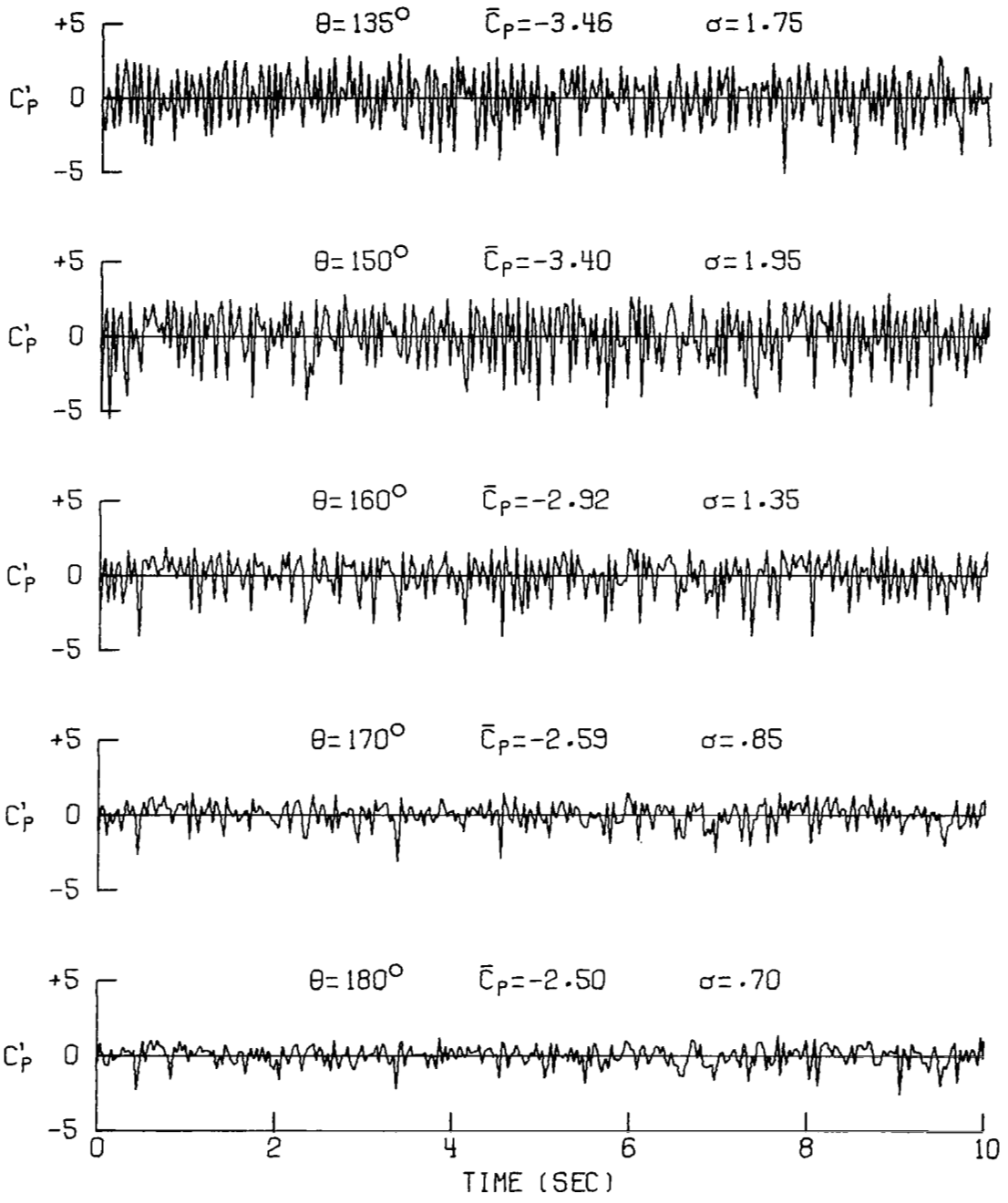

(a) Concluded.

Figure 13.- Continued.

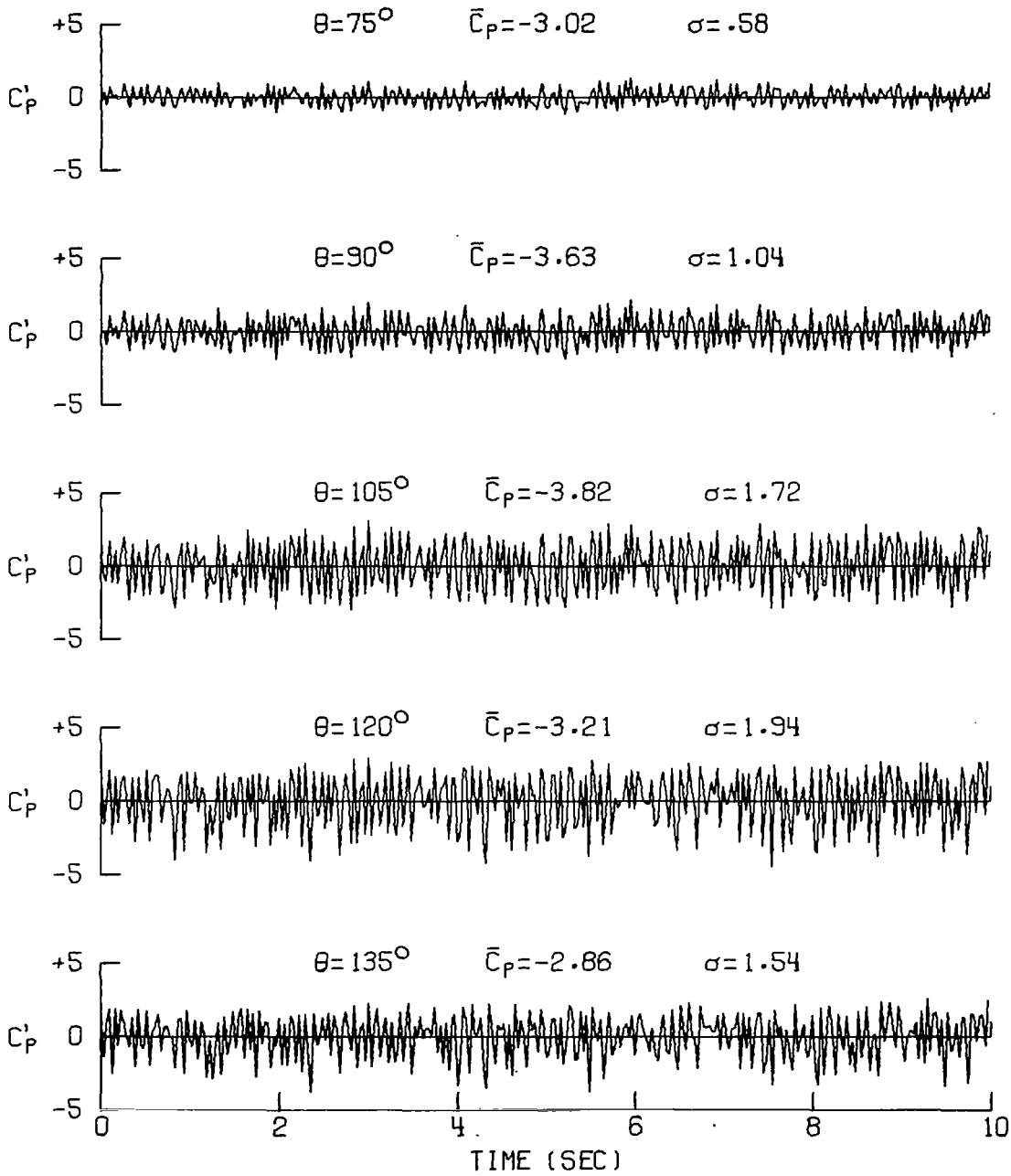

(b) Pressure ports at r/D = 0.70.

Figure 13.- Continued.

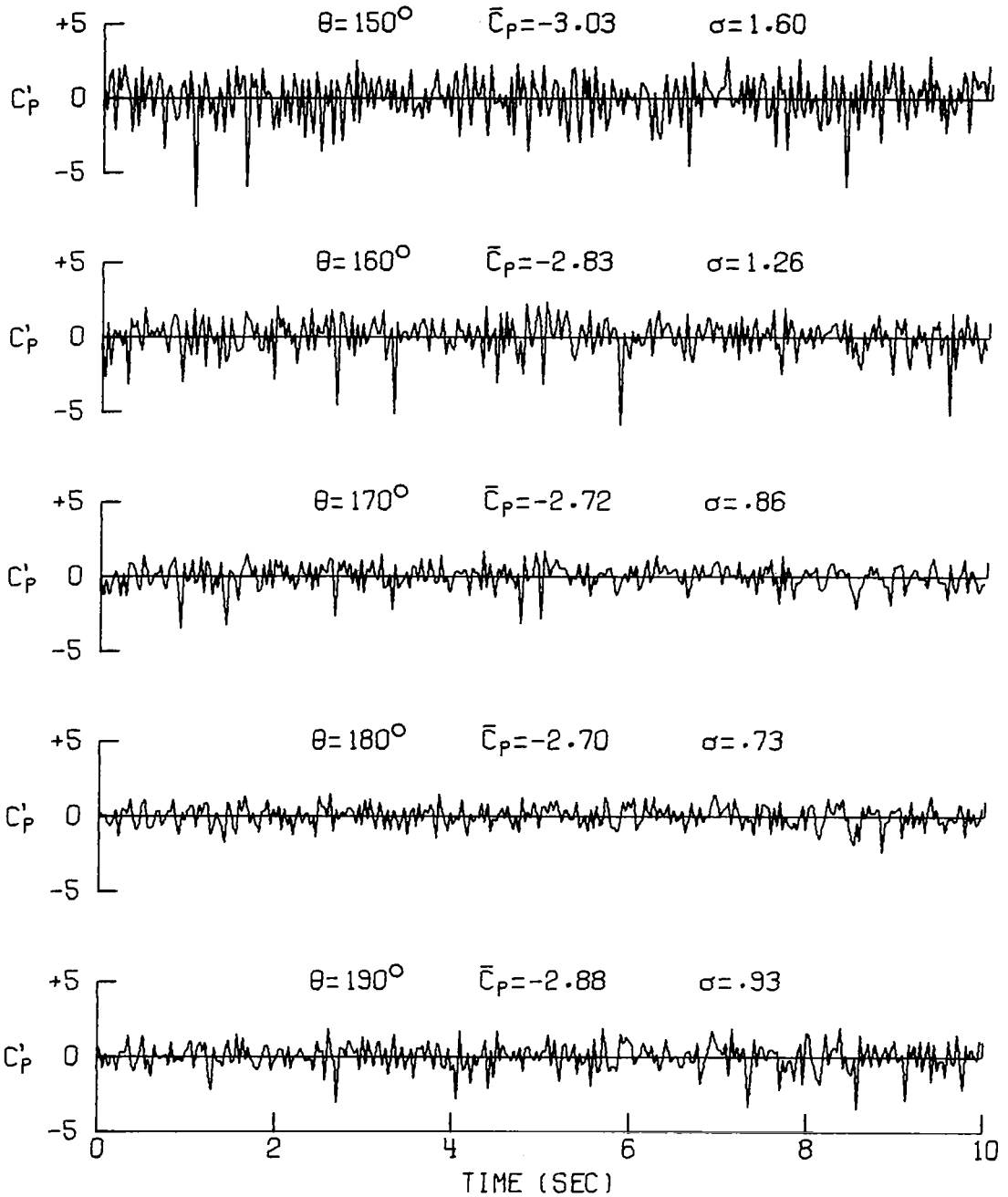

(b) Concluded.

Figure 13.- Continued.

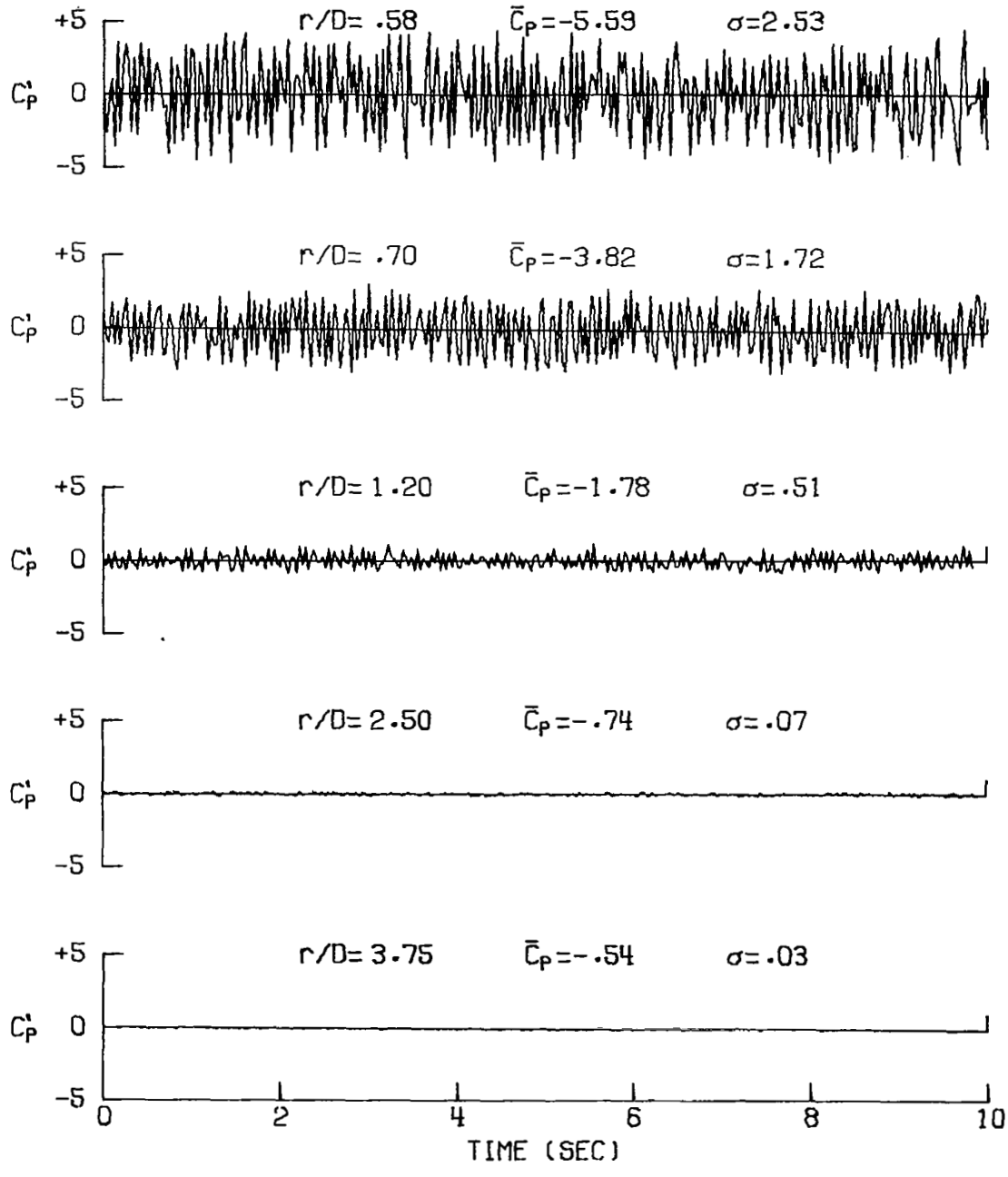

(c) Pressure ports at $\theta = 105^{o}$.

Figure 13.- Continued.

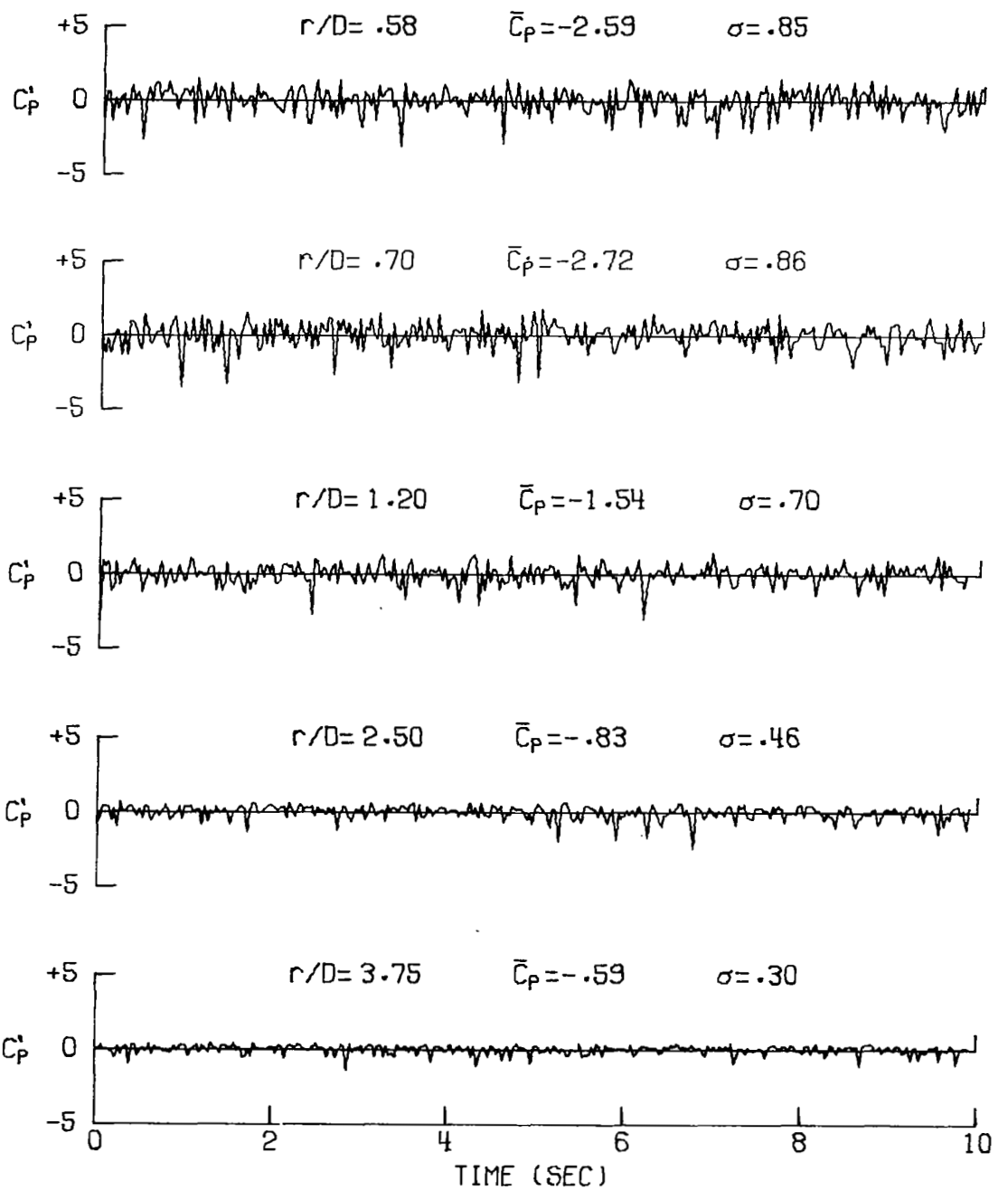

(d) Pressure ports at $\theta = 170^{o}$.

Figure 13.- Concluded.

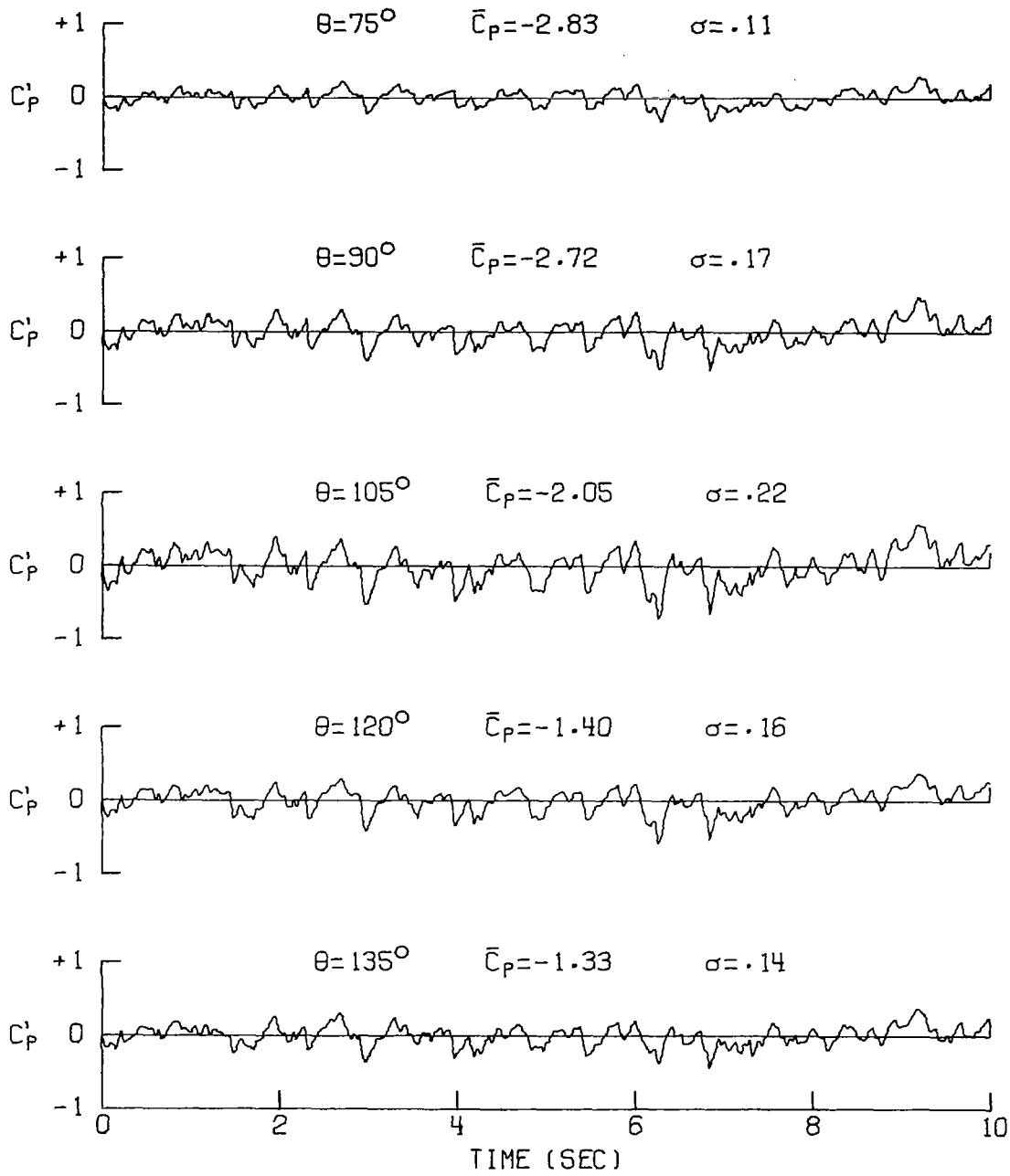

(a) Pressure ports at r/D = 0.70.

Figure 14.- Time variation of C_p with pressure-transducer output filtered. R = 8.0; M_j = 0.93.

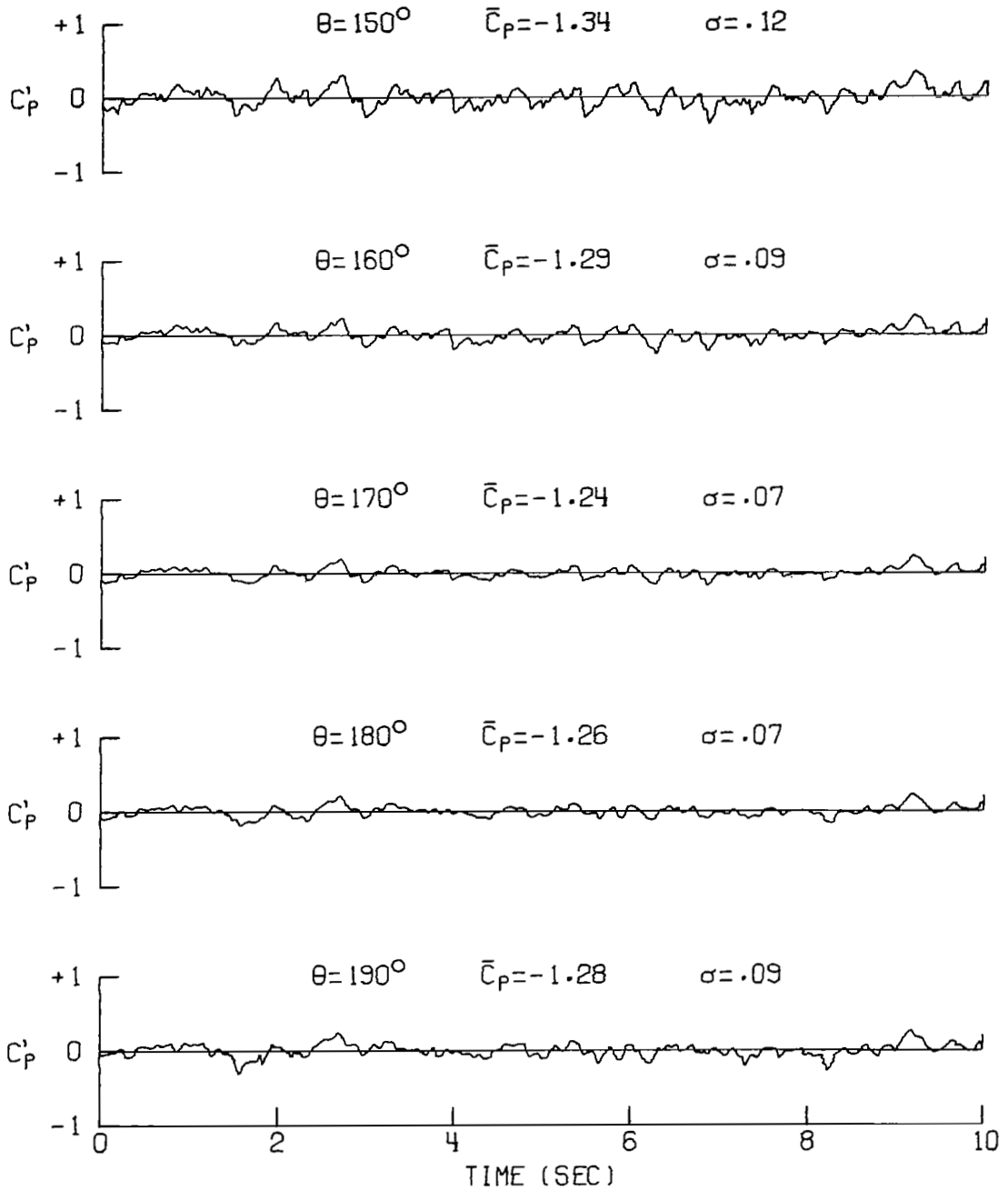

(a) Concluded.

Figure 14.- Continued.

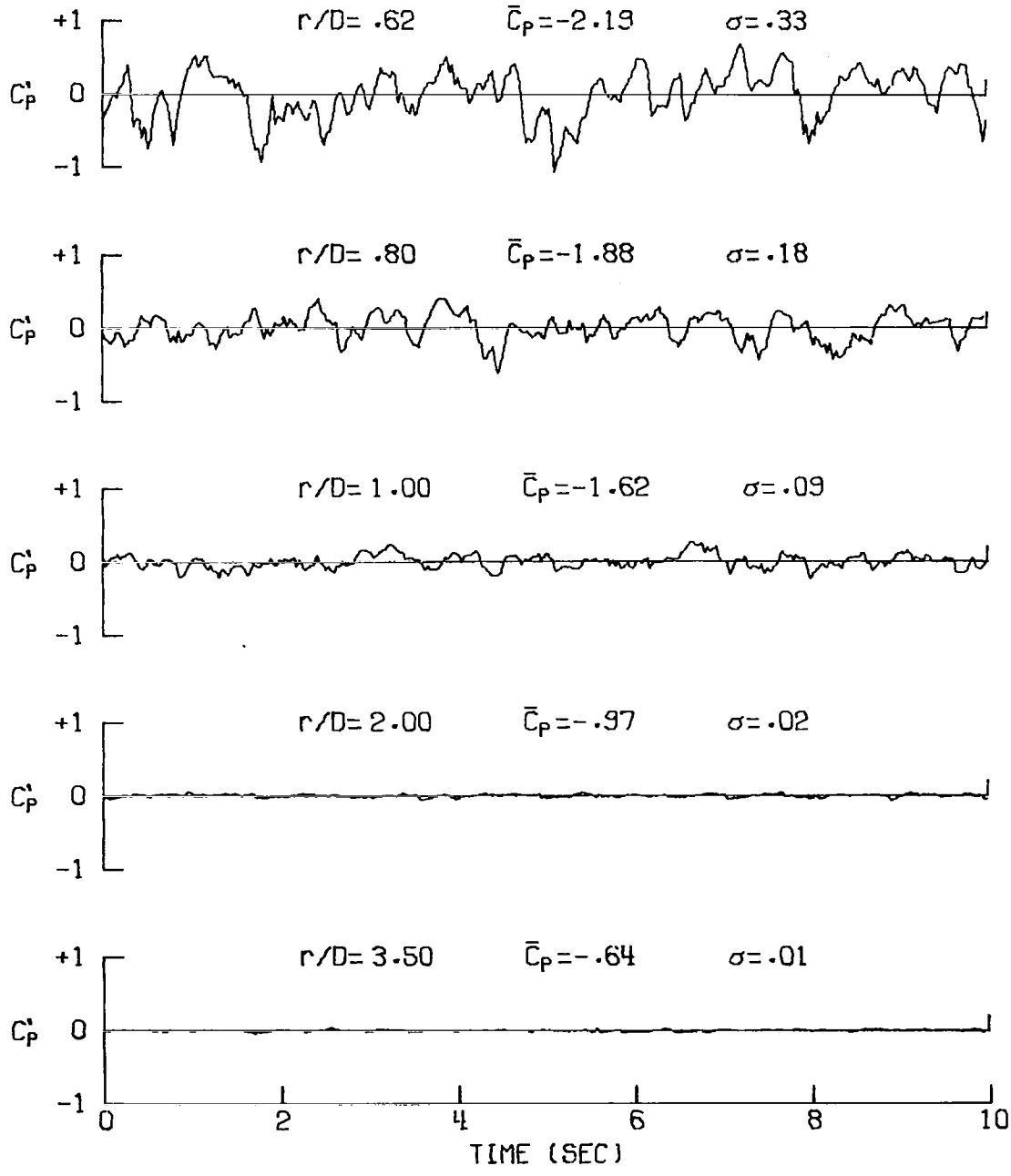

(b) Pressure ports at $\theta = 105^{o}$.

Figure 14.- Continued.

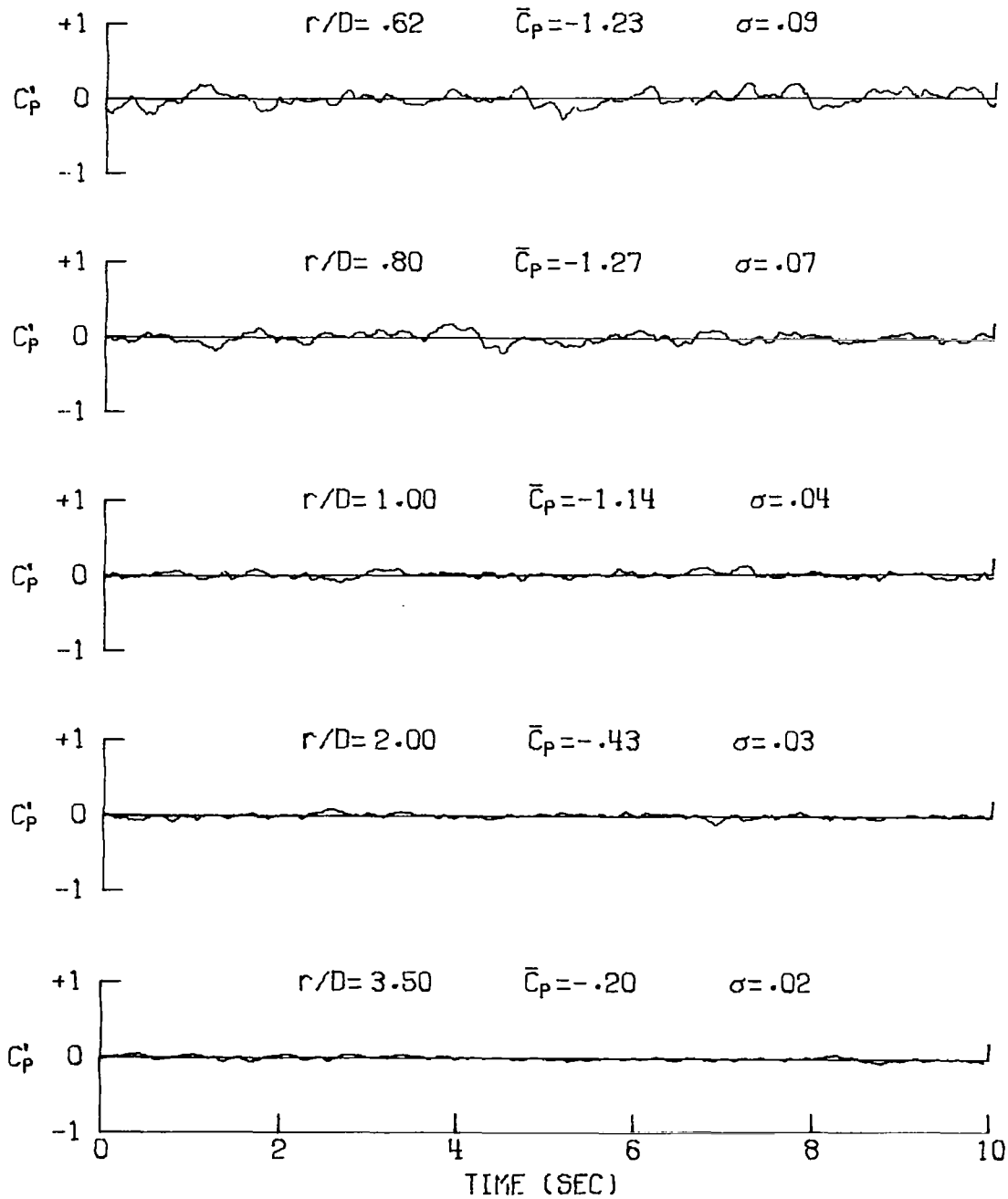

(c) Pressure ports at $\theta = 170^{o}$.

Figure 14.- Concluded.

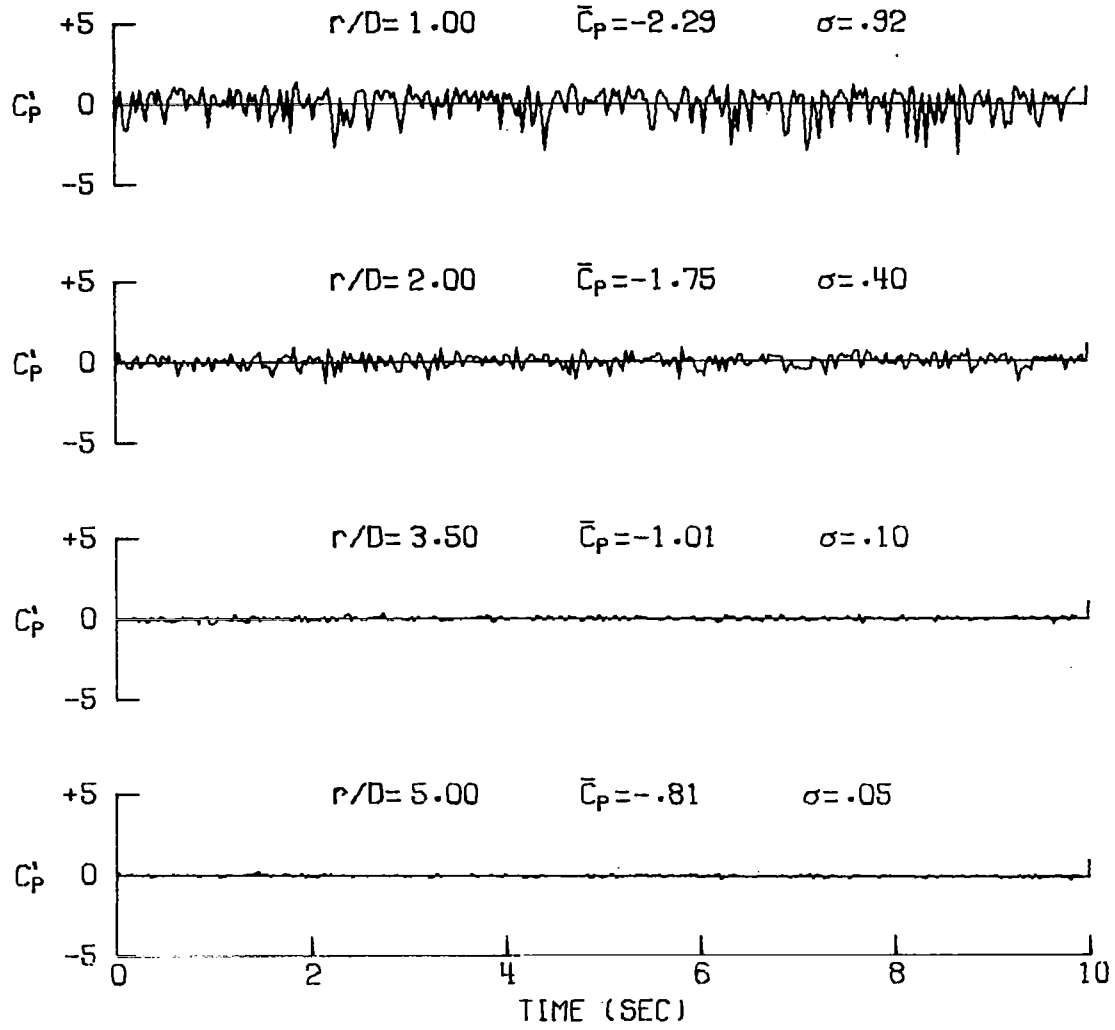

(a) Pressure ports at $\theta = 105^{o}$.

Figure 15.- Time variation of C_p with pressure-transducer output not filtered. R = 8.0; M_j = 0.93.

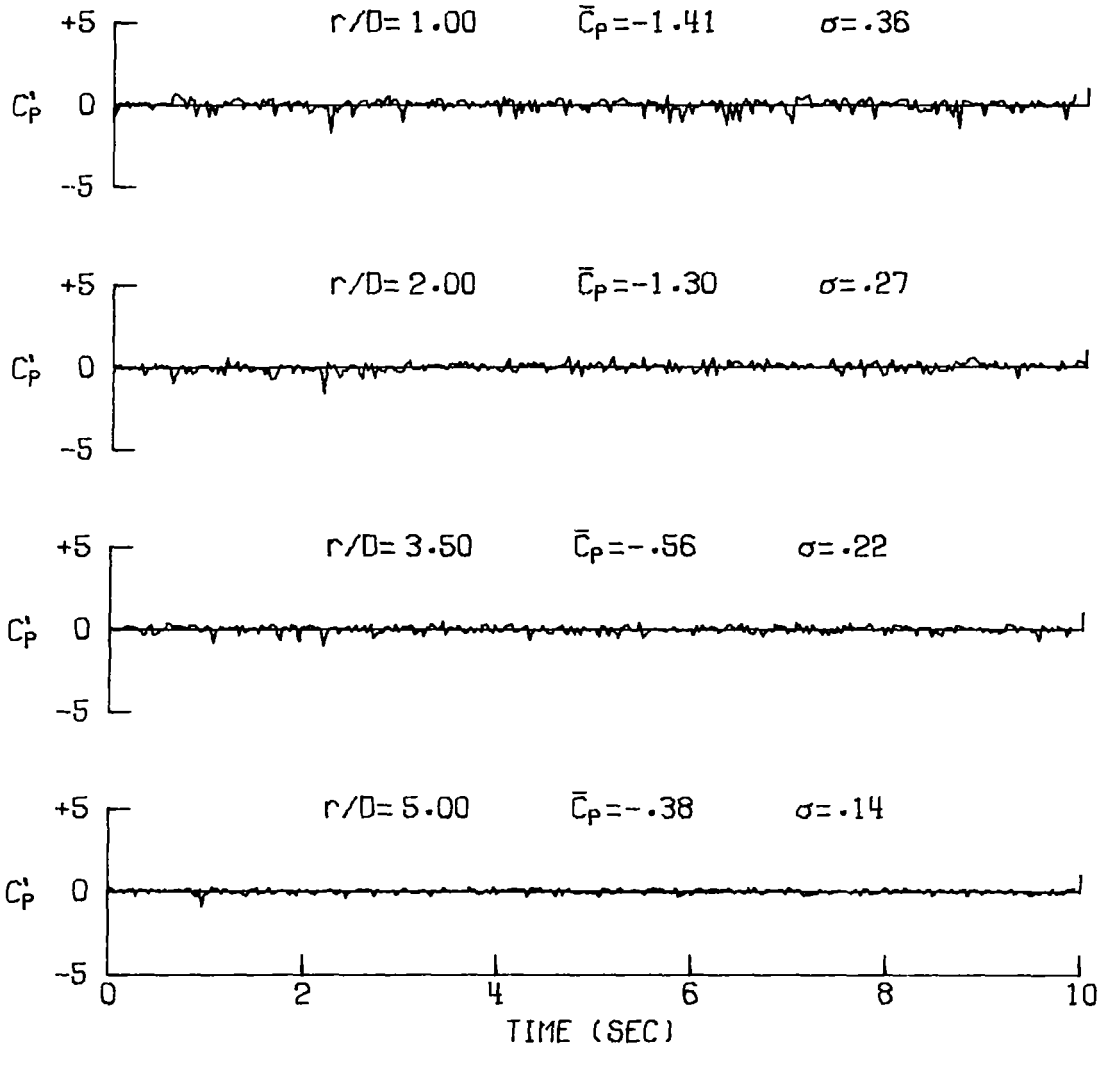

(b) Pressure ports at $\theta = 170^{o}$.

Figure 15.- Concluded.

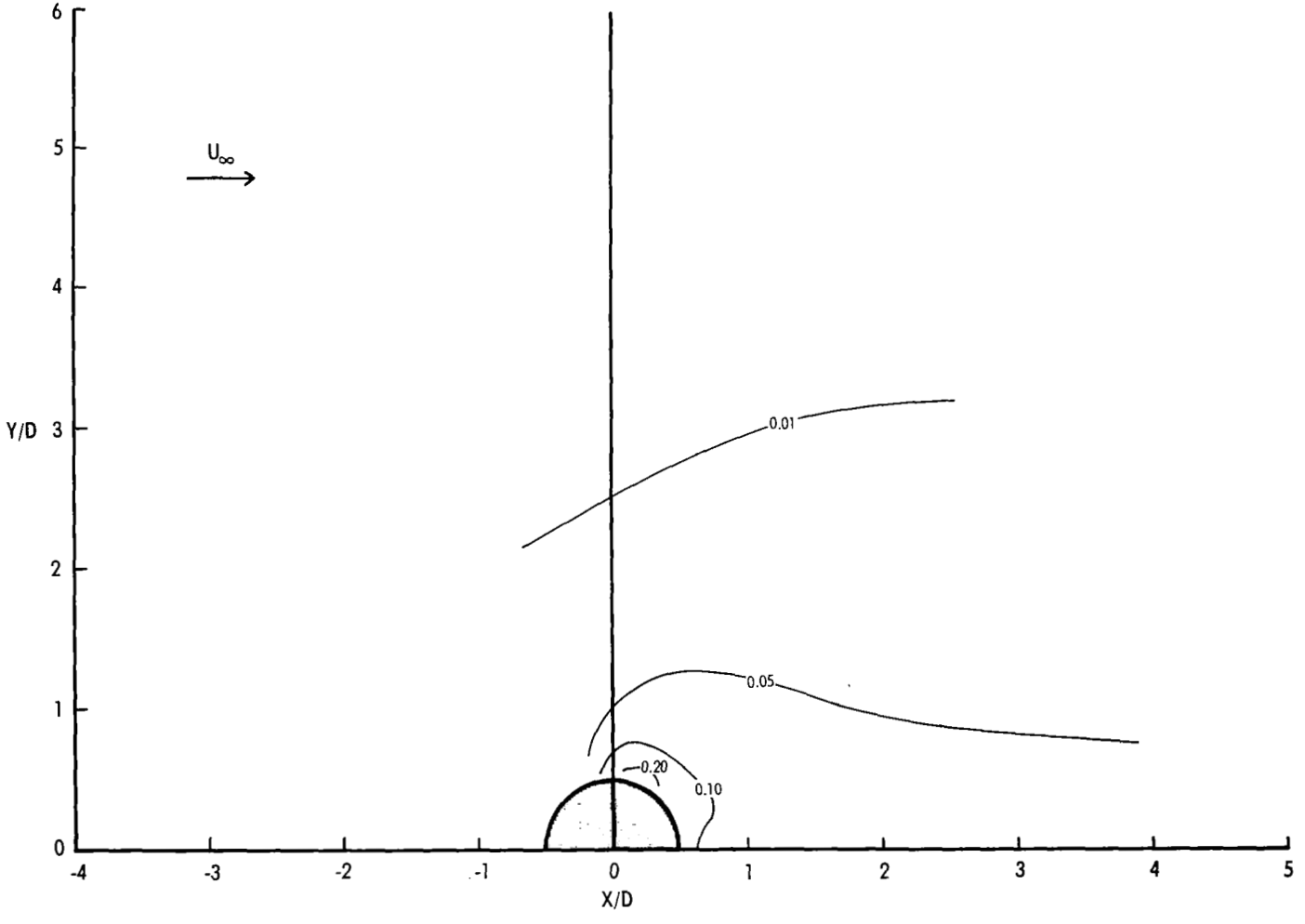

(a) R = 4.1; M_j = 0.48.

Figure 16.- Contours of constant σ.

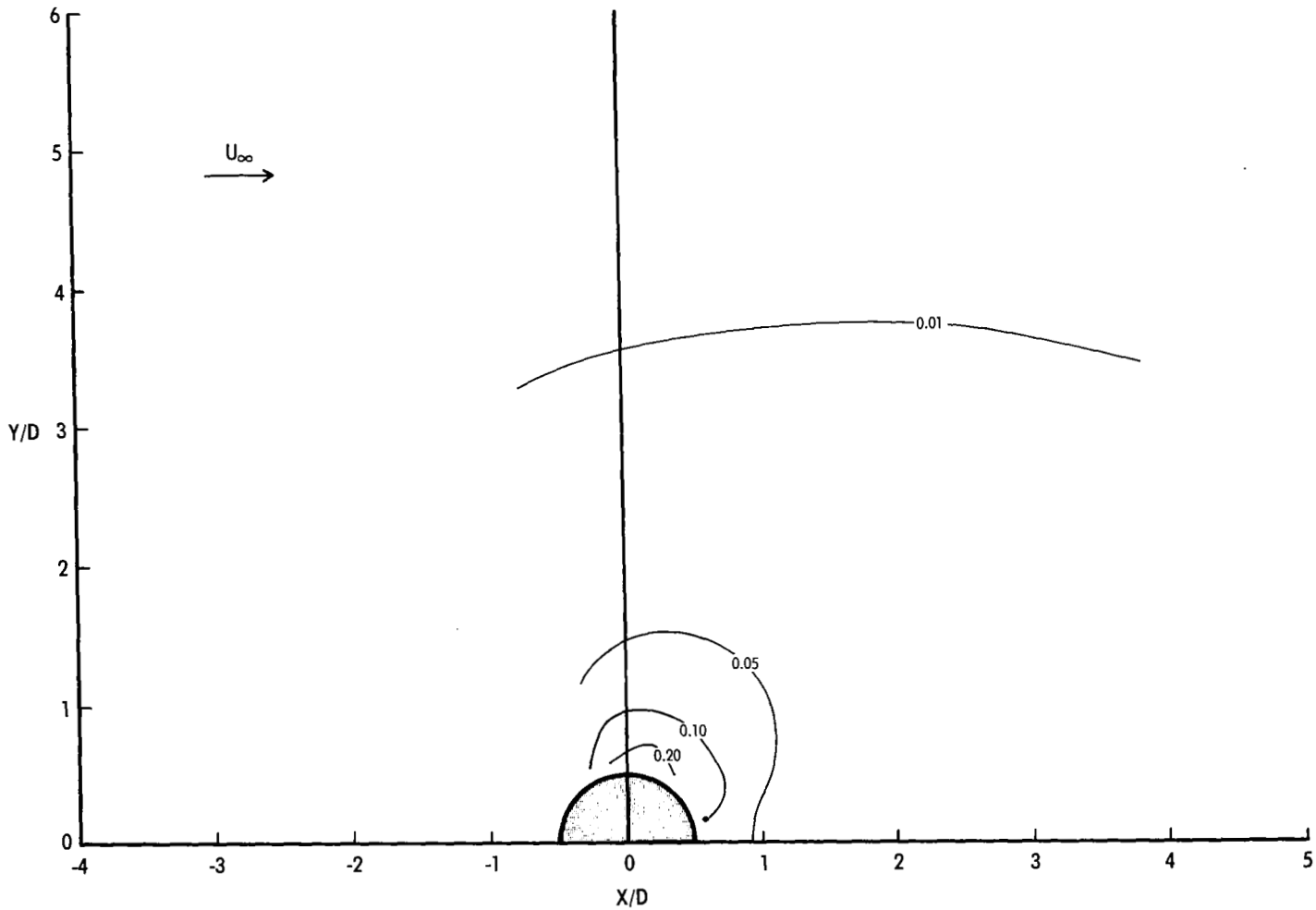

(b) R = 8.0; M_j = 0.93.

Figure 16.- Concluded.

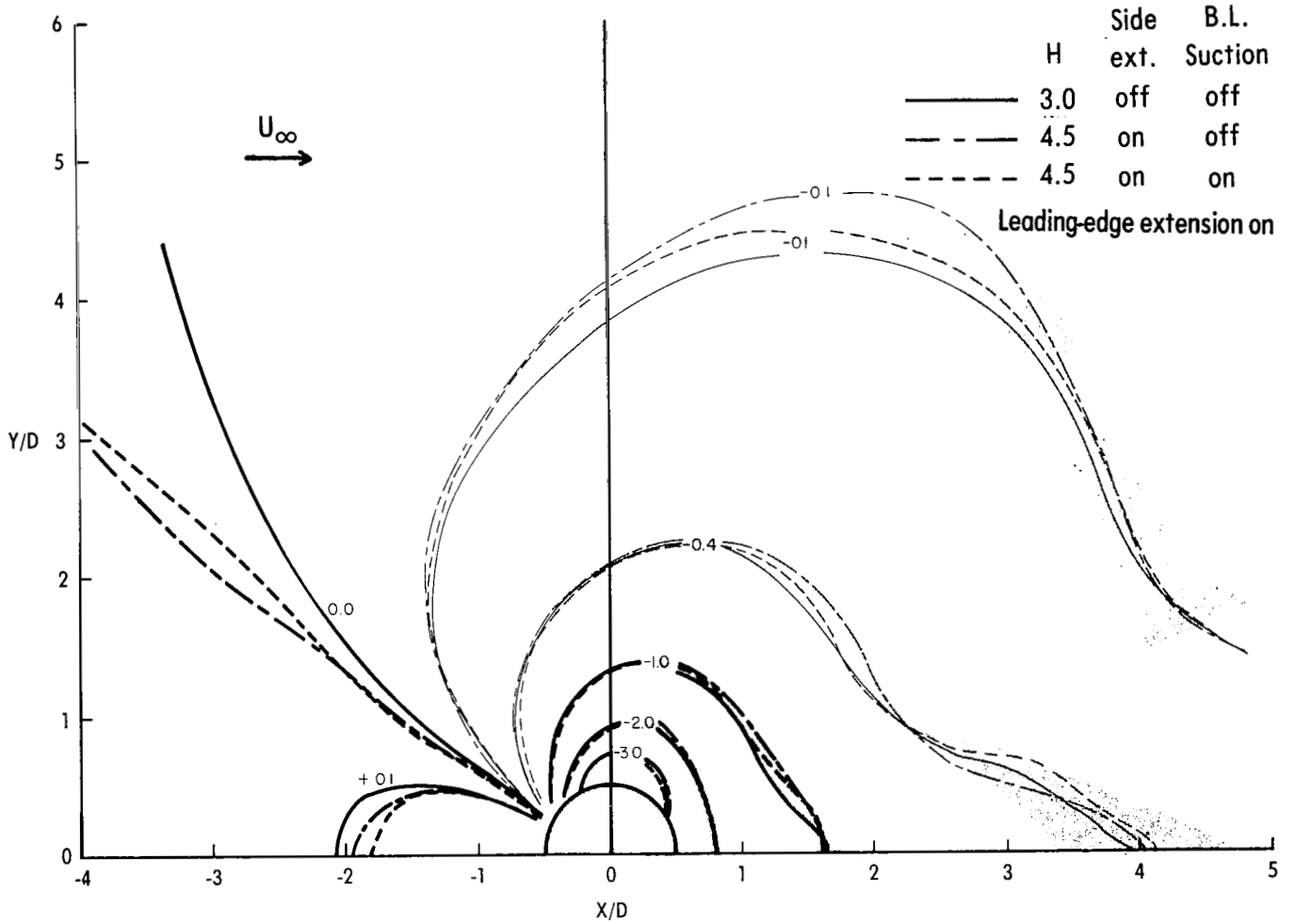

(a) Uncertainty due to measured fluctuations in C_p. $\Delta C_p = \sigma$.

Figure 17.- Effect of test conditions (see table 1) on pressure distribution and uncertainty bands.

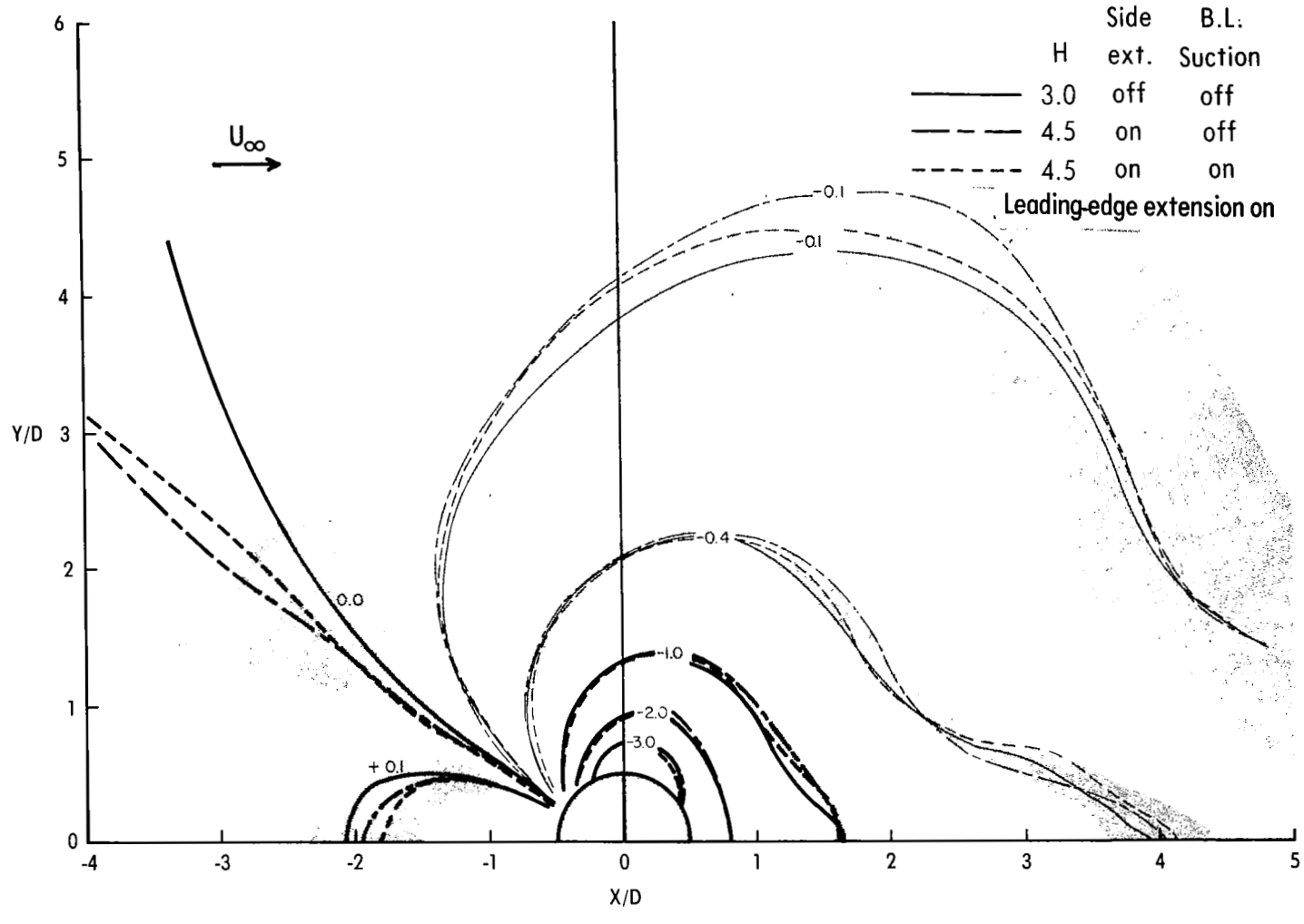

(b) Uncertainty due to pressure-transducer errors. $\Delta C_p = 0.036$.

Figure 17.- Concluded.

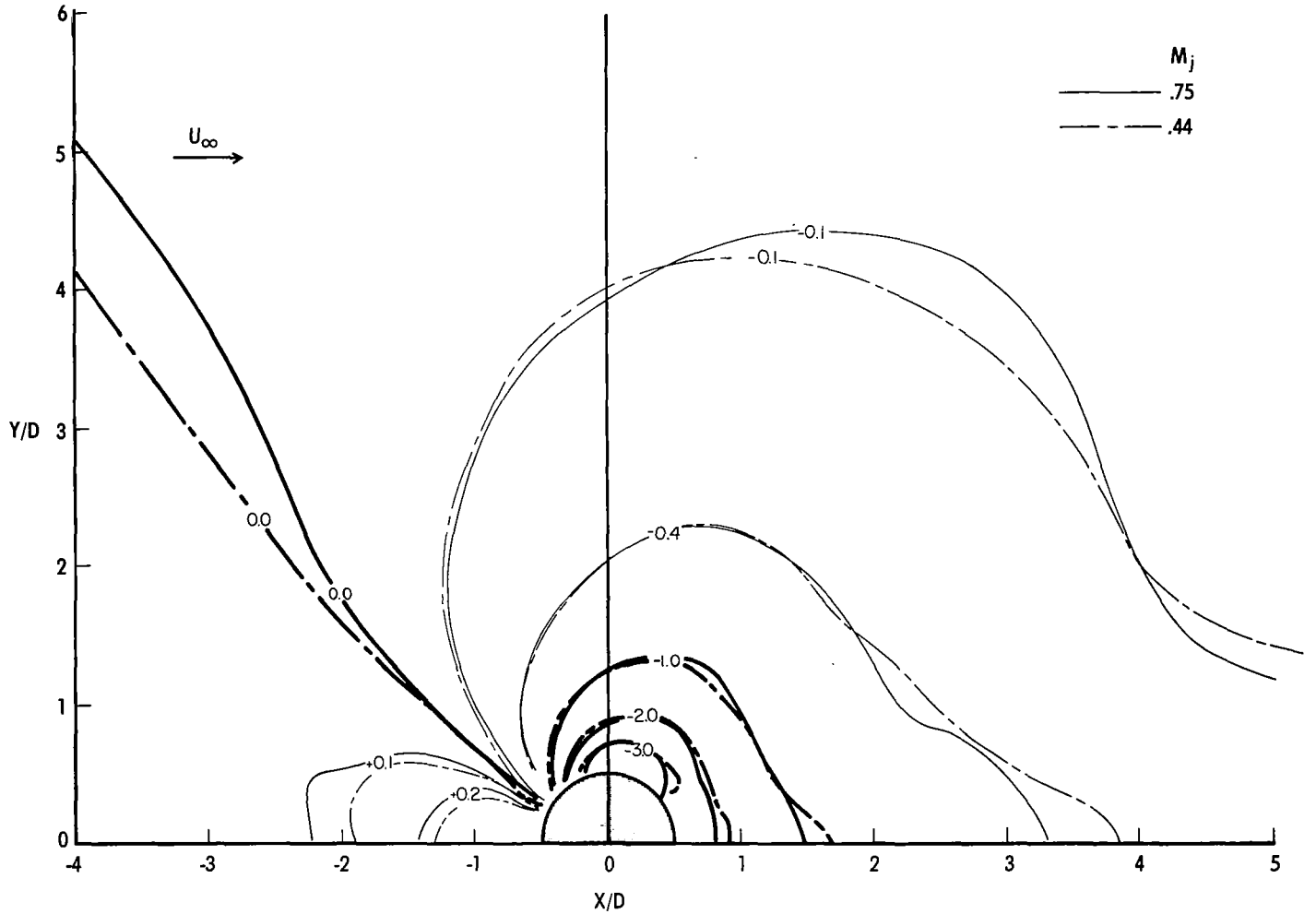

(a) R = 4.

Figure 18.- Effect of changing jet Mach number on pressure distribution.

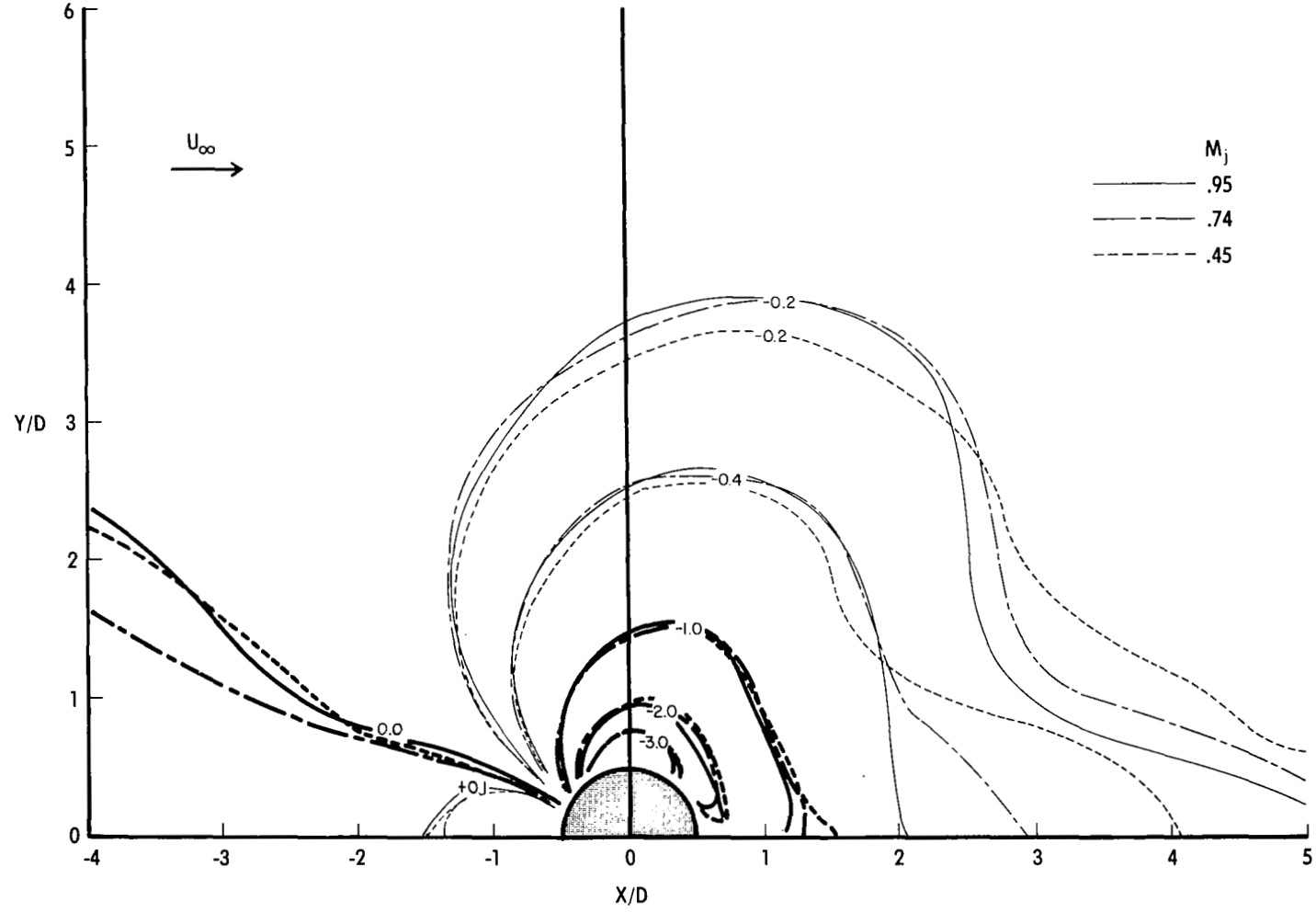

(b) R = 5.

Figure 18.- Continued.

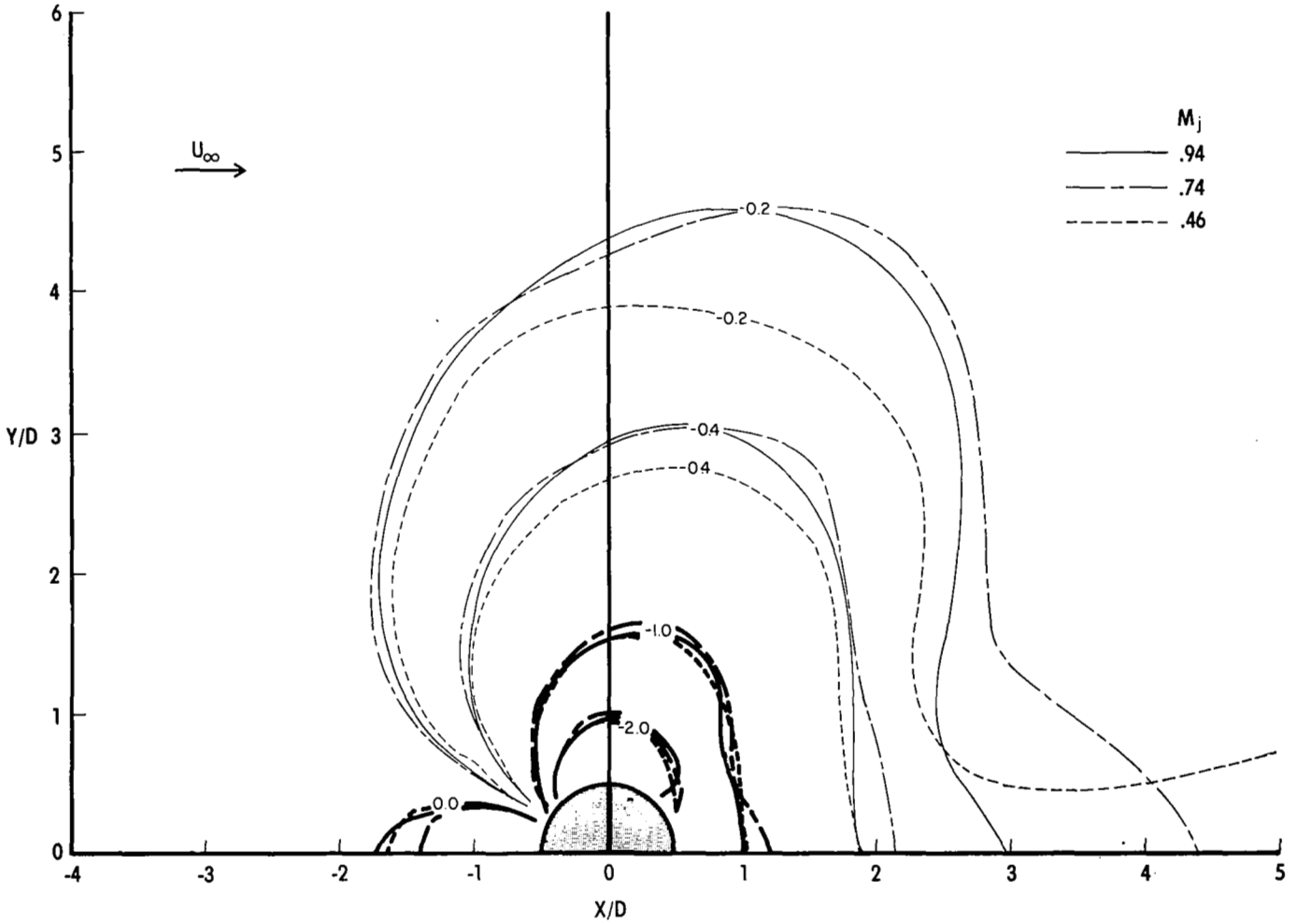

(c) R = 6.

Figure 18.- Continued.

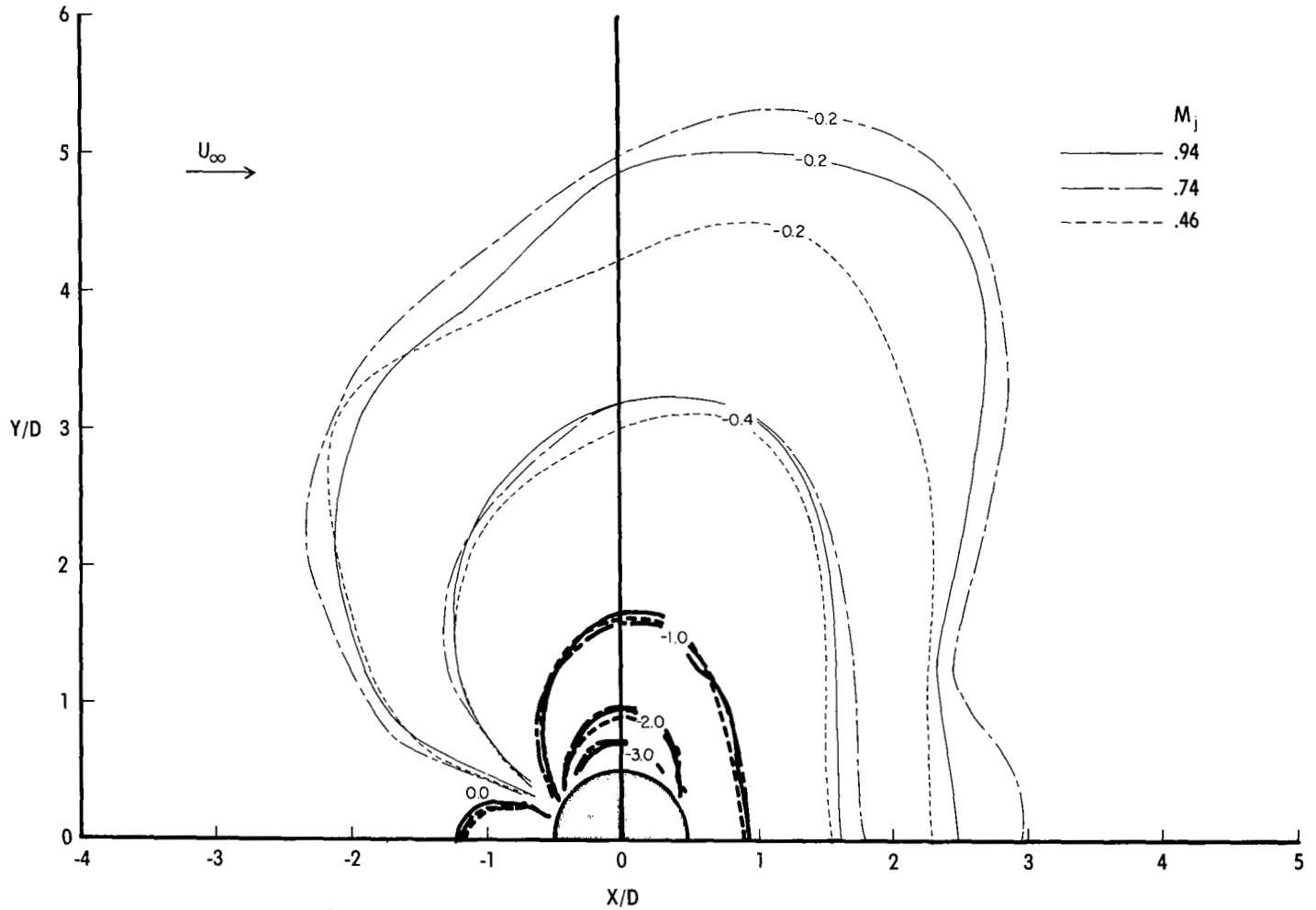

(d) R = 7.

Figure 18.- Continued.

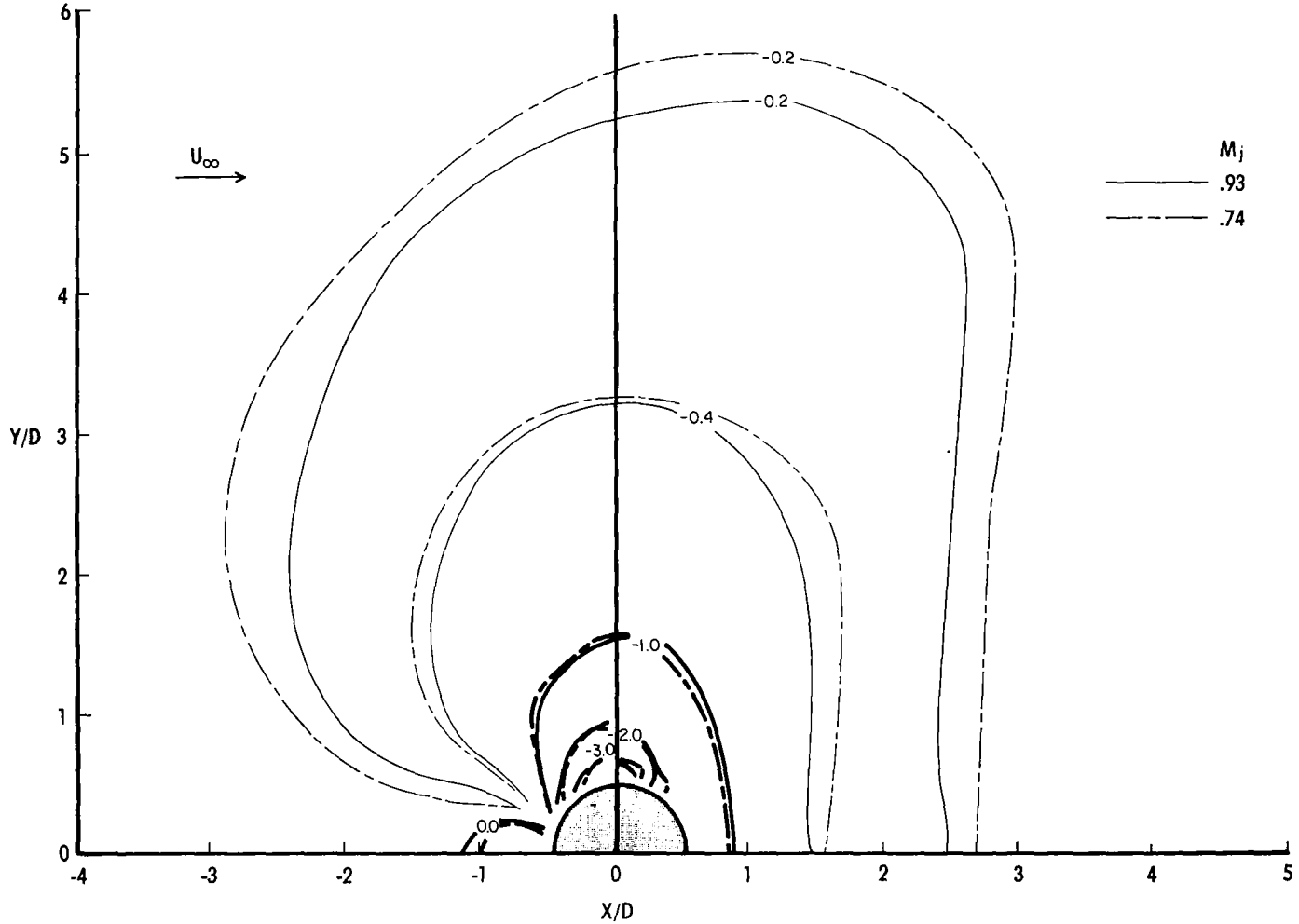

(e) R = 8.

Figure 18.- Continued.

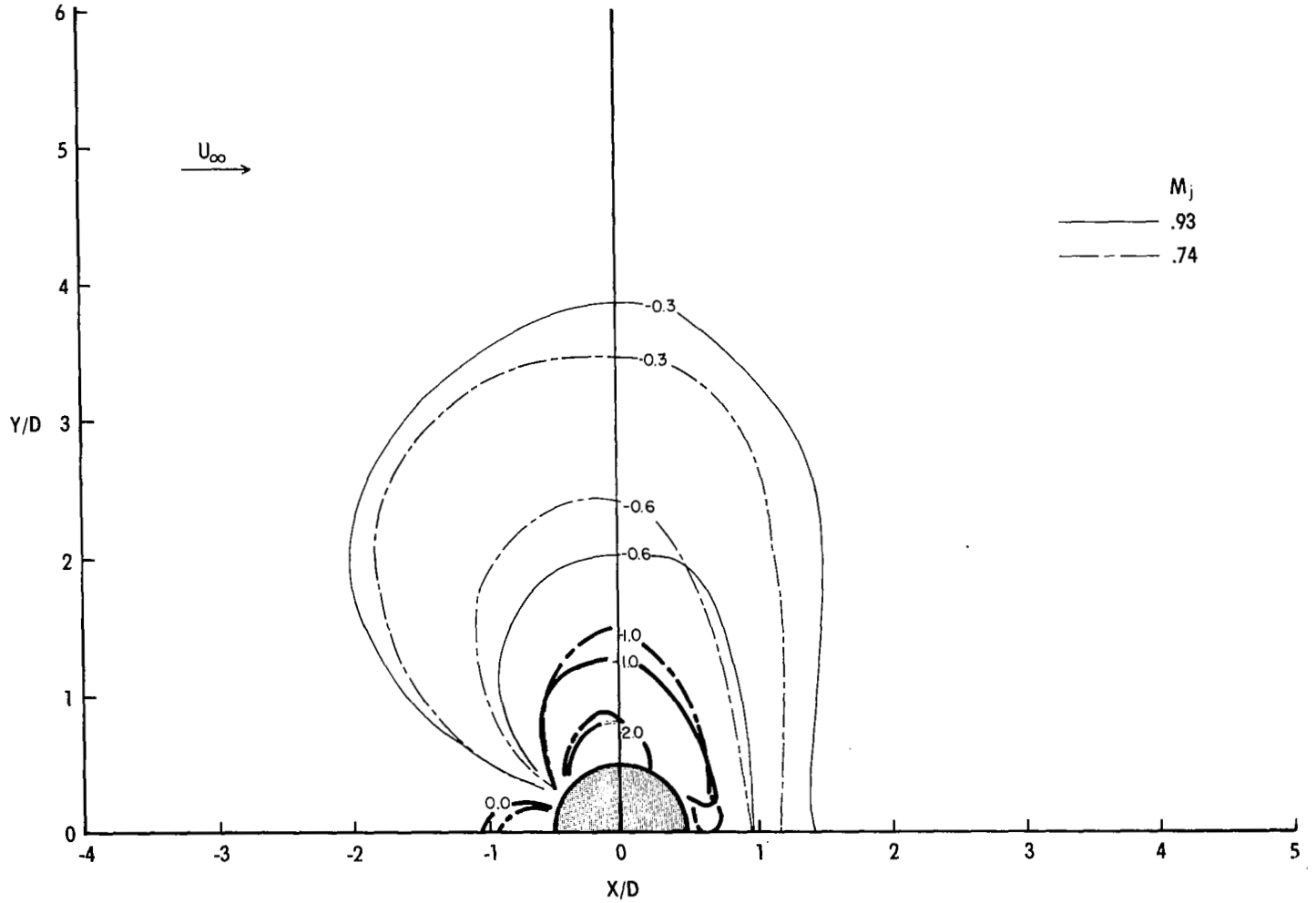

(f) R = 10.

Figure 18.- Concluded.

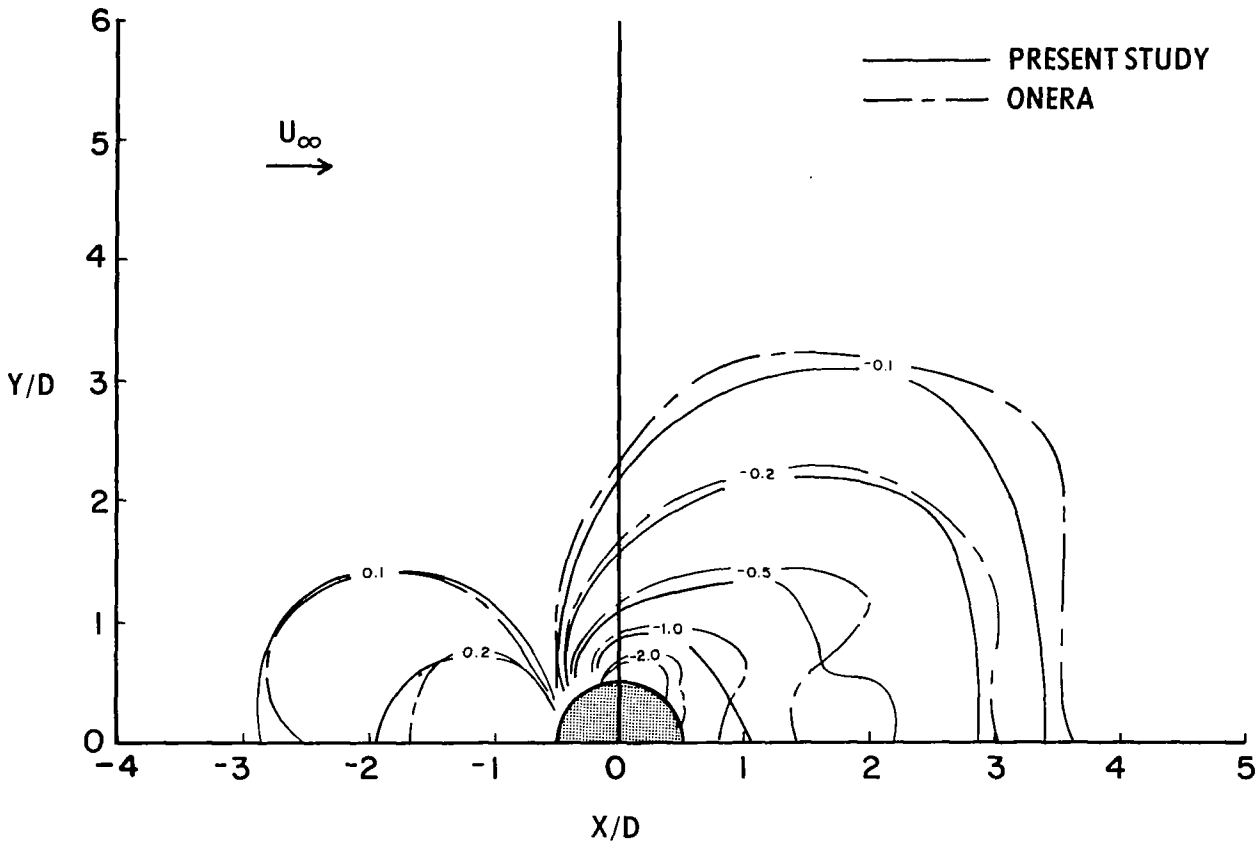

(a) R = 2; M_∞ = 0.09.

Figure 19.- Comparison with Soullier (ref. 21).

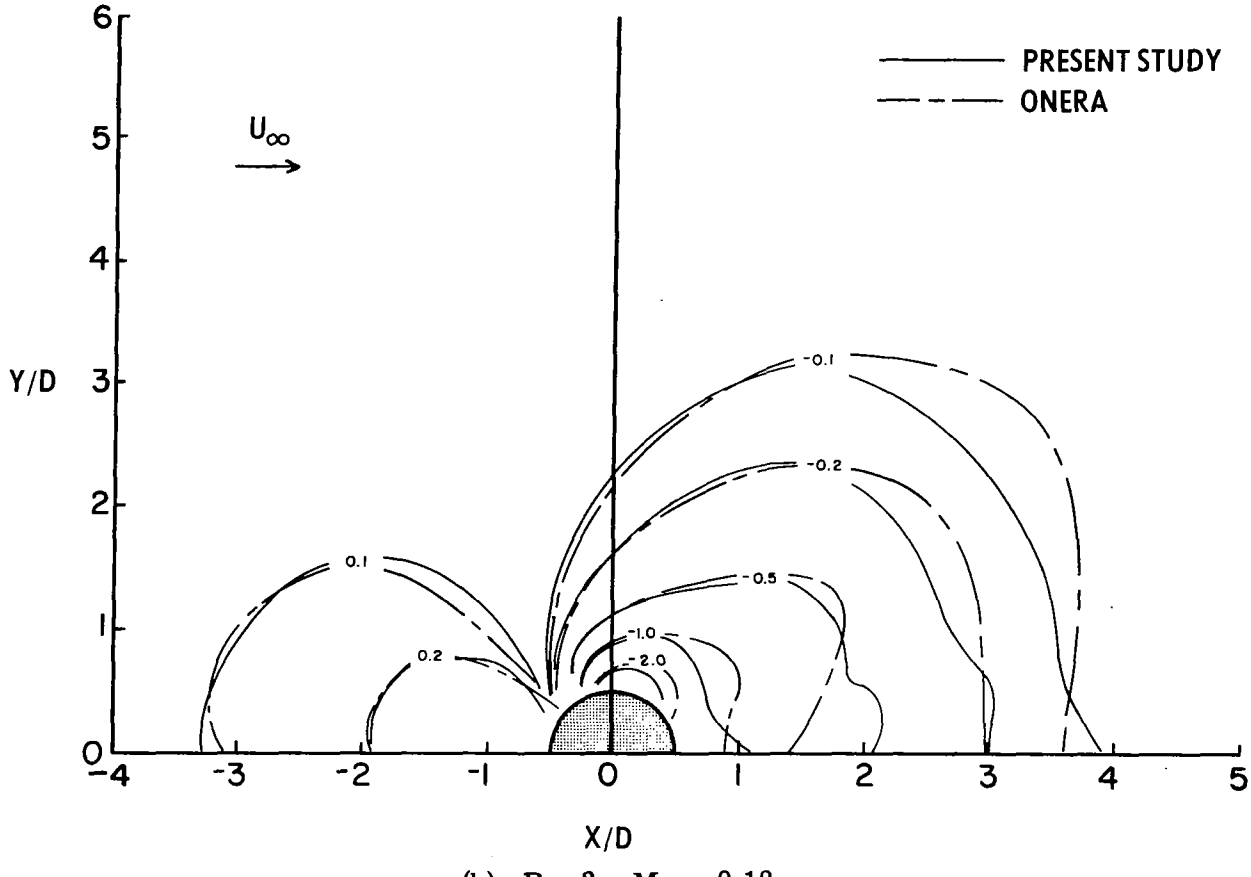

(b) R = 2; M_∞ = 0.18.

Figure 19.- Continued.

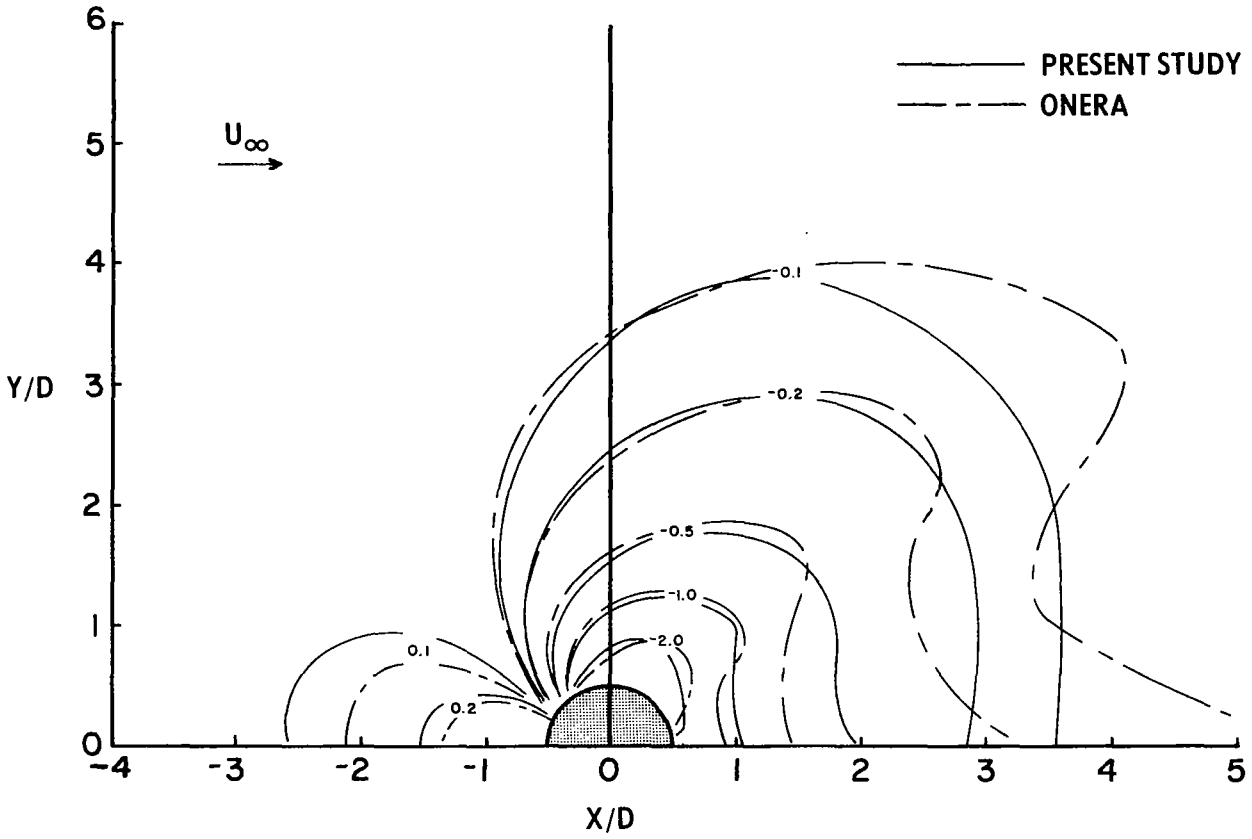

(c) R = 3; $M_\infty = 0.09$.

Figure 19.- Continued.

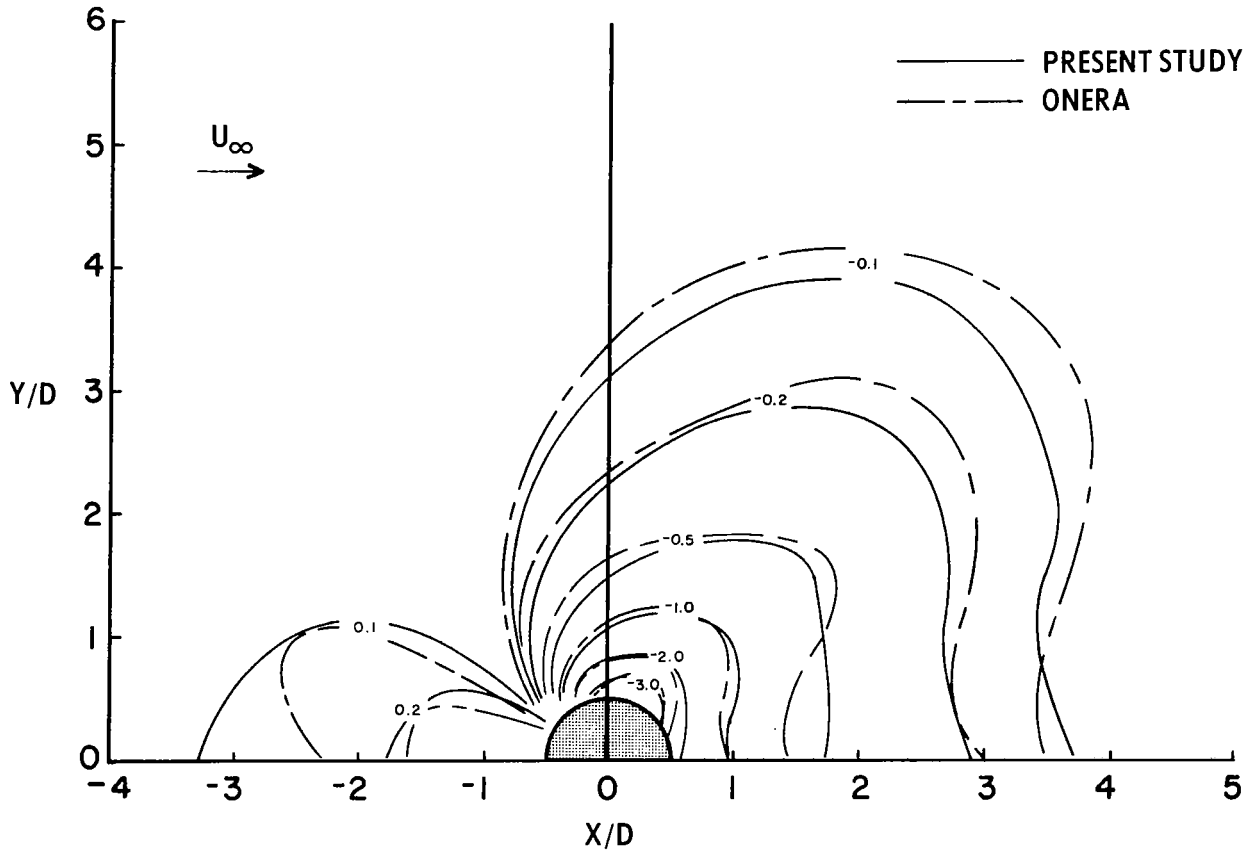

(d) R = 3; $M_\infty = 0.18$.

Figure 19.- Continued.

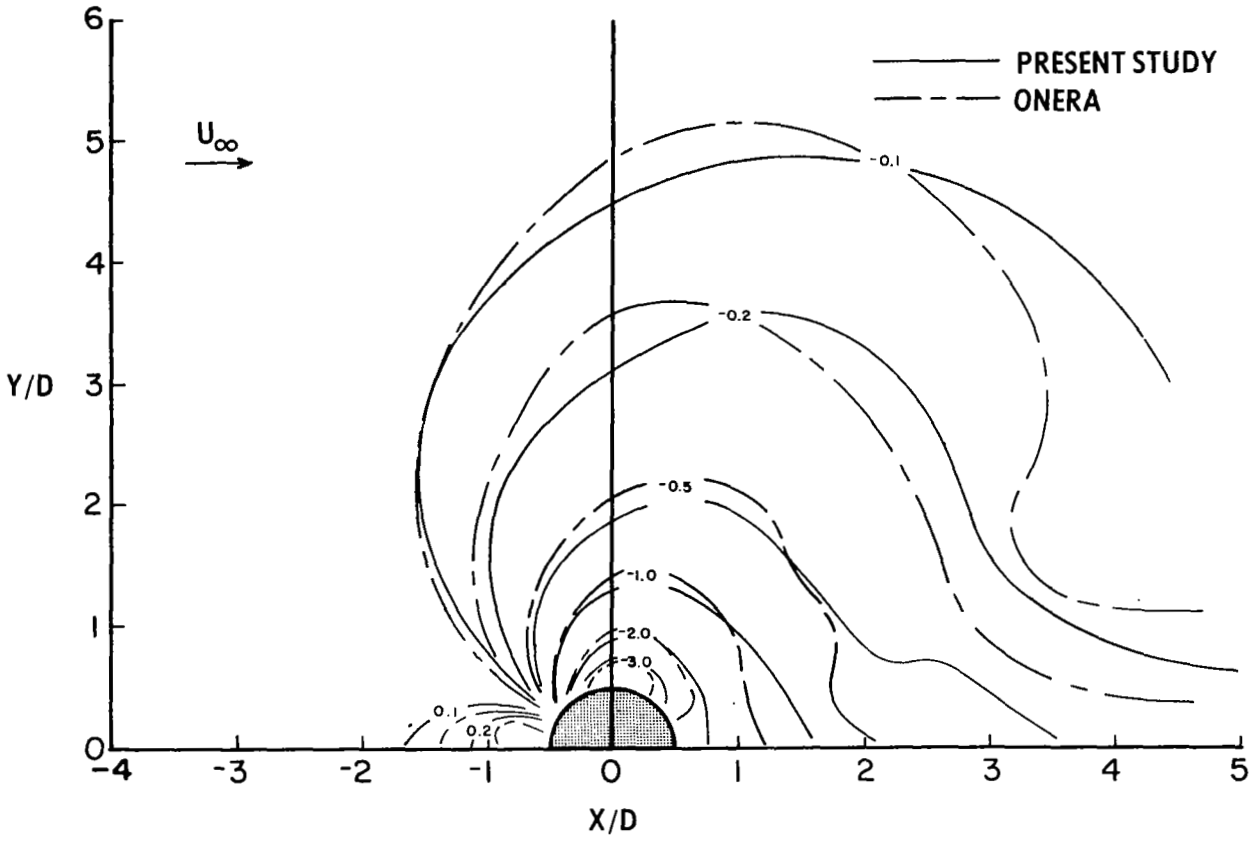

(e) R = 4; $M_\infty = 0.09$.

Figure 19.- Continued.

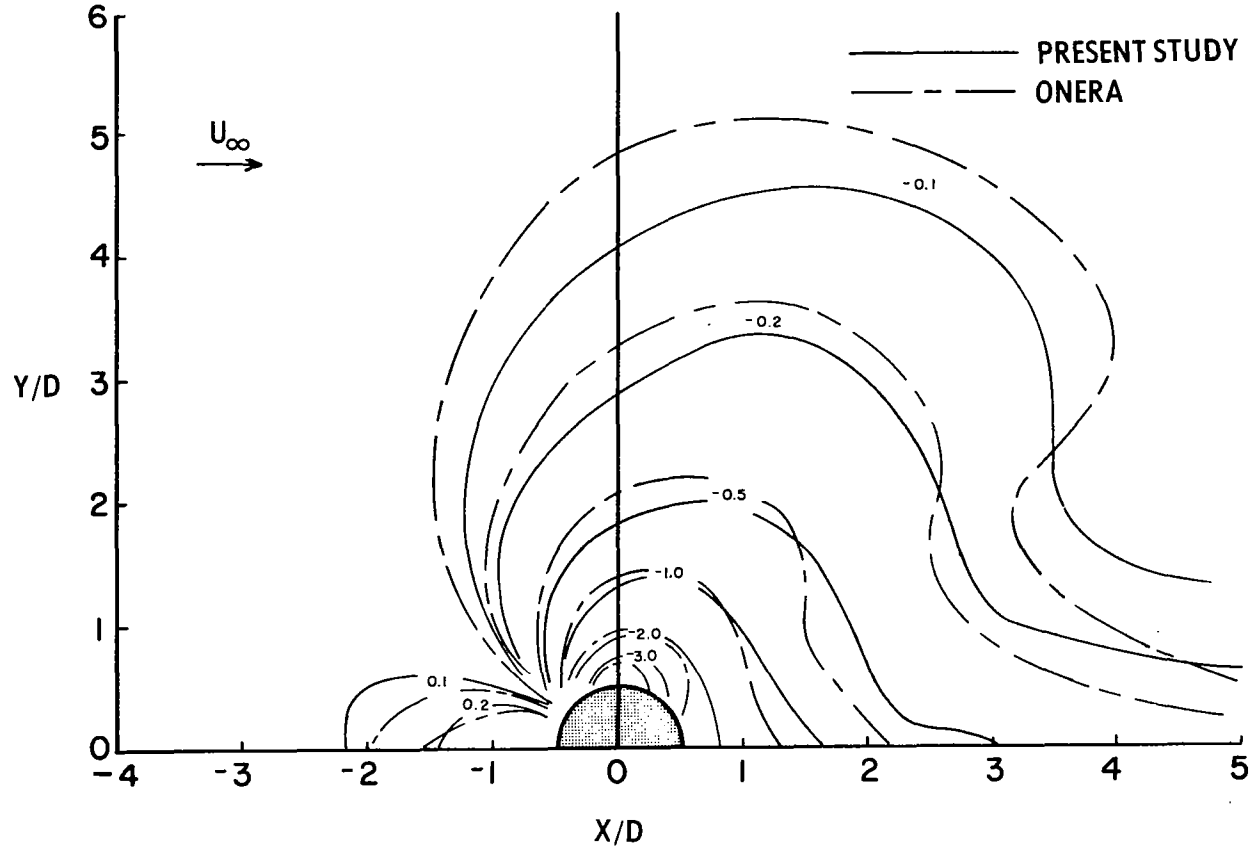

(f) R = 4; M_∞ = 0.18.

Figure 19.- Continued.

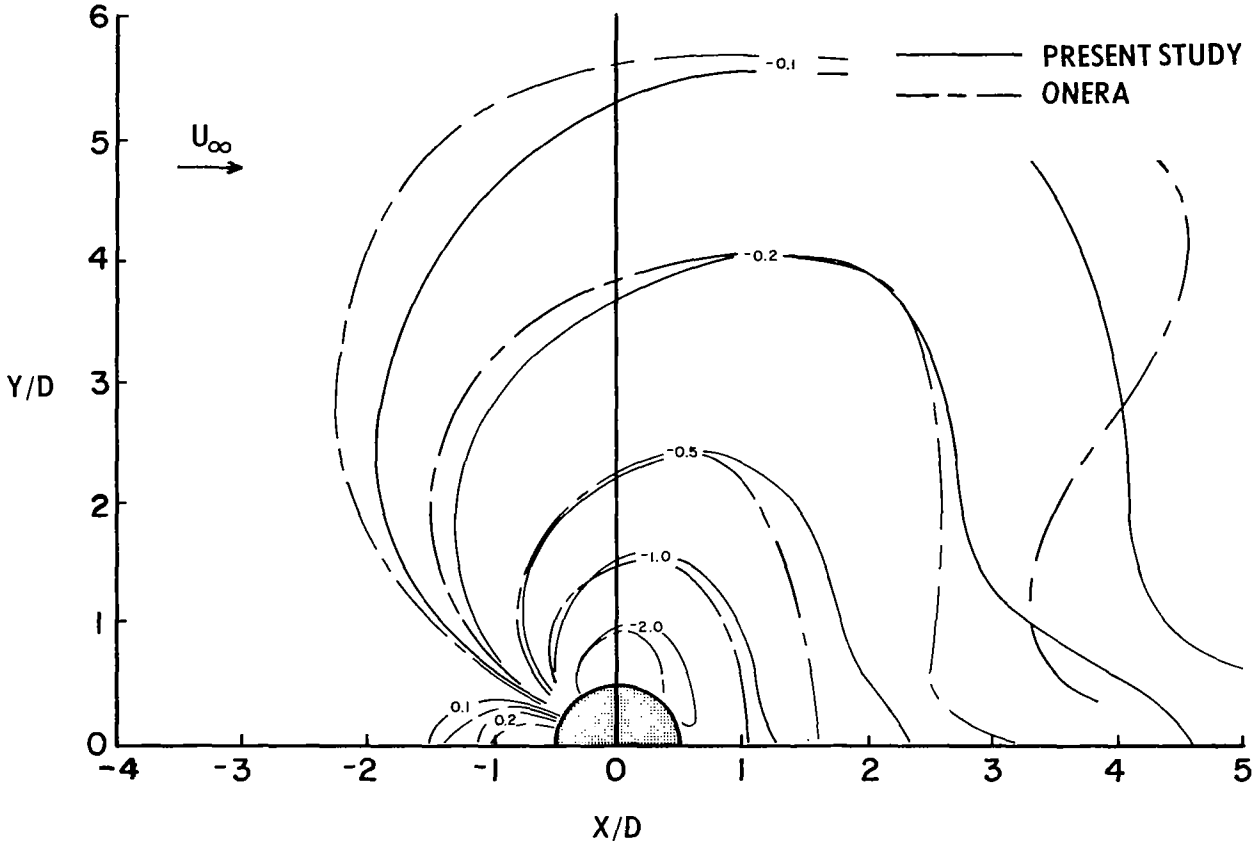

(g) R = 5; $M_\infty = 0.18$.

Figure 19.- Continued.

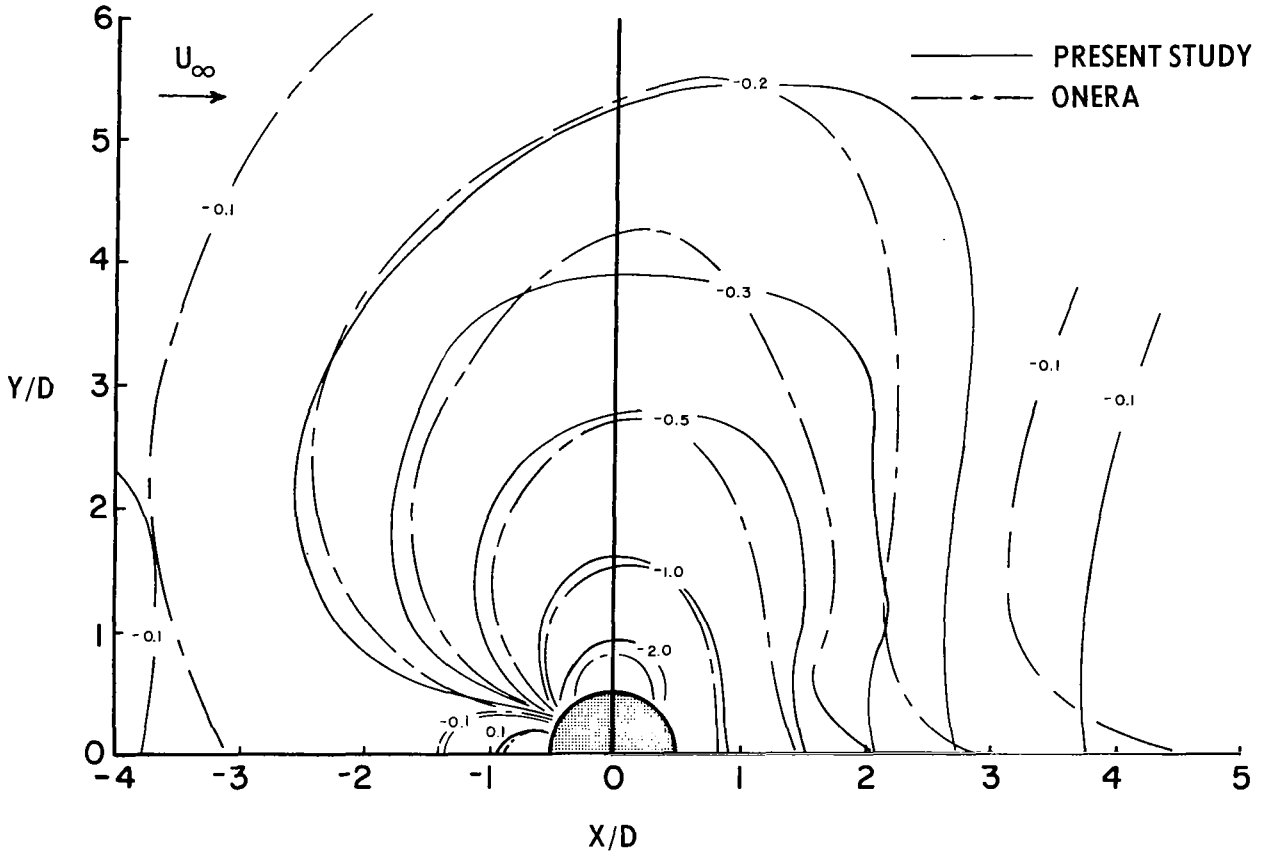

(h) R = 7; $M_\infty = 0.09$.

Figure 19.- Continued.

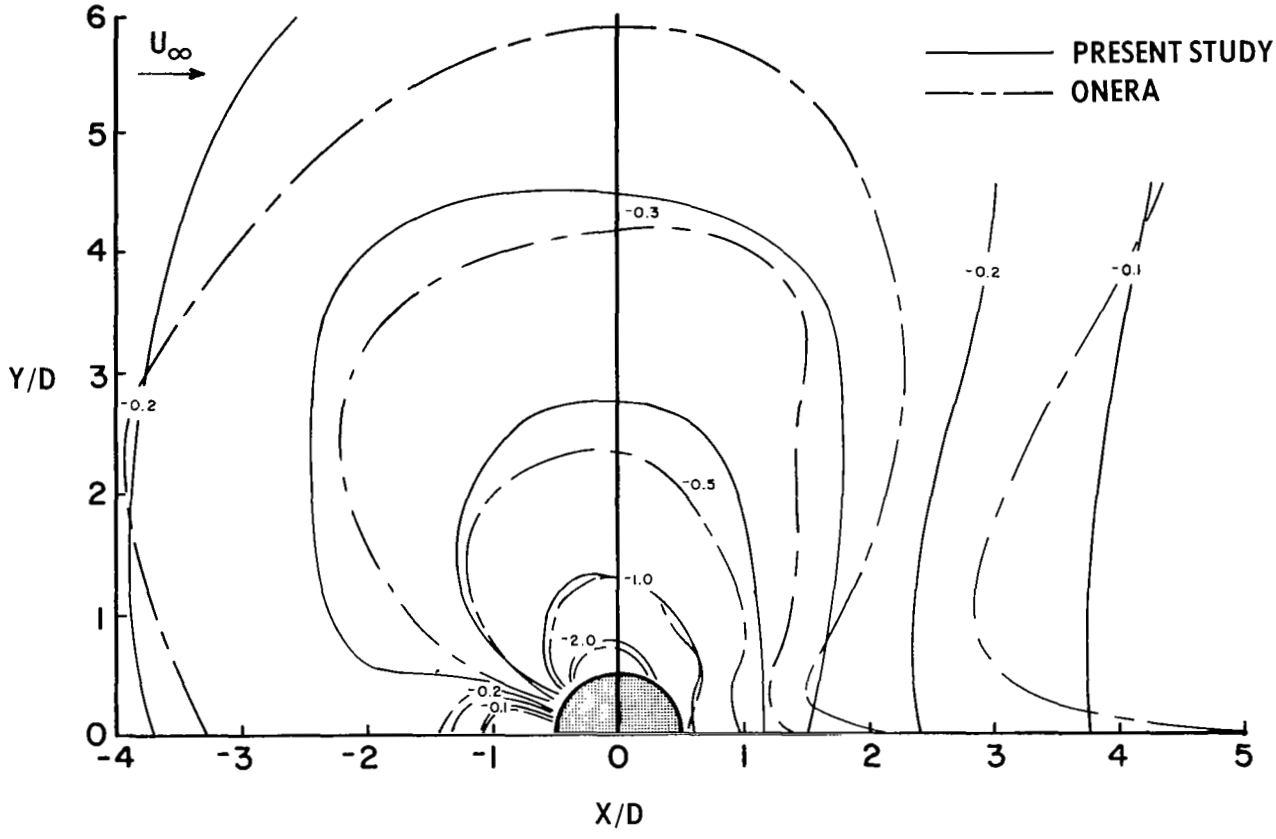

(i) R = 10; $M_\infty = 0.09$.

Figure 19.- Concluded.

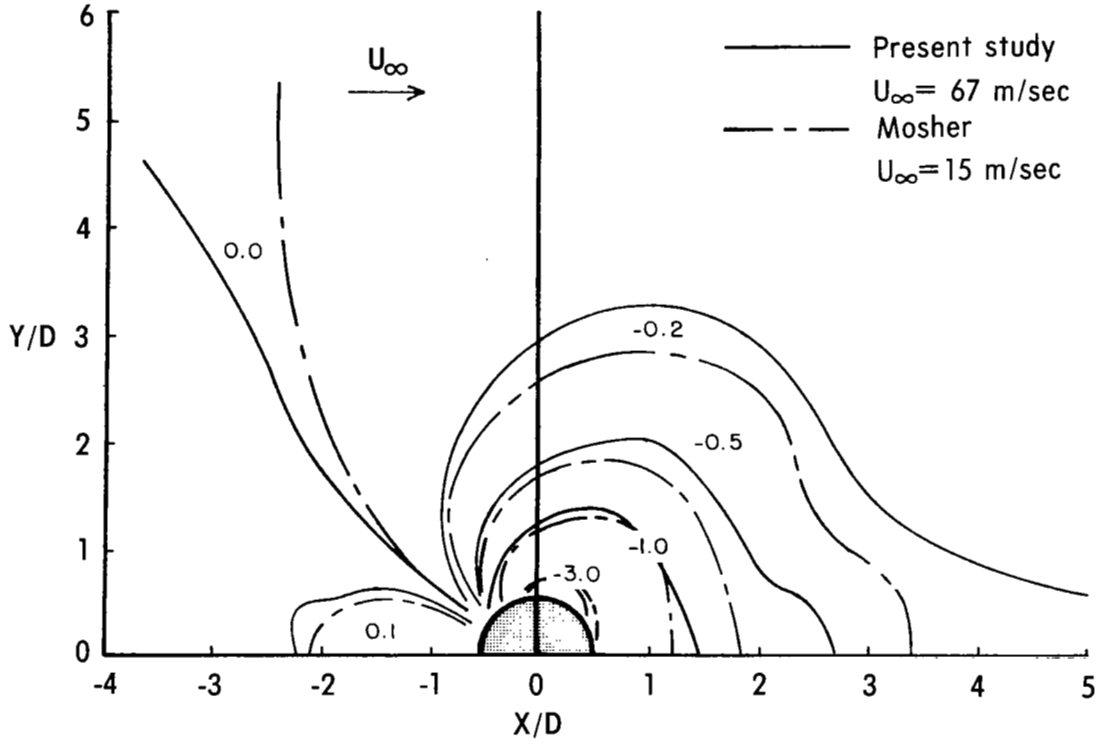

(a) R = 4.

Figure 20.- Comparison with Mosher (ref. 28).

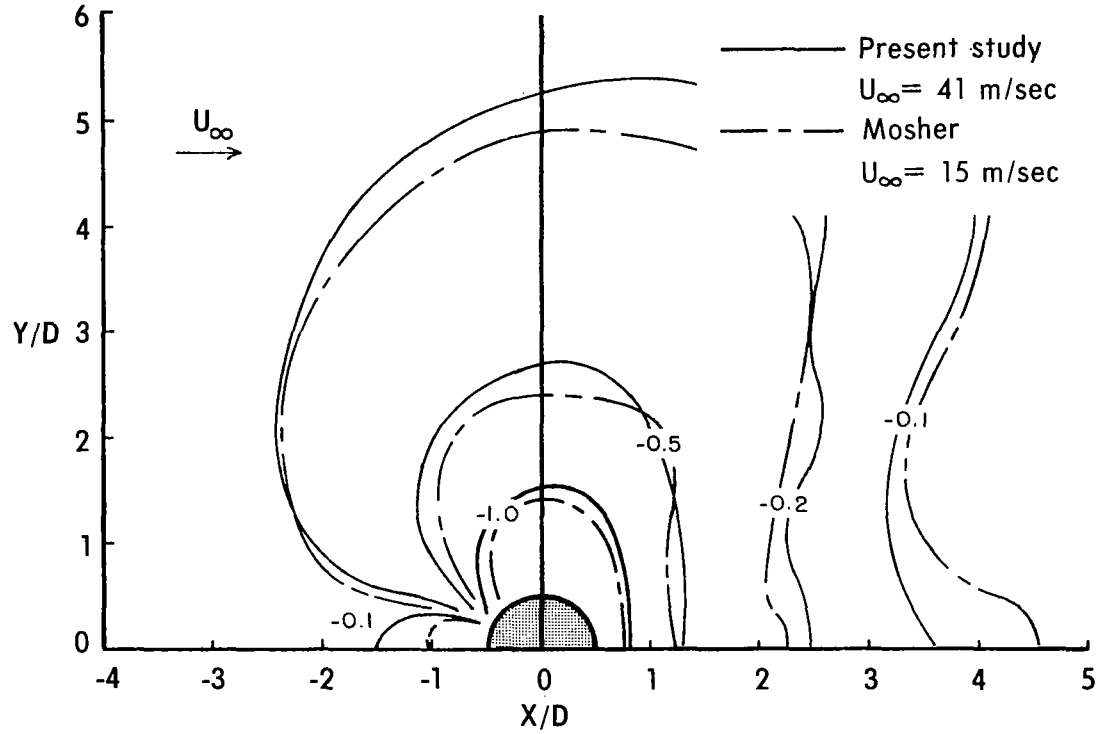

(b) R = 8.

Figure 20.- Concluded.

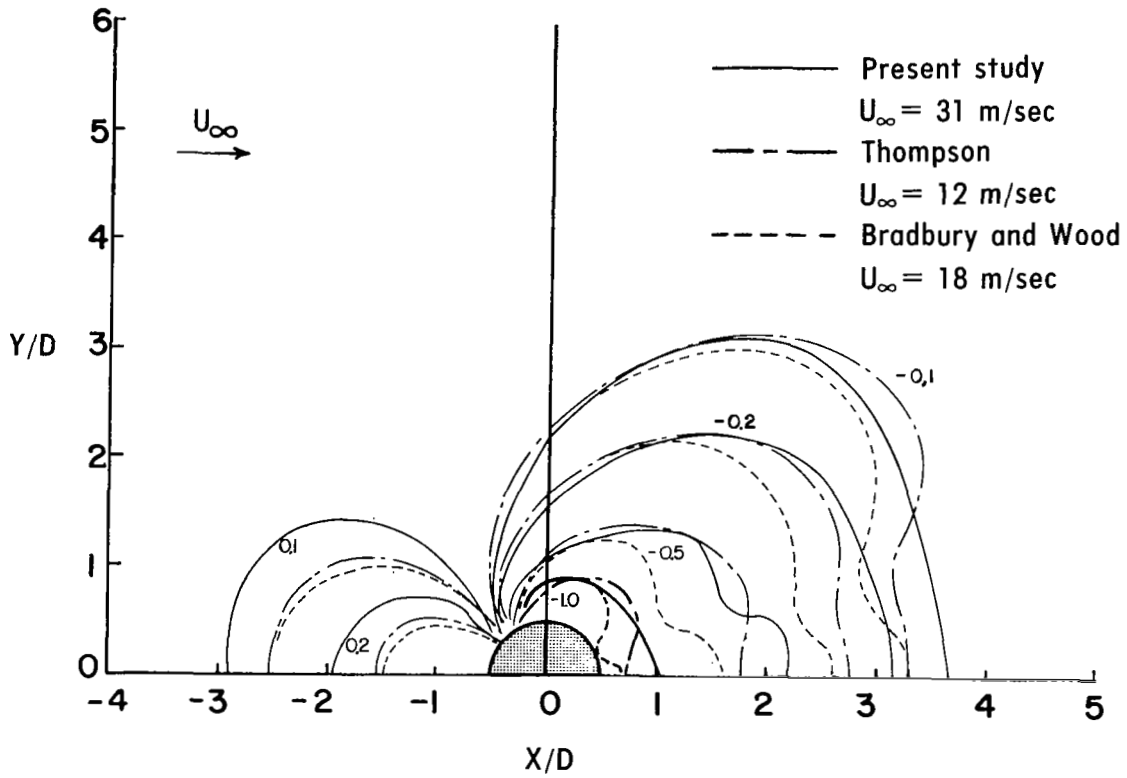

(a) R = 2.

Figure 21.- Comparison with Thompson (ref. 15) and with Bradbury and Wood (ref. 18).

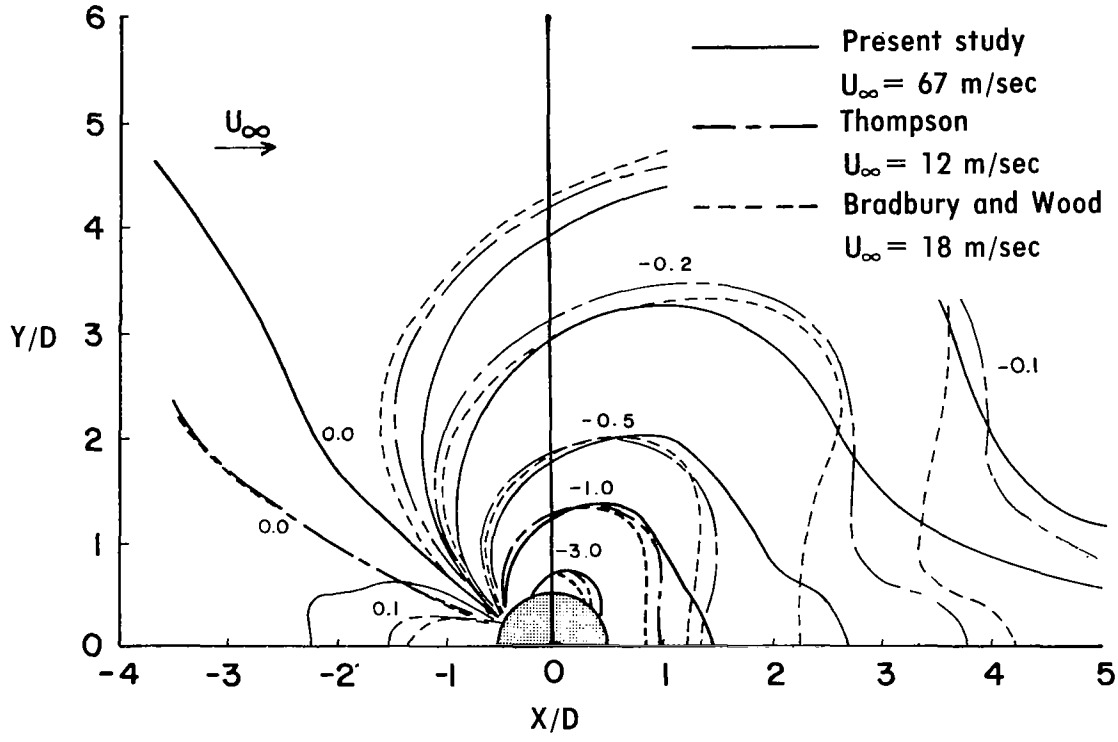

(b) R = 4.

Figure 21.- Continued.

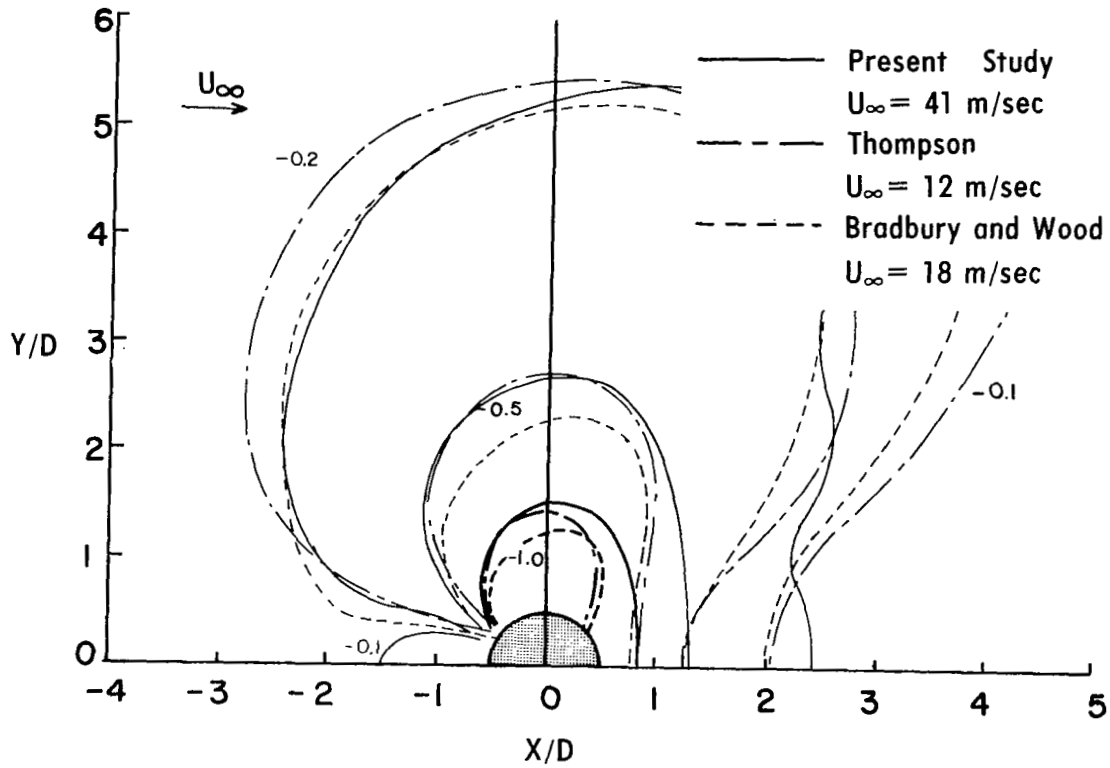

(c) R = 8.

Figure 21.- Concluded.

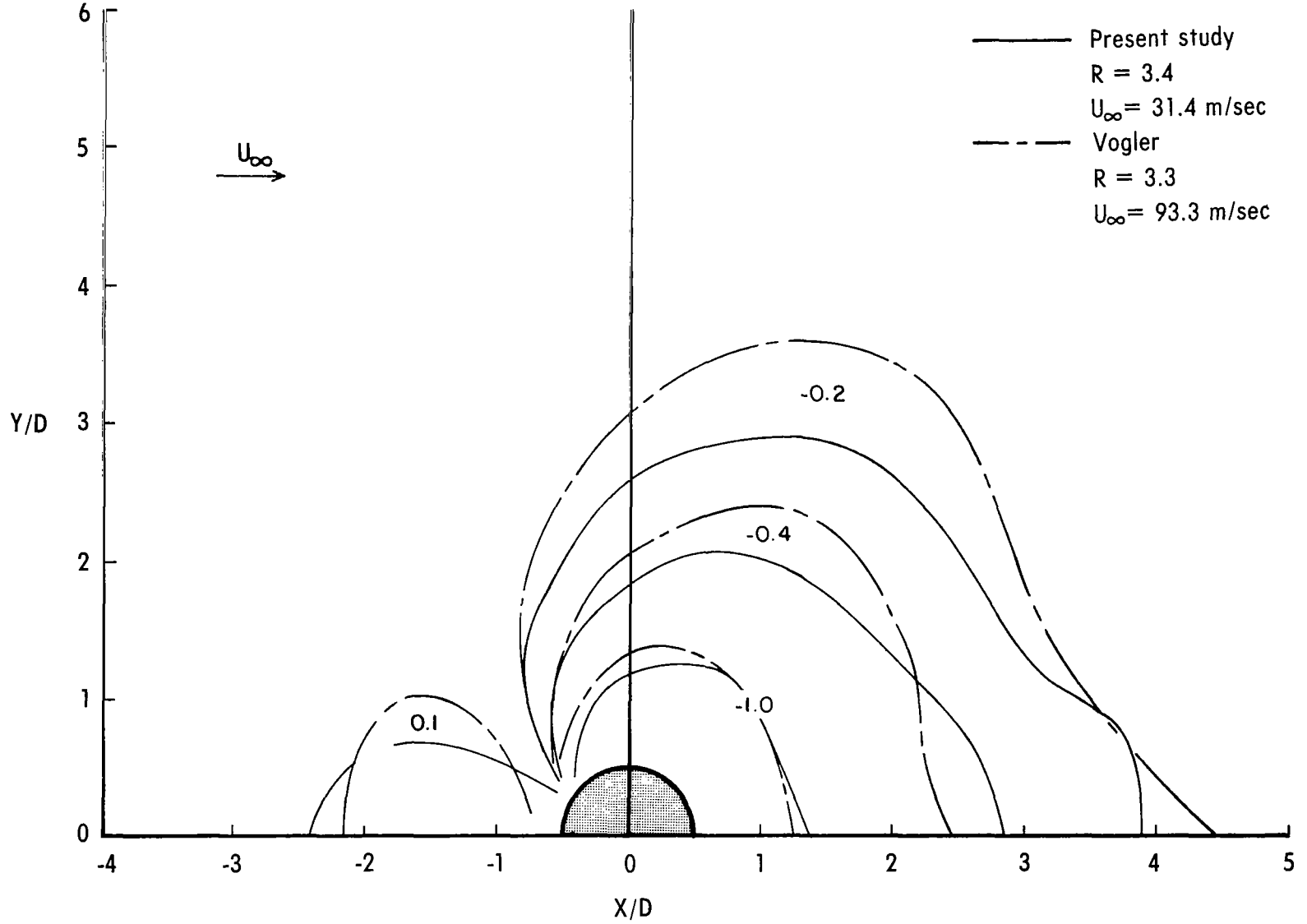

Figure 22.- Comparison with Vogler (ref. 17).

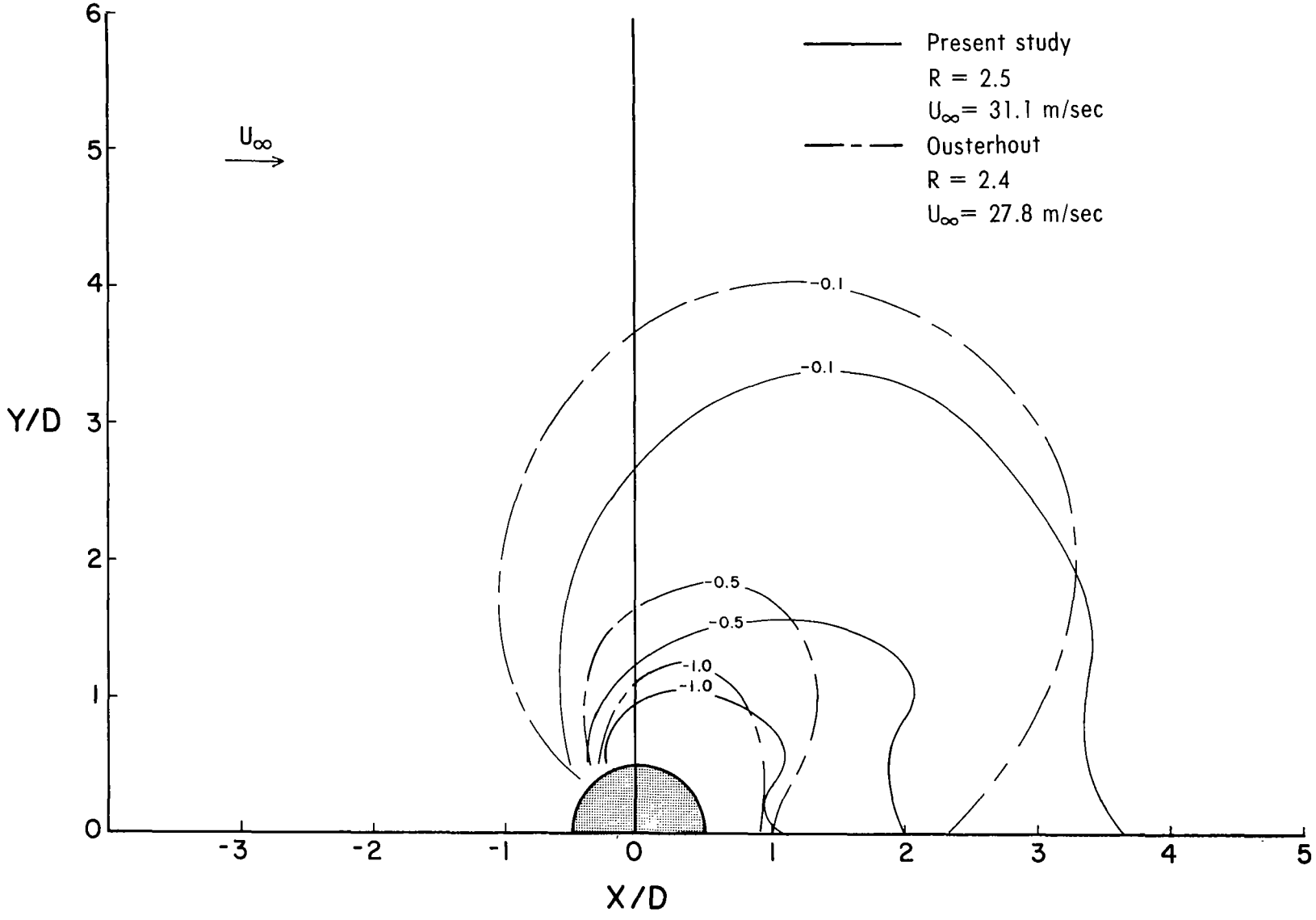

Figure 23.- Comparison with Ousterhout (ref. 23).

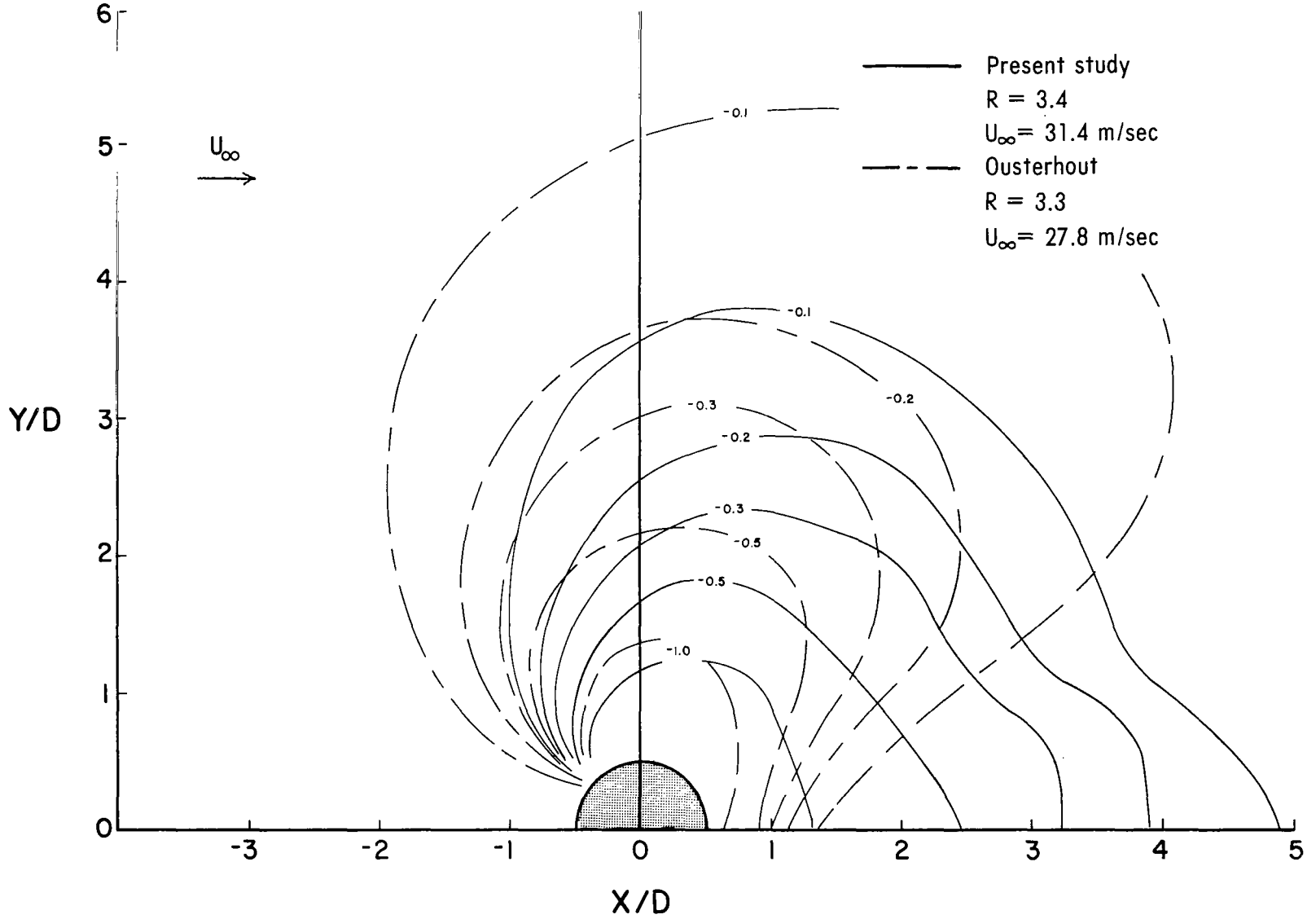

Figure 23.- Concluded.